Extended Theories of Gravity: The Early Universe and Stellar Interiors

Mariam Campbell

Thesis presented for the degree of

Doctor of Philosophy

Department of Mathematics & Applied Mathematics
University of Cape Town

Supervisor: **Prof. Peter K. S. Dunsby**

29 May 2025

DECLARATION

I, Mariam Campbell, declare that this thesis, titled *Extended Theories of Gravity: The Early Universe and Stellar Interiors*, submitted for the degree of Doctor of Philosophy at the University of Cape Town, is my own original work, except where otherwise indicated through proper citation and referencing.

- This work has not been previously submitted, either in whole or in part, for the award of any degree or qualification at this or any other institution.
- All sources of information, ideas, data, and text used in the preparation of this thesis have been fully acknowledged.
- I have not engaged in plagiarism, fabrication, falsification, or any other form of academic dishonesty in producing this work.
- I understand that any violation of the above may result in disciplinary action under the regulations of the University of Cape Town.
- None of this work has been previously published elsewhere, with the exception of the following:
  - Transitioning from a bounce to R^2 inflation

    Richard Daniel, Mariam Campbell, Carsten van de Bruck and Peter K. S.

Dunsby, Journal of Cosmology and Astroparticle Physics **06**, 030 (2023). The arXiv link: 2212.01093.

– Some exact relativistic star solutions in $f(R)$ gravity

Mariam Campbell, Sante Carloni, Peter K. S. Dunsby and Nolene F. Naidu, Class. Quantum Grav. **42**, 085014 (2025). The arXiv link: 2403.00070.

– Bouncing cosmologies in the presence of a Dirac-Born-Infeld field

Mariam Campbell, Richard Daniel, Peter K. S. Dunsby and Carsten van de Bruck, Physical Review D **110**, 043505 (2024). The arXiv link: 2405.06031.

Date: 29 May 2025

Signature:

ABSTRACT

This thesis explores two central themes within extended theories of general relativity: the cosmological dynamics of the early universe and the formulation of mathematical frameworks for modeling relativistic stars, with the overarching aim of testing and constraining model parameters in modified gravity.

In the cosmological context, a perturbative analysis of scalar-tensor theories demonstrates that a stable bi-scalar tensor model can yield a cosmic bounce preceding natural inflation. A detailed dynamical systems study of a Dirac–Born–Infeld (DBI) field further shows that initial conditions favorable to a bounce become increasingly likely as the system approaches the ultrarelativistic limit. A key result, derived for the first time in a spatially closed Friedmann-Lemaître-Robertson-Walker (FLRW) spacetime, reveals that the introduction of a negative cosmological constant does not lead to cyclic behavior in the DBI framework, implying that additional exotic degrees of freedom may be necessary to achieve cyclicity.

In the study of relativistic stars, this thesis presents two new exact, physically viable solutions to the Tolman–Oppenheimer–Volkoff (TOV) equations within extended gravity models. For theories with a quadratic correction to the Einstein–Hilbert action, the solutions describe (1) a quasi-isotropic stellar configuration with a shell and double-layer structure resembling a dipole distribution, and (2) a configuration characterized by a

quartic correction to the Newtonian potential and a smooth boundary matching. These results highlight the effectiveness of analytical methods in capturing the astrophysical behavior of compact objects in modified gravity. Moreover, the structural and compositional differences identified in these stellar models, relative to standard general relativity (GR), suggest potentially observable signatures that could be probed by future astrophysical observations.

ACKNOWLEDGMENTS

First, I want to acknowledge the National Research Foundation of South Africa and the University of Cape Town Science Faculty for funding my Ph.D. through the NRF Scarce-Skills PhD Scholarship and the Science Faculty Equity Scholarship, respectively.

Next, I would like to thank a few people whose presence has been invaluable during my academic career. The greatest thanks go to my supervisor, Prof. Peter Dunsby. In my final year as an undergraduate, I knocked on his door to ask about a final-year undergraduate project. He welcomed me in and said, "I'll teach you general relativity. Do as I say, and you'll be great." The rest is history. Thank you for your invaluable support during my academic career, not only as a supervisor but also for exposing me to countless opportunities (too many to list) that helped build my career and shape me into the scientist I am today. A special mention goes to my collaborators Prof. Carsten van de Bruck, Dr. Richard Daniel, Prof. Sante Carloni, and Dr. Nolene Naidu, with whom I enjoyed working and learned so much from scientific ideas to different approaches to problem-solving. An extended thanks goes to Prof. Sante Carloni for his hospitality during my visits to the University of Genova, Italy. I also want to express my gratitude to him, not only as a collaborator but also as a mentor. His kind, patient, and understanding support throughout my Ph.D. has been invaluable, and I have often drawn inspiration

and motivation from our discussions.
I would also like to extend my thanks to Prof. Álvaro De La Cruz Dombriz for facilitating my visits abroad to Granada and Madrid in Spain, and Split, Croatia. These opportunities have allowed me to build an international scientific network that has been instrumental in my growth, both professionally and personally.

I want to give a special acknowledgment to the unexpected connections and friendships. To Dr. Thomas Steingasser: Thank you for hosting me at MIT along with Prof. David Kaiser and Prof. Alan Guth, and for making my stay in Cambridge, MA, one of the most memorable experiences of my life. Your dedication to creating opportunities for me during my time there did not go unnoticed.
To Dr. Veronica Errasti Díez, who took me under her wing as a mentee and friend. Thank you for your mentorship and friendship. I met you at a time when I most needed someone like you, and I am so grateful to have you in my life.
To Thomas and Vero, I want to express my appreciation for your unwavering belief in me as a scientist, for encouraging me to step outside my comfort zone, and for your much-needed support and motivation during the final three months of my Ph.D.

Lastly, to my mother, Gaironesa. I could never repay the years of sacrifice and support you have given me. The woman from whom I draw the most of my strength, 'thank you' could never be enough. I only aim to make you proud.

NOMENCLATURE, CONVENTIONS AND ACRONYMS

Units. Geometrized units are assumed, i.e., $c = 8\pi G = 1$, unless stated otherwise.

Differential geometry. The Misner, Thorne, and Wheeler convention is adopted [200] where the signature of a spacetime metric is $(-,+,+,+)$. Einstein's summation convention for repeated indices is applied, and the nature of the indices is given in Table 1.

Notation. The covariant and partial derivatives with respect to a coordinate x^μ are

$$\frac{\partial f}{\partial x^\mu} \equiv \partial_\mu f \equiv f_{,\mu}, \tag{1}$$

$$\nabla_{\partial/\partial x^\mu} f \equiv \nabla_\mu f \equiv f_{;\mu}, \tag{2}$$

respectively, for a general function or tensor f. The Riemann and Ricci tensors are defined, respectively, as

$$R^\alpha_{\beta\sigma\gamma} = \Gamma^\alpha_{\beta\gamma,\sigma} - \Gamma^\alpha_{\beta\sigma,\gamma} + \Gamma^\mu_{\beta\gamma}\Gamma^\alpha_{\sigma\mu} - \Gamma^\mu_{\beta\sigma}\Gamma^\alpha_{\gamma\mu}, \tag{3}$$

$$R_{\alpha\beta} = g^{\gamma\sigma} R_{\alpha\gamma\beta\sigma}. \tag{4}$$

Acronyms. They are defined on their first appearance. Refer also to Table 2.

Symbols	Description
M_{PL}	Planck mass (2.18×10^{-8} kg)
α	Starobinsky coupling constant.
Greek indices $(\alpha, \beta, ...)$	run from 0 to 3.
Latin indices $(a, b, ...)$	run from 1 to 3.
$\Gamma^{\alpha}_{\beta\gamma}$	The metric connection, Christoffel symbols.
r	aerial radius.
$\perp$	indicates an orthogonal direction.
$c^2_{i,j}$	Squared sound speed for fluid i and $j = \{r, \perp\}$.
e_a	Unit vector orthogonal to the four velocity.
f	General function.
g_{ab}	Four dimensional metric tensor.
h_{ab}	Three dimensional induced metric tensor.
$N_a{}^b$	Two-surfaces projection tensor.
p^i_j	Isotropic pressure for fluid i and $j = \{r, \perp\}$.
u_a	Four velocity.
μ^i	Energy density for fluid i in the $(1 + 1 + 2)$ covariant formalism.
Π^i	Anisotropic pressure/stress for fluid i.
ϕ	Sheet expansion of the two-surfaces.
ρ	Energy density in the $(1 + 3)$ covariant formalism.

Table 1: List of fundamental constants and description of symbols used in this thesis.

Acronyms	Signification
BH	black hole
CCC	conformal cyclic cosmology
CMB	Cosmic Microwave Background
CMBR	Cosmic Microwave Background Radiation
DBI	Dirac-Born-Infeld
EMT	Energy Momentum Tensor
ESU	Einstein Static Universe
FLRW	Friedmann–Lemaître–Robertson–Walker
GR	General Relativity
GUTs	Grand Unified Theories
GW	gravitational wave
HBB	Hot Big Bang
LQG	Loop Quantum Gravity
LRS	Locally Rotationally Symmetric
LSS	Large Scale Structure
PSTF	Projected Symmetric Trace Free
TOV	Tolman-Oppenheimer-Volkoff

Table 2: List of acronyms and their definitions.

GLOSSARY

Bounce The transitional point between a spacetime experiencing contraction and then expansion or vice versa.

Ghost(s) A theoretical field or particle with negative kinetic energy that leads to instabilities such as unbounded energy from the vacuum.

Jump The hypersurface between connecting surfaces.

Scalaron An extra scalar degree of freedom that arises naturally when modified gravity models like $f(R)$ gravity are rewritten in a form equivalent to scalar-tensor theories.

There are more things in Heaven and Earth, Horatio,

than are dreamt of in your philosophy.

— W. Shakespeare

CONTENTS

LIST OF FIGURES

LIST OF TABLES

CHAPTER 1

OVERVIEW

1.1 Introduction

This thesis explores two major themes in cosmology and general relativity (GR): alternative theories of gravity that describe the primordial Universe and the mathematical framework used to test these models by means of astrophysical objects. These topics form the foundation of astrophysics and theoretical cosmology, especially as advances in observational data collection and precision in numerical relativity have accelerated through machine learning and artificial intelligence.

The ΛCDM model provides the best approximation to describing the Universe and passes a number of demanding tests [4, 7–9, 37, 74, 229, 234, 246, 280]. By assuming an isotropic and homogeneous spacetime, described by the Friedmann-Lemaître-Robertson-Walker metric within the framework of general relativity (GR), Einstein's relativity encapsulates the Universe's dynamics. However, as elegant as GR is, it has some shortcomings. The main challenges facing it are the following:

1. Its incompatibility with quantum mechanics. Since GR is a classical theory, it cannot describe the physics of black hole singularities or during the early Universe

at the Big Bang scale.

2. The prediction of singularities [141–143, 230, 253]. The initial singularity and at centers of black holes, the energy density and curvature becomes infinite and GR breaks down. This implies that GR is an incomplete theory since it cannot provide a full description of spacetime at these points.

3. GR does not naturally predict dark matter and dark energy. Observational phenomena such as galaxy rotation curves [41, 118], the distribution of large-scale structures, and cosmic acceleration [234, 241] are only fully explained by introducing dark matter and dark energy within the ΛCDM paradigm.

4. The cosmological constant problem [286, 287]. Introduced by Einstein [103, 105] and later interpreted as a representation of dark energy [270], its theoretical prediction is off by at least 10^{120} times the observed value predicted by quantum field theory [60, 273, 274].

Attempts to overcome the shortcomings of general relativity (GR) often involve extending or modifying the Einstein–Hilbert action by introducing an additional scalar degree of freedom.

To address the incompatibility of GR (a classical theory) with quantum mechanics, various approaches have been proposed to develop a theory of quantum gravity. Many of these approaches involve increasing the number of spacetime dimensions, leading to major research areas such as string theory [95, 281] and loop quantum gravity [244]. Although these frameworks have gained significant attention, their predictions have yet to be experimentally verified. Rovelli explores the foundational and conceptual issues of quantum gravity in his book of the same name [245].

To address the initial singularity problem inherent in the Hot Big Bang (HBB) model, one possible remedy is to replace the singularity with a *bounce*. In this scenario, the Universe undergoes a period of contraction followed by a bounce, when the scale factor

reaches a minimum, after which cosmic expansion begins. This mechanism, often used as a prelude to inflation, also offers a framework for constructing cyclical models of the Universe [36, 155].

Another approach to resolving the initial singularity is the concept of an *Emergent Universe*, originally proposed by Ellis and Maartens [109, 112]. This model envisions a universe that emerges from an Einstein static state, i.e., non-expanding, spatially closed ($k > 0$), and supported by a positive cosmological constant. However, such models depend on the existence of an initial Einstein static state to describe the eternal past and typically require significant fine-tuning.

In contrast, models developed within the framework of loop quantum gravity have been shown to alleviate these issues. In such models, a non-singular, past-eternal, oscillating universe can naturally evolve into an emergent inflationary phase [203].

Modifying gravity to theoretically explain observational phenomena such as dark matter and dark energy is commonly pursued through models like scalar-tensor theories, fourth-order gravity theories, quintessence, and interacting and/or dynamical dark energy models.

Throughout this thesis, modified theories of gravity will be explored in the context of extensions to the Einstein–Hilbert action, with a focus on their ability to describe early-universe evolution and dynamics, as well as astrophysical objects. The ultimate goal is to constrain model parameters through these applications.

1.2 The Early Universe

The origin of the Universe has long been a subject of both scientific inquiry and philosophical reflection. The foundational concept of how the Universe came into existence, later termed the Big Bang, was first proposed by Lemaître in 1927 [175, 189–191]. A Belgian physicist and priest, Lemaître suggested that the Universe began from a single point and was expanding, based on solutions to the Einstein field equations. He was also

the first to derive what is now known as the Hubble–Lemaître law [107], which relates a galaxy's distance to its redshift. This name was adopted following a unanimous vote by members of the International Astronomical Union (IAU) [167]. Importantly, Lemaître correctly interpreted observational data as evidence for the expansion of the Universe, laying the foundation for what would become the Big Bang theory.

In the 1940s and 1950s, Gamow, along with his students Alpher and Herman, developed the Hot Big Bang (HBB) model. They proposed that the early Universe was in a hot, dense state, and as it expanded, it cooled. This cooling process would allow for Big Bang nucleosynthesis, the formation of light elements in the early Universe [13, 125, 126]. Gamow and his collaborators also predicted the existence of the cosmic microwave background radiation (CMBR), a relic thermal radiation from the early Universe [63]. Peebles offers an insightful review of the discovery of the Hot Big Bang model, including the pivotal developments in 1948 involving Gamow and his students [228].

Observational confirmation of the CMBR occurred in 1965, when Penzias and Wilson accidentally discovered this residual radiation [1, 233]. Despite these early successes, the HBB model faced several significant shortcomings:

- The horizon problem [199, 242]. Observations show that the CMBR is nearly uniform in temperature across vast distances and causally disconnected regions of the Universe needed to somehow "communicate" to achieve thermal equilibrium.

- The monopole problem [2, 239]. Grand Unified Theories (GUTs) predict magnetic monopoles and other exotic particles that should have formed in the early Universe, but there is no observational evidence for it.

- The structure formation problem [139, 178, 221, 227, 288]. The HBB model predicts an early universe with a uniform matter and radiation distribution, however, it struggles to explain the formation of large-scale structures like clusters of galaxies.

Nearly a decade and a half after the discovery of the CMBR, Guth, then working on grand unified theories (GUTs), proposed that a phase of exponential cosmic expansion

could resolve the horizon problem of the Hot Big Bang (HBB) model, as well as the extreme fine-tuning required in its initial conditions in the absence of inflation. He called this idea the *Inflationary Universe* [136]. Inflation, a period of rapid expansion, occurs shortly after the Big Bang and is driven by a high-energy vacuum state. This phase of rapid expansion predicts a spatially flat universe [91, 201, 275], and the Planck collaboration's observational constraint of $\Omega_K = 0.0007 \pm 0.0019$ [7] stands as a major success for inflationary cosmology.

Inflation also accounts for the large-scale uniformity and structure of the Universe without requiring an extreme degree of fine-tuning. Guth's original model, based on supercooling during cosmic phase transitions, was conceptually simple, but suffered from what became known as the *graceful exit problem* [42, 135]. In this scenario, although the accelerated expansion renders the Universe flat and homogeneous, it leads to eternal inflation [136].

This problem was independently resolved in 1982 by Linde [182], and by Albrecht and Steinhardt [10], using a model known as *new inflation*. In this approach, the false vacuum of Guth's "old inflation" is replaced by a gently sloped energy plateau, allowing inflation to proceed and then come to an end as the inflaton field slowly rolls down the plateau (see Fig. 1.1).

Linde made significant contributions to improving Guth's original model of inflation. In 1983, he developed the concept of *chaotic inflation* [183], which proposed that inflation could begin from a random, "chaotic" initial state. In this scenario, quantum fluctuations drive exponential expansion, giving rise to the universe we observe today, without requiring finely tuned initial conditions.

To make this variant of inflationary theory more widely applicable and realistic, Linde also investigated the dynamics of the inflaton field and the shape of its potential. His insights demonstrated how inflation could naturally start, end, and transition smoothly into the Big Bang phase. This framework offers greater flexibility in modeling inflation and strengthens its viability as a mechanism for generating a universe like our own.

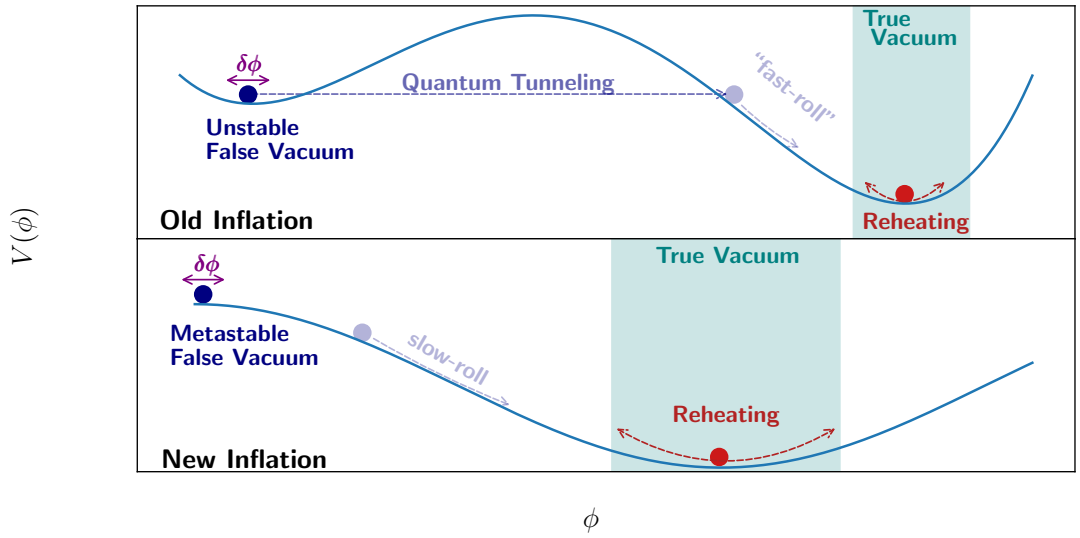

Figure 1.1: Guth's "old inflation" compared to Linde's "new inflation".

During the 1980s, numerous inflationary scenarios were proposed and critically examined in light of improving observational constraints. Before Linde introduced his concept of *new inflation*, Starobinsky had already proposed an R^2 correction to the Einstein-Hilbert action in 1980 [262]. His work, motivated by the desire to resolve the Big Bang singularity through quantum effects of matter fields, demonstrated that the de Sitter solution is unstable both in the future and the past, eventually decaying into a matter-dominated FLRW universe. However, Starobinsky's model does not explain how the universe initially entered the de Sitter phase.

A similar issue arises in scalar field-driven models of inflation, although it has been shown that for large-field inflation, phase-space trajectories possess a local attractor [44]. In both Starobinsky's and scalar field-driven inflationary models, the problem of initial conditions can be addressed either through quantum cosmology or by introducing a cosmological bounce prior to the onset of inflation. This is addressed in Parts I and II.

Quantum cosmology, in particular, suggests that a de Sitter phase can emerge spontaneously through a semi-classical tunneling event. This mechanism is argued to favor Starobinsky's model over scalar field-driven inflation, as discussed by Hawking et al. in

[144].

Currently, single-field inflationary models are strongly favored by experimental data, with recent results from the Planck collaboration providing robust support for slow-roll models featuring a concave potential [8]. However, these models face a fundamental limitation when it comes to explaining the origin of the Universe. Within the classical framework of single-field inflation, an initial singularity is unavoidable, as demonstrated by the Borde-Guth-Vilenkin (BGV) theorem [40]. In fact, the BGV theorem states that *"inflationary models require physics other than inflation to describe the past boundary of the inflating region of spacetime."*

To overcome this issue, theories must either go beyond the classical regime or introduce new dynamical mechanisms. One such idea is a **cosmological bounce**, which aims to avoid the initial singularity by positing that the Universe transitions from a contracting phase to an expanding one. Such a bounce can arise from quantum gravity effects (e.g., in loop quantum gravity or string theory), exotic matter fields, or modifications to general relativity [36, 45, 154, 215].

The earliest attempt to avoid the initial singularity was made in 1973 by Parker and Fulling [224]. They studied a classical gravitational field minimally coupled to a quantized neutral scalar field with mass, within a spatially closed FLRW spacetime. The objective of their work was to investigate the influence of quantum theory on the classical singularity theorems. Their findings showed that quantum effects in this setup can lead to a violation of the energy conditions, and they numerically demonstrated how a bounce could occur in a Friedmann cosmology. In their model, singularity avoidance arises from a quantum coherence effect, which depends on specific phase relationships in the quantum state's specification. However, their model does not provide conclusive evidence that quantum effects will always prevent gravitational collapse, as their bouncing solutions eventually re-collapse after completing a cycle.

Another approach to bypass the initial singularity is the concept of colliding branes, known as the Ekpyrotic Universe, which is rooted in M-theory [164]. The original Ekpy-

rotic model eliminated the need for inflation; however, Linde identified several inconsistencies, such as the prediction of a Big Crunch instead of a Big Bang and the possible presence of ghost fields [158–160]. A variant of the Ekpyrotic model, called Anamorphic Cosmology [153], allows for cosmological fluctuations similar to those in standard inflation, while matter experiences an Ekpyrotic bounce. These models aim to construct cyclic cosmologies [174], echoing the ideas of Tolman and Ward from 1932 [34, 268].

A more radical alternative to traditional bouncing models is *conformal cyclic cosmology* (CCC) [231, 232], proposed by Penrose. CCC describes a universe undergoing an infinite sequence of cycles, each beginning with a Big Bang and ending in a state that transitions into the next Big Bang. This transition is made possible through conformal geometry, which connects the end of one cosmic epoch (aeon) to the beginning of the next.

It is evident that new frameworks must be developed to identify signatures of bounce behavior in the early Universe. In [184], Liu et al. investigated whether such evidence could be extracted from cosmological surveys. Their model, a parametrization of the primordial spectrum with characteristics indicative of a nonsingular bounce, places upper limits on bounce parameters using a combination of CMB, LSS, and SN1a data. They conclude that if a nonsingular bounce precedes inflation, it must occur rapidly and at a very high energy scale, making direct experimental verification challenging.

An alternative, model-independent approach to probing bounce cosmologies arises from the observed relic abundance of dark matter, produced during the pre-bounce contraction and post-bounce expansion phases [177]. Li et al. divide the bounce epoch into three stages: (1) pre-bounce contraction, (2) post-bounce expansion, and (3) dark matter freeze-out. They argue that if a significantly lower abundance of dark matter with a small annihilation cross-section is detected, contrary to standard cosmological predictions, it would constitute a smoking-gun signal for the existence of a Big Bounce in the early Universe.

Further potential signatures of bouncing cosmologies have been studied in the CMB

bispectrum. In [88], Delgado et al. examined bounce models inspired by Loop Quantum Gravity (LQG), where the behavior of the model is governed by a parametrized scale factor and the Ricci scalar at the bounce. They found that the cumulative signal-to-noise ratio of the bispectrum features induced in the CMB by these models is high enough to be potentially detectable with current Planck data.

As we enter the era of precision cosmology, particularly through the lens of gravitational wave astronomy, new avenues for testing inflationary scenarios have emerged. The detection of high-frequency stochastic gravitational waves associated with the Cosmic Graviton Background (CGB) would pose a significant challenge to the standard inflationary model and motivate the consideration of alternative cosmological scenarios [271]. The CGB refers to relic gravitons that decoupled near the Planck time, leaving behind a thermal background of gravitational radiation. Vagnozzi et al. argue that a realistic inflationary phase would dilute the CGB to an undetectable level. Therefore, any future detection of the CGB would not only challenge the standard inflationary paradigm but could also provide compelling evidence in favor of bouncing cosmologies or emergent universe models, both of which predict a comparatively stronger CGB.

Although current detection methods are incapable of probing the high-frequency stochastic gravitational wave background associated with the CGB, whose characteristic strain peaks around 75 GHz, future technological advancements may enable the observation of this primordial graviton background, offering novel insights into the physics of the early Universe.

In the context of $f(R)$ gravity, Oikonomou investigated how a pre-inflationary de Sitter bounce influences the energy spectrum of primordial gravitational waves [218]. The study demonstrates that such a bounce can significantly suppress the energy spectrum, with the effect depending on both the duration of the bounce and the specific dynamics of the chosen $f(R)$ model. The universe's evolution is modeled in distinct phase patches, each governed by a particular form of $f(R)$ gravity, except during the matter- and radiation-dominated eras, which are described by the corresponding matter fluids.

The study concludes that the resulting gravitational wave signal could be detectable by future gravitational wave experiments such as the Big Bang Observer [79, 81], in contrast to scenarios without a pre-inflationary bounce.

The study of bouncing cosmologies often serves as a foundation for developing cyclic models. In canonical scalar field models, achieving cyclic behavior typically requires incorporating bounces, which are realized through either modifications to gravity or exotic matter-energy conditions. Cyclic models of this type have to

1. violate the strong energy condition or consider a spacetime with positive spatial curvature,

2. fine-tune the initial conditions when replacing the initial singularity with a bounce and,

3. incorporate dark energy; modeled as a cosmological constant that best describes our current universe. In the standard ΛCDM cosmology, a positive Λ leads to an eternal accelerated expansion.

Popular and successful cyclic models are

- Ekpyrotic models [174]. It describes cyclic cosmology as a series of brane collisions, where a brane collision describes the Big Bang.

- Cyclic Anamorphic Cosmology [152]. An alternative to Ekpyrotic models, the key feature of the model is a classically stable, non-singular bounce that transitions from a contracting phase to an anamorphic smoothing (anisotropic scaling) phase. This bounce is achieved through modifications to the Horndeski theory, ensuring stability and the absence of singularities. The stages of the cyclic anamorphic model include:

    1. Exiting the dark-energy epoch and entering a period of contraction.

    2. A non-singular bounce connecting the contraction phase to the anamorphic smoothing phase.

3. The anamorphic phase sets the initial conditions for the standard HBB, leading to the current observable universe.

The basic requirements for achieving an ideal cyclic universe are illustrated in Fig. 1.2. However, realizing such a model is challenging due to the difficulty of reconciling it with observational data and the unresolved issues in the emergent scenarios that many bounce or cyclic models struggle to address.

An alternative class of early universe models involves non-canonical scalar fields. These fields, often described by Lagrangians with non-standard kinetic terms, allow for richer dynamical behavior. They can impose constraints on the field's rate of change, preventing it from evolving too rapidly even with steep potentials. Such models offer enhanced control over the dynamics in scenarios like slow-roll inflation or smooth contraction phases in bouncing cosmologies, including emergent phenomena that are typically difficult to achieve in canonical frameworks.

A notable study by Bag et al. [28] revisits emergent cosmology models, highlighting the challenges posed by the instability of the Einstein Static Universe (ESU) within general relativity. They explore how modified gravity theories can provide a more robust framework for realizing emergent scenarios. By examining Braneworld Cosmology, Loop Quantum Cosmology (LQC), and Asymptotically Free Gravity, they identify a new minimum in the effective potential corresponding to a stable ESU. One of their most significant results is the demonstration that while a stable ESU supports emergent cosmology, it is not essential. Specifically, in the context of LQC with a non-canonical scalar field, they show that even without a stable ESU, the universe can oscillate around the true vacuum of the effective potential, still enabling an emergent scenario.

Furthermore, their study suggests that this LQC model yields values for the spectral index n_s and the tensor-to-scalar ratio r that are consistent with Cosmic Microwave Background (CMB) observations for steep potentials.

The most common non-canonical scalar fields, offering alternatives and extensions to

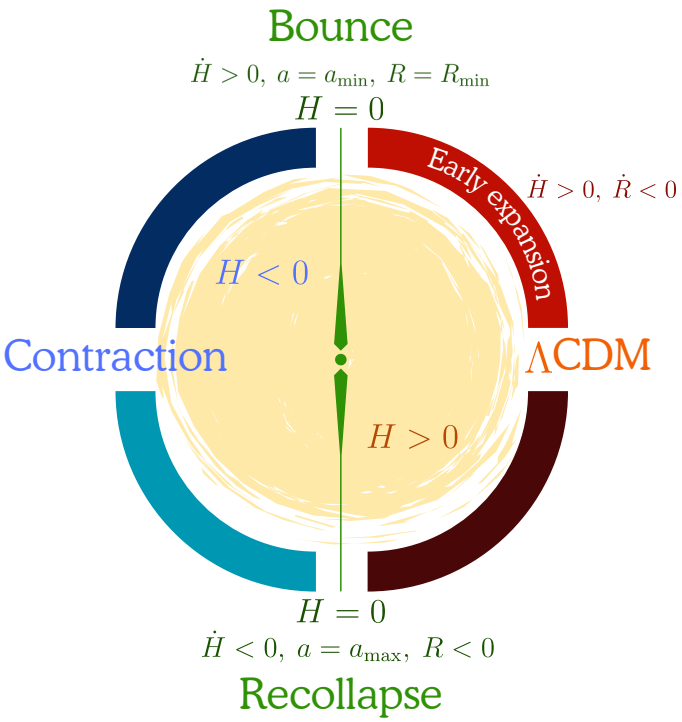

Figure 1.2: An ideal cyclic cosmology and the required conditions on the cosmological parameters.

standard inflation, are

1. DBI inflation: Driven by the Dirac-Born-Infeld action, these models possess an inherent speed limit that is imposed on $\dot{\phi}$, leading to inflation with suppressed higher-order corrections [157].

2. K-essence: Provides mechanisms for both inflation and late-time acceleration by introducing a kinetic energy-dominated phase [24, 64].

Our study, in Part II, focuses on a DBI field and the conditions conducive for a bounce.

Extending the range of inflationary scenarios beyond the standard slow-roll models, Dirac-Born-Infeld (DBI) fields offer a framework to study non-canonical inflationary dynamics that arise naturally in string theory. DBI fields are a class of scalar fields whose action originates from the dynamics of D-branes moving in a higher-dimensional warped internal space [157]. The field ϕ is typically interpreted as the position of the brane in the extra dimensions.

The distinctive feature of DBI inflation is the form of its kinetic term in the Lagrangian, which imposes a natural speed limit on the scalar field's evolution, analogous to the Lorentz factor in special relativity [11, 257]. This relativistic effect allows the field to slow-roll without requiring the flatness of the potential $V(\phi)$, a condition usually necessary in canonical slow-roll inflation. Consequently, DBI inflation permits inflationary dynamics with steeper potentials than those typically allowed by standard models [38, 65, 66, 163, 165, 261].

However, this relativistic mechanism comes with a trade-off: it tends to amplify non-Gaussianities in the primordial perturbations. The shape and amplitude of these non-Gaussianities depend on the warp factor and the potential, and they propagate at a reduced effective sound speed. These modifications influence both the power spectrum and the bispectrum of primordial fluctuations. As a result, these characteristic signatures may leave observable imprints in the Cosmic Microwave Background (CMB), offering a means to constrain such models and potentially uncover the physical origin of inflation [62, 114, 150, 172, 173, 276].

The deceleration mechanism of the DBI field is a novel feature. Its non-canonical nature imposes a speed limit on $\dot{\phi}$, ensuring that the evolution of the scalar field ϕ remains slow, even in the presence of steep potentials. This property offers significant advantages in bouncing cosmologies. Ensuring a smooth and controlled contraction phase is essential to avoid instabilities or singularities in bouncing models. The DBI deceleration mechanism restricts the field's speed during contraction, preventing it from rolling too rapidly down steep potentials, where chaotic dynamics could otherwise emerge.

A smooth and nonsingular bounce requires a careful balance between the scalar field's energy components and the underlying spacetime dynamics. The DBI field naturally regulates the evolution of ϕ during the bounce; its deceleration mechanism introduces a form of dynamic friction, which helps stabilize the field and suppress rapid oscillations or instabilities. As a result, the DBI field is an attractive candidate for driving bouncing cosmologies. Its deceleration mechanism helps prevent uncontrolled contraction and

singularities, while also stabilizing the dynamics of the bounce.

In Part II, we present an extensive dynamical systems analysis of the DBI field in a spatially closed spacetime. We expand the analysis to include solutions representing a bounce and assess whether an additional degree of freedom that triggers re-collapse could support a cyclical cosmological model. This includes original work that has been published, and it addresses bouncing cosmologies in the presence of a DBI field for the first time in the literature [52].

1.3 Astrophysical compact objects

Astrophysical objects serve as ideal candidates for testing extensions to general relativity. Spanning a vast range of scales, they probe gravity in different regimes, including:

- **Compact objects** such as neutron stars, which test gravity under high-density conditions [82, 123, 209, 289].
- **Stellar systems**, which examine gravitational dynamics on kiloparsec scales [33, 185, 207].
- **Black hole environments**, where strong gravitational fields provide a setting for exploring potential quantum gravity effects [21, 149, 169, 192, 194, 290].

Astrophysical phenomena also occur in extreme high-energy settings, such as supernovae [145, 210], active galactic nuclei (AGN) [6, 25], and gamma-ray bursts [16, 56], making them excellent laboratories for testing modified gravity theories that predict different energy-momentum relations or couplings between gravity and matter at high energies.

Methods for probing deviations from general relativity include:

1. **Gravitational wave observations**: Events involving black hole or neutron star mergers allow for testing deviations in waveform structures predicted by modified gravity theories. Although current data from LIGO and Virgo have not conclusively

ruled out scalar-tensor theories and others (discussed in Sec. 1.5), ongoing studies continue to analyze curvature dependence and higher-order corrections [31, 32, 80, 117, 196].

2. **Orbital decay in binary pulsars**: The loss of energy through gravitational radiation in binary pulsar systems provides a powerful tool for testing theories such as scalar-tensor gravity or massive gravity, which predict different decay rates and orbital dynamics [33, 185, 207].

3. **Black hole imaging**: High-resolution imaging of black hole shadows and accretion disks, as conducted by the Event Horizon Telescope (EHT), constrains deviations in spacetime geometry predicted by extended gravity theories. Such theories often result in altered shadow sizes or different matter dynamics near the event horizon [21, 149, 169, 192, 194, 290].

4. **Neutron star observations**: The mass-radius relation, pulsar timing, and gravitational wave data from binary neutron star inspirals offer sensitive tests of universal relations proposed in extended gravity theories [82, 123, 209, 289].

Some extensions to general relativity, particularly in the context of exotic compact objects, such as magnetars [26], boson stars [30, 116, 179], or hypothetical wormholes [29, 137, 186], predict distinct observational signatures not accounted for by standard GR. As such, the physical properties of astrophysical objects offer a rich and dynamic environment for studying gravity. A key theoretical objective is to improve the modeling of compact objects in these scenarios to enhance the sensitivity of observational tests and uncover potential deviations from general relativity.

1.4 Relativistic stars in gravity and its challenges

In this section, we discuss several challenges encountered when studying relativistic compact objects in general relativity (GR) and its extensions, and how Part III of this thesis

aims to address them. One major challenge is the difficulty in finding exact solutions for relativistic compact objects, particularly within extended theories of gravity, where the analyses are predominantly numerical.

Numerical approaches to gravitational problems often involve simplifying assumptions, such as relaxing boundary conditions, to accommodate the chosen numerical scheme or to enhance numerical stability [22, 27, 120, 121, 127, 285]. For instance, the Tolman–Oppenheimer–Volkoff (TOV) equations, which describe the equilibrium structure of spherically symmetric matter distributions, are highly nonlinear and typically require numerical methods for their solution. This complexity is further compounded when investigating modifications to GR, such as including higher-order curvature invariants in the Einstein–Hilbert action.

While numerical solutions are valuable, semi-analytical approaches offer distinct advantages. These include the ability to express model parameters explicitly in terms of observable quantities, impose stricter boundary conditions, and derive analytical constraints. This thesis seeks to contribute toward this goal. In Chapters 7 and 8, we present a dimensionless formulation of the TOV equations within the (1+1+2) covariant formalism and establish a new framework for deriving exact solutions for the interior of relativistic stellar objects in an $f(R)$ gravity framework.

Another major challenge in constructing relativistic stars in the context of gravity theories lies in matching the spacetime geometry outside the stellar configuration. An exact solution to Einstein's vacuum field equations, describing the spacetime around a static, spherically symmetric mass, was discovered by Schwarzschild in 1916 [250]. Remarkably, just four months later, Droste independently derived the same solution in his PhD thesis [197]. His work was later communicated by his advisor, Lorentz, and subsequently published in [93, 94].

This solution was quickly acknowledged and validated by contemporary physicists, notably Eddington and Pauli, who played significant roles in interpreting and popularizing its implications [100, 225]. The Schwarzschild metric remains foundational in the study of

black holes and other compact astrophysical phenomena, as it offers a simple, analytical description of spacetime outside a static, spherically symmetric configuration.

It provides a valuable framework for testing general relativity (GR), both in the weak-field limit, where the metric reduces to the Newtonian potential with relativistic corrections, and in the strong-field regime. Empirical validation of GR using the Schwarzschild solution has been achieved across diverse contexts, such as Solar System tests [37, 54, 98, 101, 124, 133, 238, 255, 256, 269], and observations of binary pulsars [83, 168, 266].

A natural extension of general relativity (GR) involves the inclusion of quadratic terms or linear combinations of quadratic curvature invariants, first considered by Weyl in 1918 [277]. These higher-order curvature terms become dominant in strong-field regimes, as they scale with higher powers of the curvature tensor. In these regimes, such as the early universe, the vicinity of black holes, or within dense compact stars like neutron stars, the contribution from quadratic terms can outweigh the linear Einstein-Hilbert term. Consequently, these environments provide ideal conditions for testing and constraining higher-order gravity models. Part III of this thesis focuses on describing relativistic stars in the context of higher-order gravity theories.

Buchdahl was the first to study the uniqueness of the Schwarzschild metric in pure R^2 gravity [49, 211], showing that it is the only spherically symmetric, asymptotically flat vacuum solution of the R^2 field equations. Whitt later extended this result to quadratic gravity of the form $R + \alpha R^2$ [278]. A significant property of quadratic gravity, and one reason it is widely studied in spherically symmetric spacetimes, is that the Schwarzschild metric remains the only static, spherically symmetric, asymptotically flat vacuum solution with a regular horizon, provided $\alpha > 0$ [198].

However, Pechlaner and Sexl demonstrated that while the metric in quadratic gravity may be asymptotically flat, its linear approximation around Minkowski spacetime does not correspond to the linearized Schwarzschild metric [226]. This discrepancy raised the question of whether the Schwarzschild solution remains valid outside a matter distribution

(point-like or extended) in $f(R)$ gravity. Deruelle et al. addressed this issue in [90] by generalizing the Israel junction conditions for $f(R)$ theories of gravity (discussed in more detail in Chapter 10). They analyzed boundary conditions across a brane, modeled as an infinitesimally thin domain wall, and examined the Einstein limit. Their study shows that a specific non-minimal coupling of matter on the brane to gravity introduces the possibility of a new class of braneworld scenarios. The conditions required for the existence of the Schwarzschild solution for a generalized $f(R)$ theory of gravity were later addressed by Nzioki et al. in [217].

When considering less exotic spacetime models that are more consistent with observational constraints, the Schwarzschild metric remains the simplest vacuum solution naturally supported by quadratic gravity. In 1945, Einstein and Straus examined how cosmic expansion influences the gravitational field around a localized mass [106]. They concluded that the spacetime expansion has no significant influence on the local static field surrounding a star, except at the boundary of the star's embedding region in the expanding universe.

Extending this idea to $f(R)$ gravity, Clifton et al. showed that for $f(R) = R^n$ models, no known spherically symmetric vacuum solution can be consistently matched to an expanding FLRW background [69, 72]. Compact objects thus serve as ideal laboratories to constrain extended theories of gravity, providing observable signatures that place stringent limits on model parameters. Although the lack of exact solutions limits some aspects of theoretical analysis, particularly at the boundaries of such objects, existing observations have already imposed meaningful constraints. These issues are addressed in more detail in the following section.

1.5 Current observational constraints

With the advent of precision measurements from gravitational wave signals, particularly those emitted from neutron star cores and mergers, a new avenue for testing theories of

gravity has emerged. A recent study [99] demonstrated that the long-ringdown phase of binary neutron star mergers can provide stringent constraints on the properties of nuclear matter at densities that are otherwise inaccessible in laboratory settings. These constraints complement those derived from direct mass-radius measurements and further narrow the viable forms of the neutron star equation of state (EOS).

The detection of the gravitational wave signal GW170817, along with its electromagnetic counterpart GRB170817A, has played a crucial role in constraining extended theories of gravity. A number of key studies published shortly thereafter [31, 80, 117] summarized the implications of this event:

- The propagation speed of gravitational waves, c_T, parametrized as $c_T = 1 + \alpha_T$, is constrained to the interval $|\alpha_T| \leq 10^{-15}$.
- **Eliminated models:** quartic and quintic Galileon models, de Sitter Horndeski, $f(\phi)$·Gauss-Bonnet, and $G_{\mu\nu}\phi^\mu\phi^\nu$.
- **Viable models:** GR; Brans-Dicke/$f(R)$ theories; scalar-tensor theories of the form $f(\phi)R$ plus non-gravitational terms; and beyond-Horndeski extensions of scalar-tensor theories that are conformally coupled to gravity. In particular, conformally coupled models must exhibit minimal coupling strength to gravity such that they can be modeled as generalized fluids. This class includes cubic Galileons, kinetic gravity braiding, and k-essence.
- **Unconstrained models:** minimally coupled gravity and quintessence models.

Focusing specifically on astrophysical constraints in $f(R)$ theories of gravity, the galactic halo provides one of the strongest bounds, with $|df/dR| \leq 10^{-6}$ [187]. Observations within the Solar System, such as the measurement of geodetic precession by the Gravity Probe B experiment, constrain the scalar curvature to $R \leq 10^{-22}$ m^{-2} [204].

Relativistic stars have been extensively studied in the context of quadratic gravity, where constraints on the R^2 term parameter α have been derived from satellite experi-

ments, astrophysical observations, and investigations of the neutron star mass-radius relation. The Gravity Probe B experiment, designed to test the geodetic and frame-dragging effects predicted by GR, sets a bound on α of 5×10^{11} m^2 [115]. However, observations from PSR J0737–3039, a binary pulsar system, yield an upper bound $\alpha \leq 2.3 \times 10^{15}$ m^2 [48, 204].

In a perturbative analysis of neutron stars in quadratic gravity, Arapoglu et al. [23] found that deviations from GR comparable to those arising from uncertainties in the EOS occur for $|\alpha| \sim 10^9$ cm^2. Notably, this constraint is five orders of magnitude tighter than the one provided by Gravity Probe B. Moreover, they determined that the associated length scale, $\sqrt{\alpha} \sim 10^5$ cm, is only about an order of magnitude smaller than the typical neutron star radius, suggesting that deviations from GR may be subtle but non-negligible.

Additionally, the Eöt-Wash laboratory experiment, which tests for violations of the equivalence principle and deviations from Newton's inverse-square law in the weak-field regime, provides a much stricter bound of $\alpha \leq 10^{-10}$ m^2 [161].

Despite these bounds, the parameter α remains largely unconstrained in practice. For quadratic models of $f(R)$ gravity, the condition $1 + 2|\alpha|R \leq 10^{-6}$ shows that these observational limits do not decisively restrict α in current astrophysical and experimental settings.

Gravitational waves have emerged as a promising avenue for testing $f(R)$ theories of gravity, with several frameworks developed to distinguish between various $f(R)$ models [14, 55, 67, 130, 162]. In particular, Clifton and Barrow investigated the stochastic gravitational wave background in the early universe for the model $f(R) = R^{1+\delta}$, and obtained a stringent constraint on the model parameter: $0 \leq \delta < 7.2 \times 10^{-19}$ [68, 70]. This result suggests that the prospects for detecting higher-order curvature deviations from the Einstein–Hilbert action in the gravitational wave background are limited.

Despite advances in gravitational wave astronomy, constraints on the parameter α in quadratic $f(R)$ models remain inconclusive. Even with the detection of gravitational waves from inspiraling black hole binaries, the bounds on α are broad. Two notable

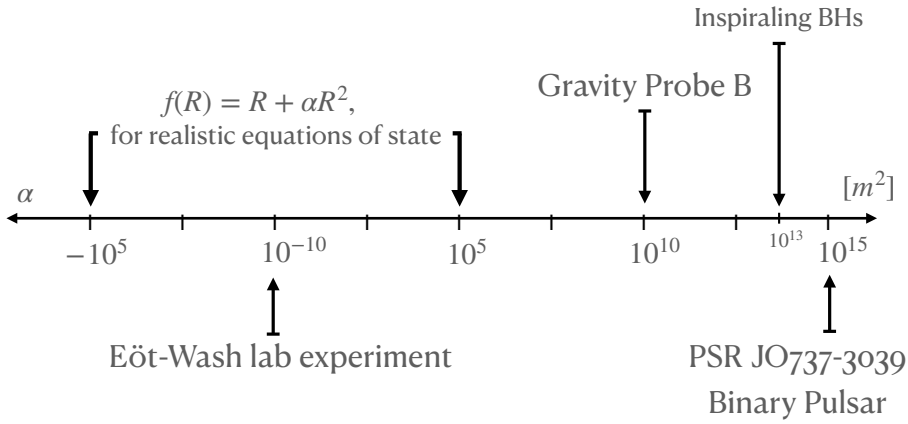

Figure 1.3: The current constraints on the quadratic gravity parameter α.

studies have estimated $\alpha \sim 10^{31}$ m^2 [170] and placed an upper limit of $\alpha \leq 1.1 \times 10^{13}$ m^2 [15] based on gravitational wave emissions from such systems.

A quadratic model of gravity with $\alpha > 0$, known as the Starobinsky model, is a popular alternative for describing inflation. The predictions of the Starobinsky model are in excellent agreement with current observational data [4, 8, 237]. In particular, Planck data reveals the closest agreement between the predicted and observed values of the tensor-to-scalar ratio (r) and the spectral index (n_s) [8]:

$$\text{Predicted} \begin{cases} n_s \sim 0.965 & \text{(nearly scale-invariant)} \\ r \sim 0.003 - 0.004 & \text{(small tensor perturbations)} \end{cases} \tag{1.1}$$

$$\text{Observed} \begin{cases} n_s \sim 0.9649 \pm 0.0042 & \\ r < 0.06 & \text{(95\% confidence interval)} \end{cases} \tag{1.2}$$

Current missions like *Euclid* [17] and future missions such as *LiteBIRD* [129, 265], *CMB-S4* [3], and the *Rubin Observatory* [122, 254] are set to refine measurements of tensor perturbations, detect primordial B-modes, and improve constraints on large-scale structure (LSS).

1.6 Modified theories of gravity

Modified theories of gravity are models incorporating scalar-tensor corrections or linear/quadratic corrections to the Riemann curvature tensor in the Einstein-Hilbert action, given by

$$\mathcal{S}_{\rm GR} = \frac{1}{2\kappa}\int d^4x\ R\sqrt{-g}, \tag{1.3}$$

where g is the determinant of the metric tensor, $\kappa \equiv 8\pi G c^{-4}$ is the Einstein gravitational constant, G is the gravitational constant, and c is the speed of light in vacuum. Modifications to gravity can be categorized into two types:

1. **Explicit modifications** of general relativity, where extra fields are added to the Einstein-Hilbert action. These include:
    - Non-minimal scalar couplings (e.g., scalar-tensor theories) [46, 47].
    - Theories with additional symmetries (e.g., Galileon or scale-invariant theories) [86, 212, 284].
    - A second tensor field $f_{\alpha\beta}$ as an extra degree of freedom. Constructing a potential $V(g^{-1}f)$ yields a massive graviton theory free of instabilities, such as ghosts [87, 147].
    - Combinations of fields with different spins [71].
2. **Implicit modifications** to general relativity:

- Replacing the Ricci scalar R with a function of curvature invariants:

$$R \to f(R, R^2, R_{\alpha\beta}R^{\alpha\beta}, R_{\alpha\beta\mu\nu}R^{\alpha\beta\mu\nu}). \tag{1.4}$$

  This introduces higher-derivative terms and new degrees of freedom. For example, if f depends only on R, an extra scalar degree of freedom is introduced,

$$\psi \sim \ln(df/dR), \qquad (Scalaron) \tag{1.5}$$

  called the scalaron, which recasts the theory as a scalar-tensor model (a subset of explicit modifications) [259].

- Increasing spacetime dimensions (e.g., string theory), motivated by unification [95, 281].

This thesis focuses on scalar-tensor theories, where the modification is either explicit or implicit. Their generalized Lagrangians are:

$$\mathcal{L}_{\rm ST} = \frac{1}{2\kappa}\sqrt{-g}\ \left[f(\phi)R - g(\phi)\partial_\alpha\phi\partial^\alpha\phi - V(\phi)\right], \tag{1.6}$$

$$\mathcal{L}_{R...} = \frac{1}{\chi}\sqrt{-g}\ f(R, R^2). \tag{1.7}$$

Equation (1.6) is the general scalar-tensor description of gravity where f and g are general functions of the scalar field ϕ, and $V(\phi)$ is the scalar field potential. Equation (1.7) is the simplest general fourth-order description of gravity where a linear, quadratic correction to the scalar curvature R is added and χ is a constant determined from the appropriate Newtonian limit.

1.6.1 Stability in extended theories of gravity

Extensions of general relativity (GR) typically introduce new degrees of freedom, which often lead to instabilities, such as the Ostrogradsky instability [220, 282, 283], which is associated with systems that have equations of motion involving higher than second-order time derivatives. In the Hamiltonian formulation, the Hamiltonian is not bounded from below, resulting in cases where the energy can become arbitrarily negative, leading to unphysical and unstable solutions. In the context of field theories, the Ostrogradsky instability can manifest itself in theories with higher-derivative terms in the Lagrangian. However, metric $f(R)$ gravity appears to be the only case that avoids the Ostrogradsky instability [282], but it contains the Dolgov-Kawasaki (DK) instability [92]. This instability is specific to the metric $f(R)$ models. It was first discovered by DK, after analyzing models of the form $f(R) = R - \mu^4/R$, since it was proposed to explain the observed cosmic acceleration and eliminate the need for dark energy [61]. The result of DK was confirmed by Nojiri and Odintsov [213, 214], who also showed that adding an R^2 term to the $f(R)$ model of DK removes this instability. Faraoni [119], proved this instability for a generalized $f(R)$ theory in the metric formalism and subsequently confirmed by Sawicki and Hu [249],

$$\frac{d^2 f}{dR^2} \equiv f''(R) > 0, \qquad \textit{Dolgov-Kawasaki stability condition.} \tag{1.8}$$

In this form, the DK instability imposes a restriction on the functional form of $f(R)$, and ensures that the scalaron is not a ghost field. In terms of astrophysical applications, it was found that the stability criterion for Schwarzschild black holes in quadratic gravity, $f(R) + R + \alpha R$, is $\alpha > 0$, which corresponds to $f''(R) > 0$ [279]. An extensive review on $f(R)$ theories in its three different formalisms, focusing on cosmological dynamics, applications to astrophysics, and its standard viability criteria, is covered in [260].

1.7 Thesis Outline

This thesis presents three models that modify the Einstein-Hilbert action, which divides the thesis into three parts. Parts I and II address early universe dynamics in the context of bouncing cosmologies for a canonical and non-canonical scalar field, respectively. Part I explores the conditions required for a bounce followed by natural R^2 inflation. The bi-scalar tensor model is introduced in Section 2.1. The conditions for a bounce, the initial conditions before the bounce, and the subsequent dynamics around the bounce are discussed in Sections 2.2, 2.3, and 2.4, respectively. Section 2.5 addresses the necessary conditions to kickstart natural inflation after the bounce. The stability of the model is investigated in Section 2.6 by analyzing the growth rates of the cosmological perturbations, and the overall evolutionary behavior of the perturbations indicates that the model is stable. To conclude Part I, we provide a summary in Chapter 3 by highlighting our key findings and discussing future research directions.

Part II explores the dynamics and linear stability of a non-canonical scalar field model, a Dirac-Born-Infeld field, in a spatially closed spacetime to analyze resulting bounce solutions. Section 4.2 outlines the dynamical construction, and Sections 4.3 and 4.4 provide a detailed analysis of dynamical systems for a power law brane tension and scalar potential, and a brane tension and scalar potential characterized by an exponential function, respectively. In Section 4.5, we consider a special case for the scalar field potential and the brane tension and numerically analyze its dynamical behavior. Section 4.6 discusses bounce solutions in the presence of a DBI field and how a recollapse can be induced so that possible cyclic solutions could appear in the phase space. Chapter 5 summarizes Part II, highlighting key findings and proposing future research directions.

Part III explores relativistic stars in $f(R)$ gravity. Chapters 6 and 7 introduce compact stellar objects in general relativity. Chapters 8 and 9 discuss the second class of locally rotationally symmetric (LRS) spacetimes in the (1+1+2) covariant formalism and the TOV equations in this formalism, respectively. Chapter 10 outlines the boundary and

physical requirements so that physically relevant solutions can be found. In Ch. 11, we present a new solution strategy to find exact solutions to the TOV equations for a generalized $f(R)$ model and find two new physically realistic descriptions of relativistic compact objects for Starobinsky gravity [53]. Chapter 12 summarizes our new results in this part, discussing their physical implications and future research directions.

The thesis is concluded in Chapter 13, summarizing the key findings in Parts I, II, and III, discussing its implications in the existing literature and its relevance for future research directions.

Part I:

An inflationary induced bounce

> There is no reason that the universe should be designed for our convenience.
>
> John D. Barrow

CHAPTER 2

NATURAL INFLATION PRECEDED BY A BOUNCE

This part presents a model in which natural inflation follows a cosmological bounce and consists of two chapters. Chapter 2 introduces a modified gravity framework recast as a bi-scalar–tensor theory, where the Lagrangian is a function $f(\phi, R)$. We examine the initial conditions during a contracting phase in a spatially closed FLRW spacetime that can lead to a bounce, the dynamics around the bounce, and the post-bounce evolution, which is driven by an R^2 term. The stability of the model is assessed via cosmological perturbation theory, analyzing the behavior of scalar, vector, and tensor modes. All cosmological dynamics in this chapter are studied in the Jordan frame and are based on work published in the article [84]. To conclude this part, Chapter 3 summarizes the key results and outlines future research directions.

The notation for the parameters and variables used in the following chapters is consistent with that of our article [84], and is self-contained within this part of the thesis.

2.1 A bi-scalar-tensor model

In this section, we consider a bi-scalar-tensor model where Eq. (1.6), with $f(\phi) = \phi^2$ and $g(\phi) = 1$, is non-minimally coupled to Starobinsky's model [262] to describe the early

universe. The action is described by

$$\mathcal{S}_{\text{Bi-ST}} = \int d^4x\sqrt{-g}\left[\frac{1}{2}\left(M_{\text{Pl}}^2 - \alpha\phi^2\right)R + \frac{1}{2}AR^2 - \frac{1}{2}(\nabla\phi)^2 - V(\phi)\right]. \tag{2.1}$$

Its Lagrangian is mapped to a bi-scalar-tensor model by defining a generalized function given by

$$f(\phi, R) = \frac{1}{2}(M_{PL}^2 - \alpha\phi^2)R + \frac{1}{2}AR^2, \tag{2.2}$$

where M_{PL} is the Planck mass, α is the coupling constant of the scalar field to Einstein's gravity and A is Starobinsky's coupling constant with $A^{-1} << M_{PL}^2$ for standard Starobinsky inflation. Naturally, this modification introduces an additional scalar degree of freedom which we define as $\partial f/\partial R \equiv f_R = \psi$. By defining the field ψ we can express the Ricci scalar, R, and the function $f(\phi, R)$ in terms of the two fields:

$$R = \frac{1}{A}\left(\psi - \frac{M_{\text{Pl}}^2 - \alpha\phi^2}{2}\right), \qquad f = \psi R - \frac{\left[\psi - \frac{1}{2}(M_{\text{Pl}}^2 - \alpha\phi^2)\right]^2}{2A}. \tag{2.3}$$

The modified field equations, by taking the variation with respect to the metric, is given by

$$\psi R_{\mu\nu} - \frac{f g_{\mu\nu}}{2} - (\nabla_\mu\nabla_\nu - g_{\mu\nu}\Box)\psi = T_{\mu\nu}^{(\phi)}\ . \tag{2.4}$$

The modified Klein-Gordon equation for the field ψ is

$$\Box\psi = \frac{1}{3}\left[\frac{M_{\text{Pl}}^2 - \alpha\phi^2}{2A}\left(\psi - \frac{1}{2}(M_{\text{Pl}}^2 - \alpha\phi^2)\right) + T\right], \tag{2.5}$$

obtained by taking the trace of Eq. (2.4) and substituting Eq. (2.3), where T is the trace of the energy-momentum tensor of the scalar field ϕ. In order to analyze the evolutionary dynamics we assume the spacetime background to be homogeneous and isotropic, described by the FLRW metric, and that the spatial curvature has a closed geometry i.e., $K > 0$,

$$ds^2 = -dt^2 + a(t)^2\left[\frac{dr^2}{1 - Kr^2} + r^2\left(d\theta^2 + \sin^2\theta d\phi^2\right)\right]\ . \tag{2.6}$$

By substituting Eq. (2.6) into the field equation, Eq. (2.4), the evolution equations for spatially homogeneous fields and ϕ are given by

$$\ddot{\psi} + 3H\dot{\psi} = \frac{1}{3}\left[\frac{M_{\rm Pl}^2 - \alpha\phi^2}{2A}\left(\frac{1}{2}(M_{\rm Pl}^2 - \alpha\phi^2) - \quad\right) + (\rho - 3P)\right] \tag{2.7}$$

$$\ddot{\phi} + 3H\dot{\phi} = -V_\phi - \alpha\phi R, \tag{2.8}$$

where an expanding Universe the extra term $3H\dot{\phi}$ is required, which is analogous to a friction term for particle motion. The quantities ρ and P are the energy density and pressure of the scalar field ϕ, respectively, given by

$$\rho = \frac{1}{2}\dot{\phi}^2 + V(\phi), \qquad P = \frac{1}{2}\dot{\phi}^2 - V(\phi). \tag{2.9}$$

The Friedmann equations in terms of the fields ϕ and ψ are

$$H^2 + \frac{K}{a^2} = \frac{\psi R - f}{6\psi} + \frac{\rho}{3\psi} - H\frac{\dot{\psi}}{\psi}, \tag{2.10}$$

$$\dot{H} - \frac{K}{a^2} = \frac{H\dot{\psi}}{2\psi} - \frac{\ddot{\psi}}{2\psi} - \frac{(\rho + P)}{2\psi}, \tag{2.11}$$

and the acceleration equation in terms of the curvature quantities and scale factor is

$$\dot{H} = \frac{R}{6} - 2H^2 - \frac{K}{a^2}. \tag{2.12}$$

In order to fully realize the dynamical evolution we consider a model for the potential energy of the scalar field ϕ. To compare the field containing the additional Starobinsky term to the original model proposed in [134], the same potential is used. It takes the form

$$V(\phi) = \frac{m^2}{2}\phi^2 + \frac{\beta}{3}\phi^3 + \frac{\lambda}{4}\phi^4, \tag{2.13}$$

where m, β, and λ are constant model parameters. The cubic term in Eq. (2.13) introduces an asymmetry that causes the potential to become unbounded in one direction,

but is counterbalanced by the higher order quartic term. In a renormalizable theory, the potential $V(\phi)$ is restricted to cubic and quartic terms, with the cubic term typically excluded by symmetry considerations since it explicitly breaks the parity symmetry i.e., $\phi \to -\phi$. Since the potential is being treated as part of an effective field theory, the cubic term is included as a small non-renormalizable correction [193]. In the following section, we address the conditions on the fields to achieve a bounce.

2.2 Conditions for a bounce

Investigations of bouncing cosmologies usually include a positive spatial curvature. The reason is that when the universe undergoes contraction, spatial curvature can slow down and reverse the contraction. Positive spatial curvature can temporarily halt the contraction and facilitate a bounce. However, a positive spatial curvature is not sufficient to sustain a bounce. Additional conditions are required. A bounce is achieved provided the following hold:

1. $\boldsymbol{H(t_b) = 0}$ — where the scale factor sits at a minimum, it has momentarily stopped contracting before it starts expanding.

2. $\boldsymbol{\dot{H}(t_b) > 0}$ — the Hubble parameter transitions from negative (contracting phase) to positive (expanding phase), resulting in a sign reversal of $\dot{a}$.

3. $\boldsymbol{(\rho + 3P) < 0}$ — the violation of the strong energy condition is a consequence of the previous point 2. To illustrate, consider

$$\dot{H} + H^2 = -\frac{1}{3}(\rho + 3P) + \frac{K}{a^2}.$$

   Imposing $H_b = 0$ from the first point 1, the bounce condition 2 in a spatially closed universe is achieved only if the strong energy condition is violated.

4. $\boldsymbol{w_b < -1/3}$ — Assuming a perfect fluid $P = w\rho$, a constraint on the equation of

state at the bounce arises as a consequence of the violation of the strong energy condition.

5. $\boldsymbol{\epsilon_b < 1}$ — the slow-roll parameter, $\epsilon \equiv -\dot{H}/H^2$, can be expressed in terms of the equation of state:

$$\epsilon = \frac{3}{2}(1+w),$$

so at the bounce we require that $w_b < -1/3$ and so placing an upper bound on the slow-roll parameter.

The analysis of the evolutionary dynamics of our model can be split into three phases: the pre-bounce, in the vicinity of the bounce, and post-bounce leading to inflation. In the following sections, we address the initial conditions necessary for a bounce which is based on the work by Güngör and Starkman [134], the dynamics around the bounce, and the resulting inflation driven by the Starobinsky term.

2.3 The initial conditions before the bounce

We assume the following initial conditions prior to the bounce.

1. The universe is slowly contracting and dominated by vacuum energy.
2. The scalar field ϕ sits in the false vacuum with an initial value ϕ_i.
3. In the cosmic past, $t \to -\infty$, the Ricci scalar is significantly smaller than the mass of the field, and so R is disregarded during this phase. Therefore, to ensure that our model initially has small R, we set the parameter A to be large, as can be seen in Eq. (2.3).
4. The location of the scalar field is situated at the extrema of the effective potential, given by

$$V^{\text{eff}}(\phi) = V(\phi) + \frac{1}{2}\alpha\phi^2 R, \quad \frac{\partial V^{\text{eff}}}{\partial \phi} = \phi(m^2 + \alpha R + \beta\phi + \lambda\phi^2) = 0.$$

We have, as illustrated in Fig. 2.1.

(a) The true vacuum,

$$\phi = 0. \tag{2.14}$$

(b) A local minimum and the false vacuum,

$$\phi_{\rm min} = \frac{-\beta^2 + \sqrt{\beta^2 - 4\lambda m^2}}{2\lambda}. \tag{2.15}$$

(c) A local maximum,

$$\phi_{\rm max} = \frac{-\beta^2 - \sqrt{\beta^2 - 4\lambda m^2}}{2\lambda}. \tag{2.16}$$

To avoid pathologies at the local minimum and ensure that the potential is positive, the condition $4\lambda m^2 < \beta^2 < 4.5\lambda m^2$ must be applied.

5. The scalaron ψ is initially at rest, where the previous assumptions in Eq. (2.7) gives an initial value for the scalaron as

$$\psi_i(\phi_{\rm min}) = \frac{8AV(\phi_{\rm min})}{M_{PL}^2 - \alpha\phi_{\rm min}^2} + \frac{1}{2}\left(M_{PL}^2 - \alpha\phi_{\rm min}^2\right), \tag{2.17}$$

where another constraint appears $\alpha\phi_{\rm min}^2 \neq M_{PL}^2$. From Fig. 2.1 we assume the natural range for the scalar field, ϕ, up to $O(10\ M_{PL})$ and the Starobinsky parameter set to $\alpha = 10^{-3}$ throughout this chapter. As discussed in Sec. 1.5 and illustrated in Fig. 1.3, the observational constraint on α remains inconclusive. Our chosen value for α is to maintain numerical stability and have a non-negligible deviation from GR where we will also see in Part III that $0 < \alpha \leq 10^{-3}$ have significant implications on the physical description of compact stellar objects. Equation (2.17) shows that if the scalar field, ϕ, evolves slowly, the scalaron, ψ, will follow its evolution.

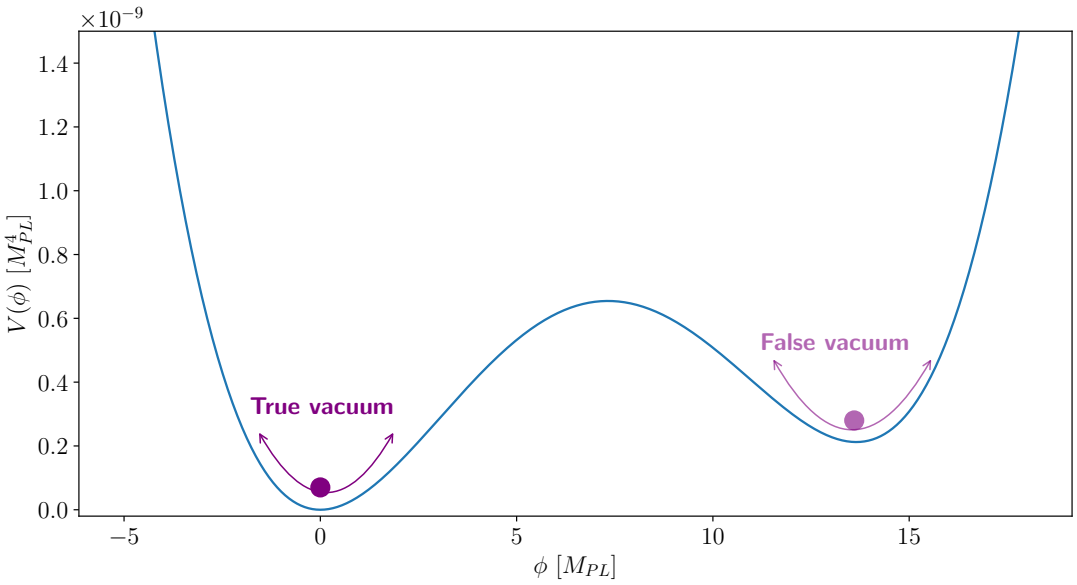

Figure 2.1: The potential energy of the scalar field ϕ, Eq. (2.13), with parameters $m = 10^{-5}\ M_{PL}$, $\lambda = 10^{-12}$, and $\beta = -\sqrt{4.4\lambda}\ m$. The potential has three extrema where we are only interested in the two potential wells: The false vacuum, the local minimum, which determines the initial conditions of the scalar field, and the true vacuum, the global minimum.

Applying the points above, the initial conditions before the bounce for the potential and cosmological parameters are

$$V(\phi_{\min}) \approx O(m^4), \tag{2.18}$$

$$R \approx \frac{8V(\phi_{\min})}{M_{PL}^2 - \alpha\phi^2} \approx O\left(\frac{m^4}{M_{PL}^2}\right), \tag{2.19}$$

$$H^2 \approx \frac{V(\phi_{\min})}{3(M_{PL}^2 - \alpha\phi^2)} \approx O\left(\frac{m^4}{M_{PL}^2}\right), \tag{2.20}$$

$$\dot{H} \approx 0. \tag{2.21}$$

2.4 Dynamics around the bounce

To show that the conditions around the bounce are independent of the scalaron ψ, let us consider the vicinity of the bounce, where the universe switches from an accelerated contraction to a decelerated contraction phase. This happens when $\dot{H} = 0$, meaning that

the Hubble parameter has a non-zero value at its extrema. Using Eq. (2.7) and $\dot{H} = 0$, Eq. (2.10) becomes

$$H^2_{\text{min/max}} = \frac{\psi R - f}{6\psi} - \frac{\rho + 3P}{6\psi} + \frac{|H|\dot{\psi}}{2} + \frac{\ddot{\psi}}{2\psi}. \tag{2.22}$$

The squared Hubble parameter at the scalar field minimum can be approximated by considering Eq. (2.17), where the ψ-field is traced by the ϕ-field if ϕ evolves slowly. Assuming that during the contracting phase the and ϕ fields do not diverge rapidly, thus avoiding the singularity, the squared Hubble parameter at the start of the bounce is given by the following equation.

$$H^2_{\text{min}} \approx \frac{2V(\phi)}{3M^2_{PL}} + \frac{V(\phi) - \dot{\phi}^2}{3\psi(\phi)} + \frac{\dot{\phi}^2}{54\psi(\phi)}. \tag{2.23}$$

This shows that, before the bounce, the dynamics are determined solely by the scalar field, ϕ. For inflation to occur, we assumed the hierarchy $\psi_i > M^2_{PL} >> \alpha\phi^2$, as will be discussed further in Sec. 2.5.

The dynamics in the vicinity of the bounce comes down to two scenarios. When the scalar field ϕ is displaced from its local minimum (false vacuum) during the collapsing phase, perhaps due to small perturbations that cause the field to grow slowly, this leads to the following:

1. the fields remaining trapped in their local minimum,

2. or the field escape their minima.

These two cases depends on how close the Ricci scalar, R, is to its critical value, which occurs where the local minimum and maximum of the scalar field, ϕ, converge to a saddle point, i.e., $\phi_{\text{min}} = \phi_{\text{max}} = -\beta/\lambda$ and

$$R_{\text{crit}} = \frac{1}{\alpha}\left(\frac{2\beta^2}{\lambda} - m^2\right). \tag{2.24}$$

Next, we discuss the conditions that leads to the scalar field escaping its false vacuum, and when the scalar field could remain trapped. We first discuss the latter:

Trapped fields

- The scalar field, ϕ, is approximately zero near or at the bounce. This can occur when $R \geq R_{\text{crit}}$, as considered in [134] where they force the local and global minimum to be in close proximity and converge to form a saddle point which allows the field to oscillate around the global minimum (true vacuum). Another scenario where the scalar field can oscillate freely is for the local maximum to possess a shallow hill, allowing the antifriction term in Eq. (2.8) to dominate, thus removing any oscillations. However, unless the initial values are finely tuned, the bouncing mechanisms will cause the fields to diverge, thus leading to a singularity. As a result, this case is not explored further.

- The scalar field is approximately equal to its value in the false vacuum, at the bounce, i.e., $\phi \approx \phi_{\text{min}}$. Here, the scalar field is not sufficiently displaced from its initial value, where it sits in the false vacuum, and it does not evolve sufficiently to alter the potential. The Ricci scalar, R, never reaches R_{crit}, and consequently the fields ϕ and ψ return to their initial values and remain trapped in their false vacuum. This scenario leads to a universe that is eternally inflating. To illustrate this, we numerically solve the evolution equations (2.7), (2.8), (2.10), (2.12) using the initial conditions given by Eq. (2.15) and Eq. (2.17). Figure 2.2 shows the scalaron and the scalar field returning to their initial values after the bounce. This outcome stems from

    1. the choice of parameter values creates a steep and deep false vacuum which only allows the fields to oscillate in this potential well but never escaping,

    2. or the choice of parameter values do not allow R to sufficiently evolve. This can occurs when the scalaron mass is large or when the coupling between the

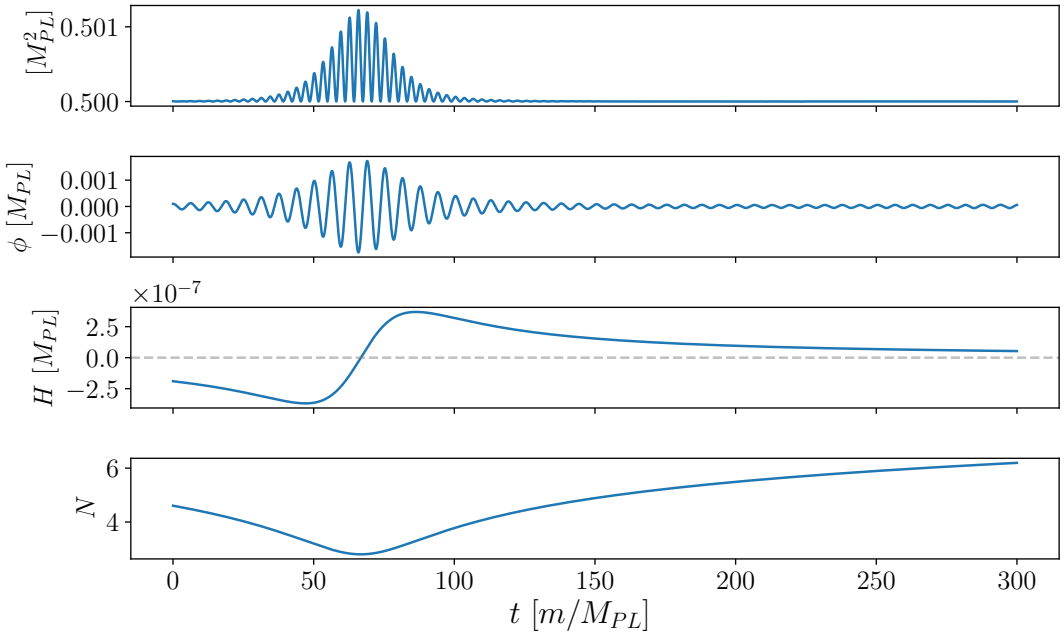

Figure 2.2: The fields depicting the case of eternal inflation, when the fields are trapped in the false vacuum, for the chosen parameter values: $m = 10^{-5}\ M_{PL}$, $\lambda = 10^{-12}$, $\alpha = 10^{-3}$, $\phi_i = 10^{-4}$, $A = 10^{12}$, $a = 10^2$, $\beta = -\sqrt{4.49\lambda}\ m$ and $K = m^2$. The scalaron tracks the scalar field and behaves as initially expected during the collapsing phase. The fields oscillate around their local minimum, growing in amplitude. The bounce occurs when the spatial curvature dominates and the field oscillations dampen as the universe enters the expansion phase.

scalar field and gravity is weak.

We also see from Fig. 2.2 that the scalaron tracks the scalar field, ϕ. This is a consequence of the field only experiencing small oscillations as the spatial curvature dominates. This behavior leads to an unchanged effective potential ($V_{,\phi} >> \alpha\phi R$) which implies that the velocity term does not dominate on the right-hand side of Eq. (2.7), therefore leaving $\psi \approx \psi_{\text{min}}$ tracing the scalar field.

A scalar field escaping its potential minimum

The scalar field value at the bounce is $0 < \phi \lesssim \phi_{\rm min}$. Here, the Ricci scalar is allowed to evolve sufficiently such that the false vacuum is retained ($R < R_{\rm crit}$) and ϕ is displaced in the false vacuum. The scalar field displays growing oscillatory behavior and eventually exits the false vacuum as it approaches or is at the bounce. This is a consequence of the change in the potential energy that provides the scalar field with enough kinetic energy so that it conquers the potential barrier. In this setup, inflation is driven by both fields following the bounce. In Fig. 2.3, we illustrate a scenario in which the scalar field settles in the true vacuum before the scalaron which now drives inflation. Sufficient inflation occurs where the lower bound is 60 e-folds, and the scalar field quickly settles in the true vacuum resulting in a period of single field inflation entirely driven by the scalaron, ψ.

2.5 Post-bounce evolution

To kickstart a post-bounce inflationary phase, we examine the conditions required. We assume that the fields experience a slow-roll and that ϕ gradually escapes the false vacuum. This allows us to approximate the cosmic friction term of Eq. (2.7) as

$$3H\dot{\psi} \simeq \frac{M_{PL}^2}{6A}\left(\frac{1}{2}M_{PL}^2 - \quad\right) - \frac{(\dot{\phi} + 2V(\phi))}{3}, \tag{2.25}$$

where we recall $M_{PL}^2 >> \alpha\phi^2$. Since we want inflation to occur after the bounce, we choose the parameter values such that $\psi_{\rm i} > 2M_{PL}^2$. This is motivated by forcing ϕ into its true vacuum, allowing the scalaron to drive inflation, whereby the slow-roll parameter is

$$\epsilon_V = \frac{M_{PL}^2}{8\psi^2}\left(\frac{M_{PL}^2 - 2\psi}{2(M_{PL}^2 - \psi)}\right)^2. \tag{2.26}$$

Choosing $\epsilon_V = 1$, post-bounce, gives $\psi_i = 2M_{PL}^2$ and so to guarantee inflation proceeds the bounce we require $\psi_i > 2M_{PL}^2$. Nevertheless, to ensure that enough inflation is

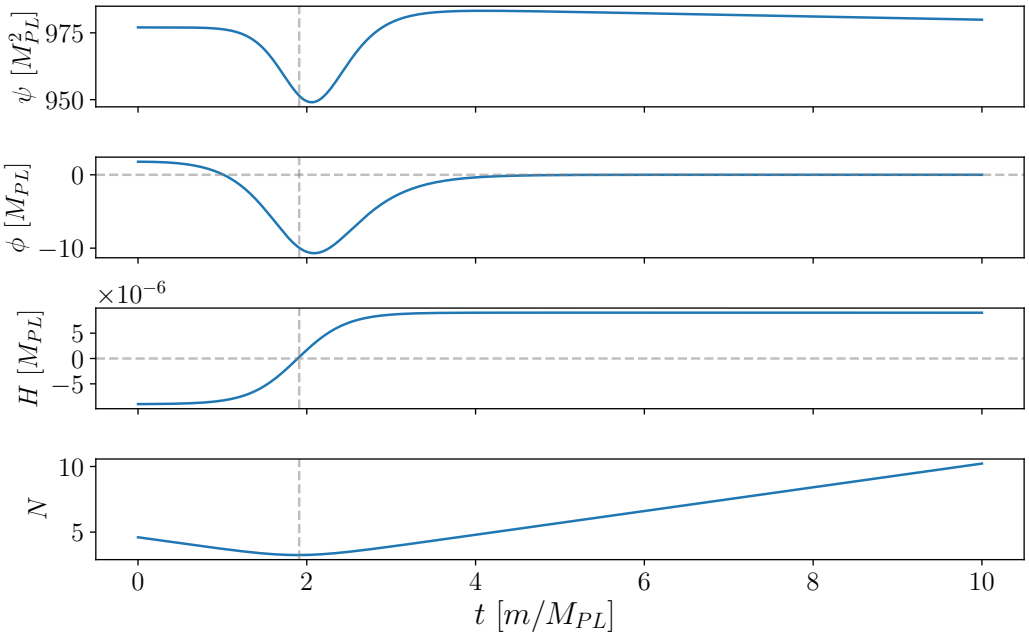

Figure 2.3: The case when the fields exit the false vacuum and R does not evolve sufficiently as to change the potential. The parameter values are $m = 10^{-5}\ M_{PL}$, $\lambda = 10^{-12}$, $\alpha = 10^{-3}$, $\phi_i = 1.785$, $A = 10^{12}$, $a = 10^2$, $\beta = -\sqrt{4.49\lambda}\ m$ and $K = m^2$. This is not a realistic case for the Universe, but it illustrates the desired dynamics that results in slow-roll inflation where ϕ exits the false vacuum, coinciding with the bounce, and ψ is driven up its potential.

achieved, the integral of the slow-roll parameter determines the condition on the value of the scalaron at the start of inflation via

$$N = \int_{2M_{PL}^2}^{\psi} \sqrt{\frac{2}{\epsilon_V M_{PL}}} d\psi, \tag{2.27}$$

where for 60 e-folds of inflation, $\psi_{\text{inflation}} > 16M_{PL}^2$.

The resulting inflation can be seen when the scalaron increases while it is driven up its effective potential due to its time-derivative remaining positive during the collapsing phase ($H_{\text{collapse}} \to -H$):

$$\dot{\psi}_{\text{collapse}} \simeq \frac{M_{PL}^2 \quad + 2A\dot{\phi}^2 + 4AV(\phi)}{18A|H_{\text{collapse}}|} > 0. \tag{2.28}$$

Therefore, while ϕ evolves towards its true vacuum, the potential energy of ψ grows and eventually dominates. This results in a unique case where the bounce naturally determines the initial conditions for inflation which is driven by the scalaron, ψ, and occurs when the Hubble parameter reaches its maximum value. These conditions impose an additional constraint on the value of ψ at the onset of inflation:

$$\psi_{\text{inflation}} = \frac{4AV(\phi_{\text{min}})}{3M_{\text{PL}}^2} - \frac{M_{\text{PL}}^2}{18}, \tag{2.29}$$

where $H^2\text{min}(\phi\text{min}) = H^2\text{max}(\phi\text{min})$ is assumed when the potential dominates in Eq. (2.23), and Eqs. (2.7) and (2.3) are appropriately substituted. These assumptions relies on a symmetrical bounce and are reasonable since we have shown that the scalaron plays only a small role during the bounce. However, due to the minimal coupling of ϕ and R, the dynamics results in an asymmetrical bounce. A constraint on the potential energy and consequently the initial conditions on ϕ is realized by considering the conditions $\psi_{\text{inflation}} > 16M_{PL}^2$ and Eq. (2.29). Taking this into account, the condition on the potential energy is $V(\phi_{\text{min}}) > \frac{387}{32A} M_{PL}^2$. The resulting inflation induced by a bounce is illustrated in Fig. 2.4. We see that the scalaron drives inflation immediately after the bounce and the Hubble parameter is nearly constant throughout the inflationary phase.

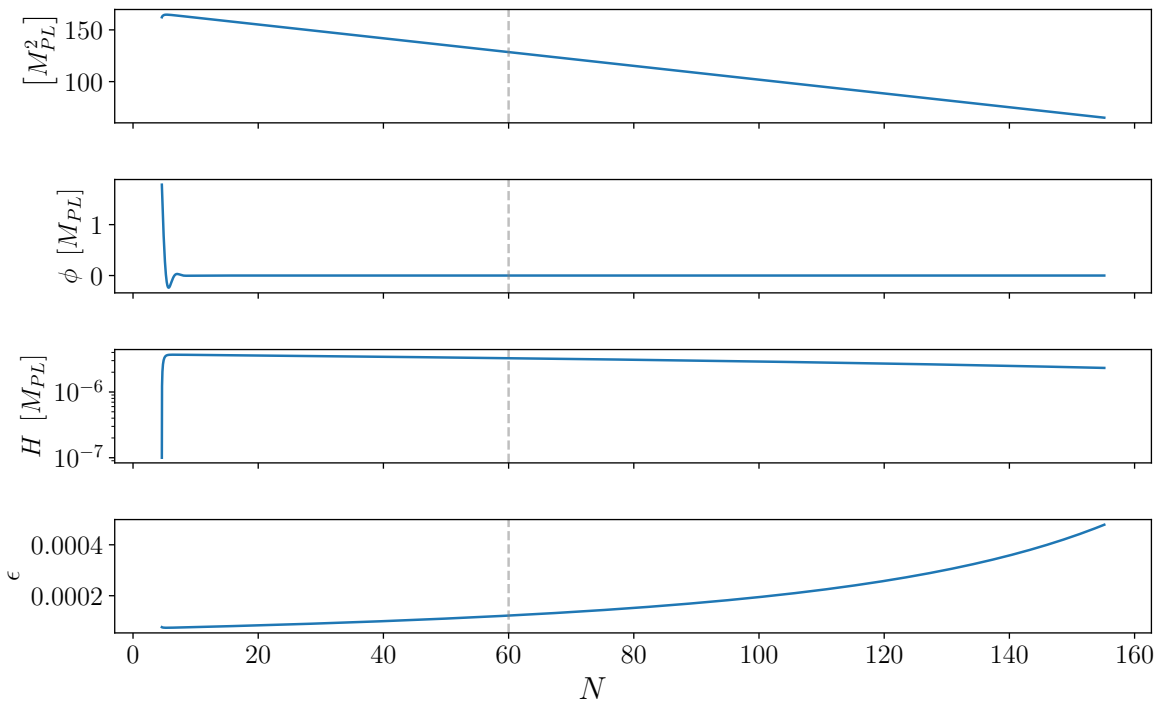

Figure 2.4: The resulting inflation from a bounce in terms of the number of e-folds that are measured post-bounce. The chosen parameters, as in the previous figures, are $m = 10^{-5}\ M_{PL}$, $\lambda = 10^{-12}$, $\alpha = 10^{-3}$, $A = 10^{12}$, $a = 10^2$, $\beta = -\sqrt{4.49\lambda}\ m$,$K = m^2$, and ψ_i is given by Eq. (2.29).

It should also be noted that a more realistic scenario is when $H^2_{\text{max}} > H^2_{\text{min}}$, however, our model predicts a smaller $\psi_{\text{inflation}}$, which results in a shorter inflationary phase. The converse is also true, i.e., if $H^2_{\text{max}} < H^2_{\text{min}}$ is achieved, then the inflationary phase lasts longer, since $\psi_{\text{inflation}}$ would be larger.

2.6 Stability analysis by cosmological perturbations

In this section, we investigate the stability of our model by analyzing the growth rates of perturbations, to linear order, in a gauge-invariant form. Metric perturbations are decomposed according to their spin with respect to a local rotation of the spatial coordinates in the hypersurfaces of constant time [43, 96, 166, 202]. At the linear order, the scalar, vector, and tensor perturbations decouple and evolve independently. This allows us to analyze them separately. During the numerical analysis, we assume that the Planck mass

is $M_{PL} = 1$ throughout this section.

2.6.1 Scalar perturbations

Scalar perturbations (spin 0) hold significant importance in understanding the structure formation of the Universe and the inflaton that drives inflation. It provides information on the small fluctuations in the scalar components of spacetime and matter fields. Here, we focus on the evolution of the scalar perturbations and the amplitude of the fluctuations. If instabilities are present, growth will appear in the perturbed fields $\delta\phi$ and $\delta\psi$.

The cosmological perturbations are performed in the longitudinal gauge which is also the most favored gauge in post-Newtonian theory [73]. Post-Newtonian perturbations are responsible for modeling non-linear structures via N-body simulations. The metric [195, 263] describing a first-order scalar perturbation in the Newtonian gauge is

$$ds^2_{(s)} = -(1+2\Phi)dt^2 + a^2(1-2\Psi)\gamma_{ij}dx^i dx^j, \tag{2.30}$$

where the subscript (s) denotes the metric corresponding to the scalar modes, Φ and Ψ are the perturbed metric potentials and γ_{ij} is the metric on constant time hypersurfaces and t is cosmic time. Together with Einstein's field equations, the generalized perturbed field, for a two-field system [132, 151], is described by

$$3H\left(\dot{\Psi} + H\Phi\right) + \frac{k^2 - 3K}{a^2}\Psi = -\delta\rho, \tag{2.31}$$

$$\dot{\Psi} + H\Phi = -\delta q, \tag{2.32}$$

$$3\left(\ddot{\Psi} + \dot{H}\Phi - H\dot{\Phi}\right) + 6H\left(\dot{\Psi} + H\Phi\right) + \Phi\left(3\dot{H} - \frac{k^2}{a^2}\right) = -\delta X, \tag{2.33}$$

$$\Psi - \Phi = \frac{\delta\psi}{\psi}. \tag{2.34}$$

The perturbed energy density, perturbed momentum density and δX, in terms of the scalar field, ϕ, and scalaron, ψ, are

$$\delta\rho = \frac{1}{2\psi}\left[3\dot{\psi}\left(\dot{\Psi}+H\Phi\right)-\left(\dot{\phi}^2+3V\right)\Phi \right. \\ \left. -3H\delta\dot{\psi}+\dot{\delta\phi}\dot{\phi}+\delta\psi\left(3\dot{H}-\frac{k^2}{a^2}+3H^2\right)+\delta\phi\left(V_\phi-\frac{f_\phi}{2}\right)\right], \tag{2.35}$$

$$\delta q = \frac{\dot{\delta\psi}+\delta\phi\dot{\phi}-H\delta\psi-\dot{\psi}\Phi}{2\psi}, \tag{2.36}$$

$$\delta X = \frac{1}{2\psi}\left[3\dot{\psi}\dot{\Phi}+3\left(\dot{\Psi}+H\Phi\right)\dot{\psi}+\Phi\left(6\ddot{\psi}+3H\dot{\psi}+4\dot{\phi}^2\right)\right. \\ \left. +\delta\psi\left(\frac{6K-k^2}{a^2}+6H\right)-\delta\phi\left(f_\phi-2V_\phi\right)-3H\dot{\delta\psi}-3\ddot{\delta\psi}-4\dot{\delta\phi}\dot{\phi}\right]. \tag{2.37}$$

To close the perturbed system of equations, we provide the perturbed Klein-Gordon equations,

$$\ddot{\delta\psi}+3H\dot{\delta\psi}-\left(\frac{R}{3}-\frac{k^2}{a^2}\right)\delta\psi+\frac{1}{3}\left(2f_\phi-4V_\phi\right)\delta\phi+\frac{1}{3}\psi\delta R+\frac{2}{3}\dot{\delta\phi}\dot{\phi} \\ =\dot{\psi}\left(\dot{\Phi}+3H\Phi+3\dot{\Psi}\right)+\Phi\left(2\ddot{\psi}+3H\dot{\psi}+\frac{2}{3}\dot{\phi}^2\right), \tag{2.38}$$

$$\ddot{\delta\phi}+3H\dot{\delta\phi}+\left(\frac{k^2}{a^2}-f_{\phi\phi}+2V_{\phi\phi}\right)\delta\phi-\frac{1}{2}\delta R\psi_\phi \\ =\dot{\Phi}\dot{\phi}+\Phi\left(3H\dot{\phi}+2\ddot{\phi}\right)+3\left(H\Phi+\dot{\Psi}\right)\dot{\phi}, \tag{2.39}$$

and the perturbed Ricci scalar,

$$\delta R = \frac{\delta\psi+\alpha\phi\delta\phi}{A}. \tag{2.40}$$

It is worth including the comoving curvature perturbation, $\mathcal{R}$, defined as

$$\mathcal{R} = \Psi - \frac{H}{\rho+P}\delta q. \tag{2.41}$$

This measures the scalar fluctuations of our spacetime geometry and is related to the perturbed fields, perturbed metric potentials and Hubble parameter, as

$$\mathcal{R} = \Psi - \frac{H}{\dot{H}}\left(\dot{\Psi} + H\Phi\right) = \Psi + \frac{H}{\dot{H}}\left(\frac{\delta\dot{\psi} + \delta\phi\dot{\phi} - H\delta\psi - \dot{\psi}\Phi}{4\psi}\right). \tag{2.42}$$

Performing a harmonic decomposition, the Laplace-Beltrami operator in a universe with positive spatial sections is given by

$$\frac{k^2}{a^2} = n(n+2)\frac{K}{a^2}, \tag{2.43}$$

where $n \geq 2$ is an integer eigenvalue representing the physical perturbation modes ($n = 0$ is the homogeneous mode and $n = 1$ is a gauge mode) [96, 138, 166]. The perturbed evolution equations can be simplified into two second order differential equations by considering Eqs. (2.34)–(2.36), and removing any dependence on the scalar field, ϕ, and the metric potential, Φ:

$$\begin{aligned}
&\ddot{\delta\psi} + \left[5H + \frac{\dot{\psi}}{} + \frac{(2V_\phi - f_\phi)}{\dot{\phi}}\right]\dot{\delta} \\
&\quad - \left[2(2\dot{H} + H^2) + \frac{(3\psi H - \dot{\psi})(2V_\phi - f_\phi)}{\psi\dot{\phi}} - \frac{10H\dot{\psi}}{\psi} - \frac{2\ddot{\psi}}{} + \frac{\dot{\psi}^2}{^2} + \frac{1}{3}\frac{k^2}{a^2}\right]\delta\psi \\
&= \left[4H - 6\frac{(2V_\phi - f_\phi)}{\dot{\phi}} + 6\frac{\dot{\psi}}{}\right]\dot{\Psi} \\
&\quad + 2\left[H^2 + \left(\frac{\dot{\psi}}{6\psi} - H\right)\frac{(2V_\phi - f_\phi)}{\dot{\phi}} + \frac{2}{3}\frac{(k^2 - 3K)}{a^2} + 5H\frac{\dot{\psi}}{} + \frac{\ddot{\psi}}{}\right]\Psi,
\end{aligned} \tag{2.44}$$

$$\ddot{\Psi} + 5H\dot{\Psi} + \left[2(2\dot{H} + H^2) + \frac{1}{3}\frac{k^2 - 2K}{a^2}\right]\Psi = \frac{H}{}\dot{\delta\psi} + \frac{2(2H' + H^2) - H\frac{\dot{\psi}}{\psi} + \frac{1}{3}\frac{(2k^2 - 3K)}{a^2}}{}\delta\psi. \tag{2.45}$$

To further our stability analysis, Eqs. (2.32), (2.36), (2.38) and Eq. (2.39) are solved numerically, where substituting Eq. (2.34) eliminates the dependence on Φ. All the necessary quantities are computed to determine the comoving curvature perturbation via Eq. (2.42). In order to numerically integrate our system of equations, we consider the following initial conditions:

$$\delta\phi_i = \frac{H}{2\pi}, \quad \dot{\delta\phi}_i = \frac{\dot{H}}{2\pi}, \quad \dot{\Psi} = 0, \tag{2.46}$$

$$\delta\psi_i = \alpha(8AV(\phi_{\min}) - 1)\phi_{\min}\delta\phi_i, \quad \dot{\delta\psi}_i = \alpha(8AV(\phi_{\min}) - 1)\phi_{\min}\dot{\delta\phi}_i, \tag{2.47}$$

where $\delta\psi_i$ and $\dot{\delta\psi}_i$ are determined from Eq. (2.17), and $(\delta\phi_i, \dot{\delta\phi}_i)$ is the de Sitter value. Figures 2.5 and 2.6 show the perturbed fields for a universe that is eternally inflating and a universe with finite inflation induced by a bounce, respectively. The evolution of the fluctuations is explored for a range of wavenumbers n. We see that as the fields evolve towards the bounce, the amplitude of the perturbations increase, but remain finite. Once inflation begins, the fluctuations settle to a constant value and are stretched to superhorizon scales. Equation (2.45) hints at the expected stability of the perturbations. From Eq. (2.34) we expect Ψ and $\delta\psi/\psi$ to have similar magnitudes, confirmed through our numerical results in Figs. 2.5 and 2.6. By collecting the common terms in Eq. (2.45),

$$\begin{aligned}\ddot{\Psi} = &-\left(\frac{\dot{\delta\psi}}{\psi} - \frac{\dot{\psi}}{\psi}\frac{\delta\psi}{\psi} - 5\dot{\Psi}\right)|H| - 2\left(2\dot{H} + H^2\right)\left(\Psi - \frac{\delta\psi}{\psi}\right) \\ &- \frac{K}{3a^2}\left[(n(n+2) - 2)\,\Psi - (2n(n+2) - 3)\,\frac{\delta\psi}{\psi}\right],\end{aligned} \tag{2.48}$$

we notice that for each term there is a counteracting effect between $\delta\psi$ and Ψ since they have opposing signs. This reduces divergent behavior that may arise during the collapsing phase. We note that for small values of n the first term in Eq. (2.48) is dominant and $\ddot{\Psi}$ remains negative throughout the collapse phase and bounce, which could lead to an instability. However, this instability is not present in Figs. 2.5 and 2.6 as $\dot{\delta\psi}$ grows more slowly than $\delta\psi$.

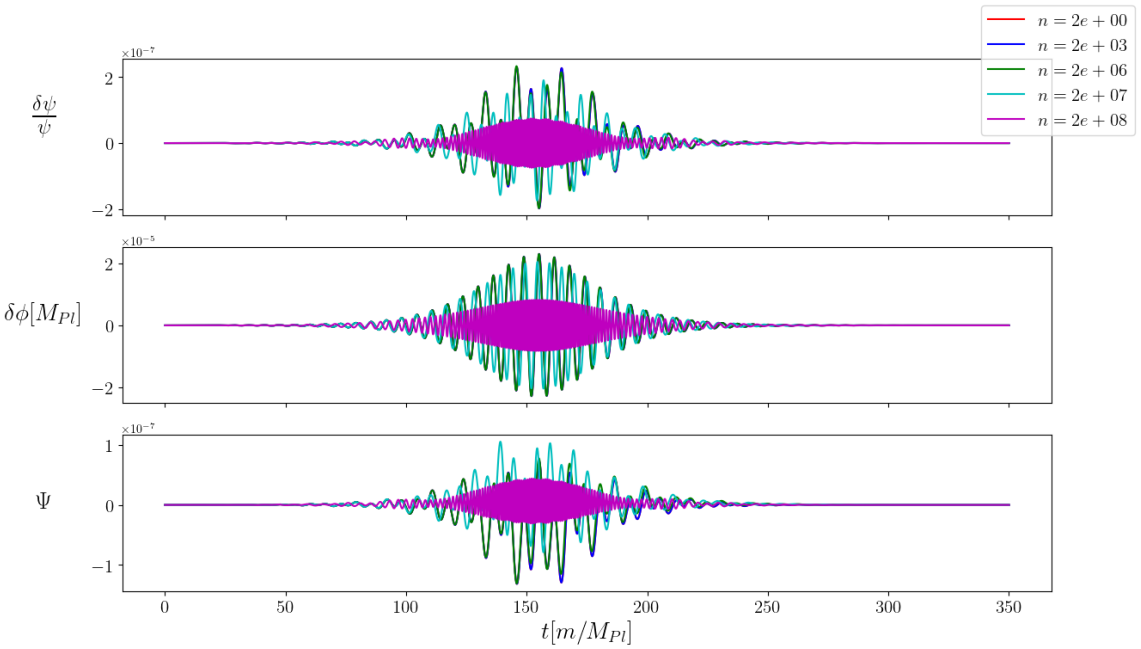

Figure 2.5: The perturbed fields for various wavenumbers when the fields are eternally inflating (c.f. Fig. 2.2). There is no significant effect in varying the wavenumber. Oscillatory behavior is evident around the bounce but is bounded in an interval $[-2, 2] \times 10^{-7}$ for the perturbed scalaron and $[-2, 2] \times 10^{-5}$ for the perturbed scalar field.

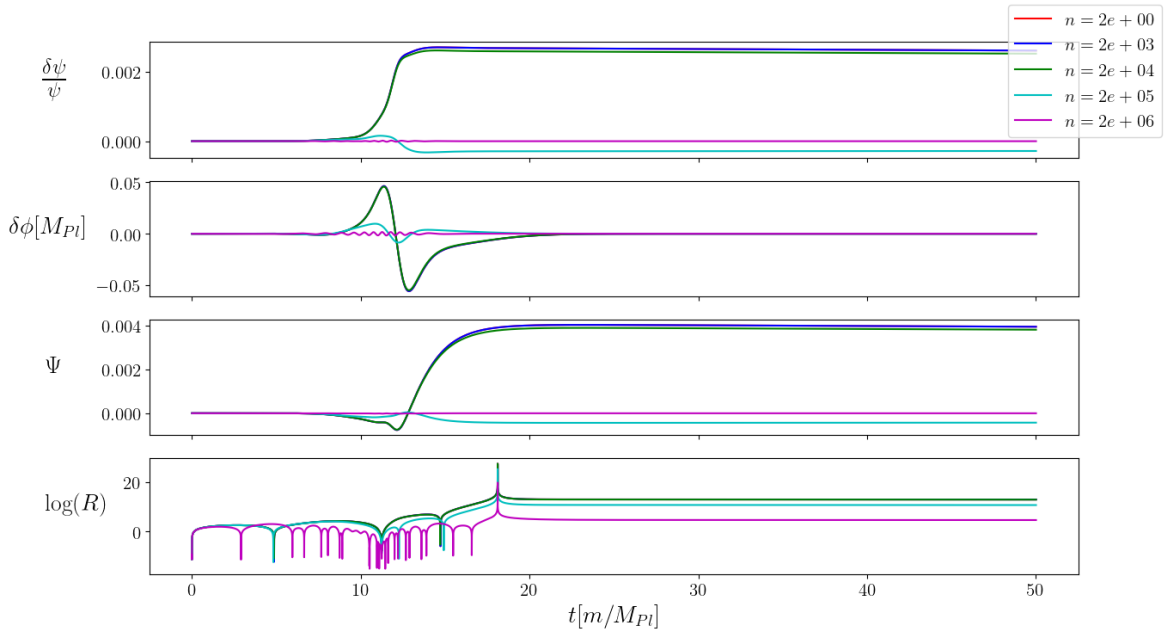

Figure 2.6: The perturbed fields for various wavenumbers when there is finite inflation (c.f. Fig. 2.3). As the perturbed scalar field vanishes post-bounce, the perturbed scalaron asymptotes to a constant non-zero value. We also note that increasing the wavenumber bounds the perturbations. Although there are more rapid oscillations through the bounce, the perturbed dynamics settles towards zero after the bounce.

2.6.2 Vector perturbations

Vector perturbations, also referred to as vorticity perturbations, are spin 1 modes arising from rotational velocity fields. During inflation the vector perturbations become subdominant and decay as the Universe expands. However, it is worth analyzing the vorticity modes around the bounce. The metric description of the vector modes is

$$ds^2_{(\mathrm{v})} = -dt^2 - 2aB_i dt dx^i + a^2(\gamma_{ij} + 2\partial_j C_i)dx^i dx^j, \tag{2.49}$$

where the subscript (v) refers to the metric corresponding to the vector modes, B_i and C_i are transverse vector-type perturbations i.e., $\nabla^i B_i = 0 = \nabla^i C_i$. The vector perturbed variable B_i represents the rotational velocity perturbation and C_i describes the shear deformation caused by the vector perturbations. The conserved momentum density in the presence of a perfect fluid is

$$\dot{\delta q_i} + 3H\delta q_i = 0, \tag{2.50}$$

where $\delta q_i = (\rho + p)v_i$, the spatial velocity perturbation is v_i, and the perturbed momentum density is related to the vorticity by taking the curl of Eq. (2.50). The vorticity is defined as $\omega^i = \epsilon^{ijk}\nabla_j v_k$. The gauge-independent vector shear, defined as $\sigma_i = \dot{C}_i + B_i/a$, has the following relation to the momentum density [151]

$$\frac{k^2 - 2K}{2a^2}\sigma_i = \frac{\delta q_i}{}, \tag{2.51}$$

a result from the $G^0{}_i$ component of the gravitational field equations.

The solution to Eq. (2.50) gives

$$\delta q_i = \delta q_i^{\mathrm{initial}} \left(\frac{a_{\mathrm{initial}}}{a}\right)^3. \tag{2.52}$$

From this we can directly deduce that during the collapsing phase ($a = a_{\max}$), the vector perturbations will be small as long as the initial amplitude $\delta q_i^{\text{initial}}$ is small. Substituting Eq. (2.52) into Eq. (2.51) leads to

$$\left(k^2 - 2K\right)\sigma_i = 2\delta q_i^{\text{initial}} a_{\text{initial}}^3 \left(a\psi\right)^{-1}. \tag{2.53}$$

Focusing on the scenario where finite inflation occurs, around the bounce the scalaron and the scale factor evolve toward their minimum values, and slowly increases after the bounce. Hence, we can deduce that the quantity $(a\psi)^{-1}$ in Eq. (2.53) will peak around the bounce and bound the vector perturbations. Subsequently, as the universe inflates, the vector perturbations will become subdominant and decay.

2.6.3 Tensor perturbations

Gravitational waves were first predicted by Einstein in 1916 [102, 104], but it was the work of Lifshitz, Khalatnikov, and Hawking [108, 140, 180, 181] that pioneered the study of general perturbations in an expanding universe which was extrapolated to observational cosmology by Sachs and Wolfe [247]. A complete covariant analysis of gravitational waves in an expanding universe was performed by Dunsby, Bassett and Ellis in 1997 [97]. Tensor perturbations, also referred to as gravitational waves, have spin 2 and are the "true" degrees of freedom of the gravitational fields in the sense that they can exist even in vacuum. The metric corresponding to the tensor mode perturbation is

$$ds^2_{(\text{t})} = -dt^2 + a^2(\gamma_{ij} + h_{ij})dx^i dx^j, \tag{2.54}$$

where the subscript (t) indicates the tensor modes, and h_{ij} is a transverse-trace-free tensor-type perturbation corresponding to the gravitational wave ($h^i{}_i = \nabla_j C^j{}_i = 0$). For a theory of the form $f(\phi, R)$, where we recall that $\psi = f_R$, the gravitational wave equation

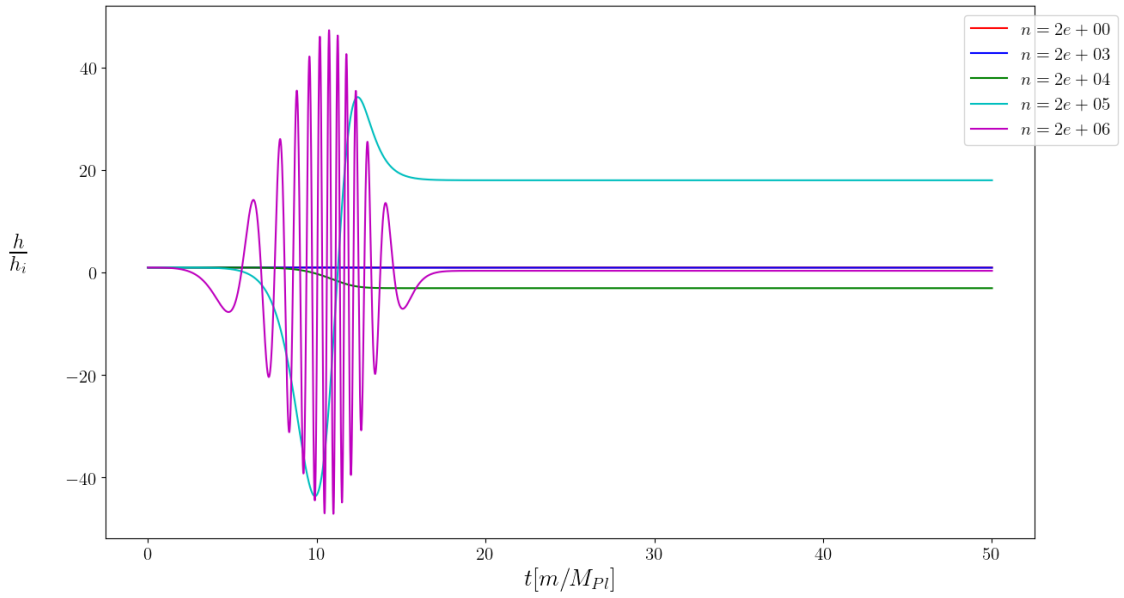

Figure 2.7: The growth of the tensor perturbation amplitude for various wavenumbers. The initial perturbed tensor amplitude is $h_i = 10^{-5}$. During the bounce, the scale factor experiences a non-zero minima, therefore we see a maximum in the amplitude around the bounce and remains finite.

in the presence of a perfect fluid is [151]

$$\ddot{h} + \left(3H + \frac{\dot{\psi}}{\psi}\right)\dot{h} + \frac{k^2 + 2K}{a^2}h = 0, \tag{2.55}$$

where h is the amplitude of the polarization states $h_{ij} = h\ e_{ij}{}^{(+,\times)}$. In the case of multiple fields, Eq. (2.55) is valid for an arbitrary number of minimally coupled scalar fields. Equation (2.55) shows that by modifying gravity, the growth of h during the collapsing phase is reduced since $\dot{\psi}/\psi$ acts as a counter friction term to the Hubble term. Consequently, the tensor modes will remain small.

CHAPTER 3

SUMMARY OF PART I

In this part, we outlined how an inflation-induced bounce can be realized, detailing the conditions on the effective potential that allow the scalar field both to trigger a bounce and to escape its false vacuum. We provided the general bounce conditions and extended them to $f(R, \phi)$ models with effective potentials featuring a false vacuum. This work builds on [134], which investigated the initial conditions leading to a bounce in a collapsing, dark-energy-dominated universe. There, the scalar field remains in its false vacuum until the bounce, after which it escapes and settles in its true vacuum.

We extended this analysis by showing that natural inflation, driven by the Starobinsky model, can follow the bounce, with the scalar field alone determining the pre-bounce dynamics. We imposed conditions ensuring that the scalaron (the R^2 degree of freedom) remains subdominant before and during the bounce yet tracks the scalar field through it. Immediately after the bounce, the scalar field decays and the scalaron drives the effective potential upward, initiating a period of inflation.

Analyzing the cosmological perturbations, we found that the coupled fields remain stable, with the scalaron enhancing overall stability. Near the bounce, the perturbed quantities exhibit oscillatory but bounded behavior, indicating no pathological instabili-

ties.

Further analysis of the perturbations can provide interesting insight into our model. For instance, scalar perturbations allow for the calculation of the primordial power spectrum, which describes the distribution of perturbation amplitudes across scales. The spectral index n_s, which determines the tilt of the power spectrum, and the running of the spectral index α_s, how n_s changes with scale, help discriminate between competing models of inflation and test the predictions of slow-roll inflation. It would be interesting to investigate these features before and during inflation. Another interesting consequence of investigating the power spectrum of primordial perturbations is that signs of peaks in the curvature spectrum indicate primordial black hole formation [236, 248]. It would be interesting to investigate if our model could allude to signs of primordial black hole formation as a consequence of a bounce. A novel model-independent approach to analyzing primordial black hole formation in the context of nonsingular bouncing cosmology was recently presented in [223].

Given that during the contracting phase conditions can yield a successful bounce followed by natural inflation, the next step is to identify the requirements for a late-time cosmological recollapse and construct a cyclic cosmology. In Part II, we undertook this task for a non-canonical scalar-tensor theory, the Dirac–Born–Infeld field [52].

Part II:

A bouncing non-canonical scalar field

> The idea is to see how far one can go without supposing supernatural intervention.
>
> Steven Weinberg, *To Explain the World: The Discovery of Modern Science.*

CHAPTER 4

A BOUNCE INDUCED DIRAC-BORN-INFELD FIELD

In Part I, we focused on canonical scalar field models minimally coupled to gravity, with an R^2 correction to the curvature, in the context of bouncing cosmologies. In this part, we consider a non-canonical model used to describe early universe evolution and perform a detailed dynamical systems analysis to determine whether it supports bouncing cosmologies and cyclic behavior. This part is based on the work published in [52], and the definitions of parameters and variables follow this article.

In the following sections of this chapter, we construct the dynamical framework for a DBI field in a FLRW spacetime with positive spatial curvature, considering two cases for the brane tension and scalar potential. This extends the work of Copeland et al. for the flat universe case [78]. We then narrow our analysis to solutions that describe bounce cosmologies and investigate whether the inclusion of an extra degree of freedom that induces recollapse can lead to cyclic behavior in phase space. We conclude this part in Chapter 5 by summarizing the key results of Chapter 4 and discussing directions for future research.

The notation for the parameters and variables used in the following chapters is consistent with that of our article [52], and is self-contained within this part of the thesis.

4.1 The Dirac-Born-Infeld field

The gravitational action that describes a DBI field is given by

$$\mathcal{S}_{\rm DBI} = \int d^4x\sqrt{-g}\left[\frac{R}{2} - \frac{1}{f(\phi)}(\gamma^{-1}-1) - V(\phi)\right]. \tag{4.1}$$

It encodes the function $f^{-1}(\phi)$ that describes the tension of the D3-brane, and the scalar field potential is $V(\phi)$. Since a DBI field modifies the kinetic energy, the term $\gamma^{-1}(f,\dot{\phi})$ acts as a Lorentzian function. It is defined as $\gamma^{-1} \equiv \sqrt{1+fX}$, where the kinetic term is $X \equiv g^{\mu\nu}\partial_\mu\phi\partial_\mu$, and becomes $X = -\dot{\phi}^2$ in the presence of a homogeneous field ϕ. Thus,

$$\gamma^{-1} = \sqrt{1-f\dot{\phi}^2}. \tag{4.2}$$

In addition, V and f are assumed to be strictly positive, thus, together with Eq. (4.2) sets the following model bounds:

$$\gamma \geq 1, \quad \text{and} \quad f^{-1} \geq \dot{\phi}^2. \tag{4.3}$$

Adopting the Friedmann-Lemaître-Robertson-Walker (FLRW) metric, the equation of motion for the scalar field ϕ is

$$\ddot{\phi} + 3H\gamma^{-2}\dot{\phi} + \frac{1}{2}f_\phi f^{-2}(1-3\gamma^{-2}+2\gamma^{-3}) + \gamma^{-3}V_\phi = 0, \tag{4.4}$$

and the field equations produce the Friedmann equation:

$$3H^2 = \frac{\gamma^2}{\gamma+1}\dot{\phi}^2 + V - 3\frac{K}{a^2}, \tag{4.5}$$

where $H(t) \equiv \dot{a}(t)/a(t)$, $a(t) \equiv a$ is the scale-factor, and K encodes the spatial curvature which is chosen as strictly positive in this chapter. The energy density and pressure of

the DBI field are given by

$$\begin{aligned} \rho_\phi &= \frac{\gamma^2\dot{\phi}^2}{\gamma+1} + V, \\ P_\phi &= \frac{\gamma\dot{\phi}^2}{\gamma+1} - V. \end{aligned} \tag{4.6}$$

When the kinetic energy approaches the brane tension, $\dot{\phi}^2 \to f^{-1}$, we see that the field approaches the limit $\gamma^{-1} \to 0$. This is called the *ultrarelativistic* limit, it can be seen from Eq. (4.4) that the acceleration of the field is governed by the tension of the brane. This leads to a deceleration in an expanding universe, as studied in [11, 257], where the Friedmann equation, Eq. (4.5), is primarily governed by the field's velocity. Conversely, in the limit $\gamma \to 1$, Eqs. (4.4) and (4.5) reduce to the standard equations of motion for a canonical scalar field.

4.2 A dynamical construction

In analysing the dynamics, we consider the DBI field non-minimally coupled to a matter source,

$$\mathcal{S}_{\text{DBI}+m} = \mathcal{S}_{\text{DBI}} + \int d^4x\sqrt{-g}\,\mathcal{L}_m. \tag{4.7}$$

By considering the FLRW metric, the Friedmann equation including a DBI field non-minimally coupled to matter is

$$3H^2 = \frac{\gamma^2}{\gamma+1}\dot{\phi}^2 + V + \rho_m - 3\frac{K}{a^2}. \tag{4.8}$$

The dynamics of the system is characterized by a set of dimensionless dynamical variables [75, 111, 235]

$$x = \frac{\dot{\phi}}{\sqrt{3\bar{\gamma}(1+\bar{\gamma})}}\frac{1}{D}, \quad y = \frac{\sqrt{V}}{\sqrt{3}D}, \quad z = \frac{H}{D}, \quad \Omega_m = \frac{\rho_m}{3D^2}. \tag{4.9}$$

Compactifying the phase space in a spacetime with positive spatial curvature [131], we define

$$D = \sqrt{H^2 + \frac{K}{a^2}}, \quad \bar{\gamma} = \gamma^{-1}, \tag{4.10}$$

where D describes the effective Hubble parameter and $\bar{\gamma}$ is bounded between $0 \leq \bar{\gamma} \leq 1$. The variables in Eq. (4.9) encodes the following physical properties.

- $\boldsymbol{x}$ is the normalized kinetic energy of the system,
- $\boldsymbol{y}$ is the normalized potential energy of the system,
- $\boldsymbol{z}$ describes expansion/contraction of the spacetime or when the spacetime is experiencing a bounce, i.e., $z = 0$, and
- $\boldsymbol{\Omega_m}$ signifies the normalized matter density, with an equation of state denoted by w_m.

The dynamical variables lead to a constraint equation,

$$\Omega_\phi + \Omega_m = 1, \tag{4.11}$$

obtained directly from the Friedmann equation, Eq. (4.8), where Ω_ϕ is the energy density of the scalar field and its equation of state is given by

$$\Omega_\phi = x^2 + y^2, \quad w_\phi = \frac{\bar{\gamma}x^2 - y^2}{x^2 + y^2}. \tag{4.12}$$

In formulating the dynamical system, we introduce a new time variable, τ, where the differential operator is defined as $\frac{d}{d\tau} = D^{-1}\frac{d}{dt}$, denoted by a prime. Equations (4.7) and (4.8) leads to a set of first-order differential equations that govern the dynamics of the

system:

$$\bar{\gamma}' = \frac{\tilde{\gamma}\,(1-\bar{\gamma}^2)}{\sqrt{1+\tilde{\bar{\gamma}}}}\left[3\sqrt{1+\tilde{\gamma}}z + \frac{\sqrt{3\tilde{\bar{\gamma}}}}{x}\left(\mu x^2 - \lambda y^2\right)\right], \tag{4.13}$$

$$x' = \frac{1}{2}\sqrt{3\tilde{\gamma}(1+\tilde{\gamma})}\lambda y^2 + \frac{3}{2}xz\left[-(1+\tilde{\gamma}) + \left(x^2+y^2\right)(1+w_\phi) + \Omega_m(1+w_m)\right], \tag{4.14}$$

$$y' = -\frac{1}{2}\sqrt{3\tilde{\gamma}(1+\tilde{\gamma})}\lambda xy + \frac{3}{2}\left[\left(x^2+y^2\right)(1+w) + \Omega_m(1+w_m)\right]yz, \tag{4.15}$$

$$z' = (1-z^2)\left[1 - \frac{3}{2}(y^2+x^2)(1+w) - \frac{3}{2}\Omega_m(1+w_m)\right], \tag{4.16}$$

where the parameters λ and μ are defined as

$$\lambda = -\frac{V_\phi}{V}, \quad \mu = -\frac{f_\phi}{f}. \tag{4.17}$$

The rate of change of these parameters,

$$\mu' = \left(1 - \frac{f_{\phi\phi}f}{f_\phi^2}\right)\mu^2\sqrt{3\bar{\gamma}(1+\bar{\gamma})}x, \tag{4.18}$$

$$\lambda' = \left(1 - \frac{V_{\phi\phi}V}{V_\phi^2}\right)\lambda^2\sqrt{3\bar{\gamma}(1+\bar{\gamma})}x, \tag{4.19}$$

shows that the dynamical system accommodates a wide range of potentials and brane tensions. When the potential energy and brane tension follows an exponential model, μ and λ become constant parameters, simplifying the dynamical system. To complete the dynamical system, we include the evolution equation of the matter density

$$\Omega_m' = -3z(1+w_m)\Omega_m + 3\Omega_m\left[(1+w)(x^2+y^2) + (1+w_m)\Omega_m\right], \tag{4.20}$$

computed directly from Friedmann constraint.

4.3 Power law brane tension and scalar potential

In this section, we examine power law forms for both the potential $V(\phi)$ and the brane tension $f(\phi)$,

$$V(\phi) = \sigma|\phi|^p, \qquad f(\phi) = \nu|\phi|^r, \tag{4.21}$$

where we choose $V(\phi) > 0$, $f(\phi) > 0$ and $(\sigma, \nu) > 0$ to be strictly positive, and p and r are free parameters.

For this case, it is worth introducing a re-parametrization of the brane tension and scalar potential:

$$\Lambda = -\frac{V_\phi}{f^q V^{q+1}}, \qquad M = -\frac{f_\phi}{f^{q+1} V^q}, \tag{4.22}$$

where $q = -1/(p+r)$. This reparametrization sets Λ and M to constants when the functions V and f follow a power law, thus simplifying the system of equations we need to solve. We note that when $q = 0$, the power law model becomes an exponential model, which is covered in Sec. 4.4. The quantities Λ and M share a relation with the normalized parameters for the scalar potential λ and brane tension μ via

$$\lambda = \left[\frac{(1-\bar{\gamma})y^2}{\bar{\gamma}(1+\bar{\gamma})x^2}\right]^q \Lambda, \qquad \mu = \left[\frac{(1-\bar{\gamma})y^2}{\bar{\gamma}(1+\bar{\gamma})x^2}\right]^q M. \tag{4.23}$$

Together with Eq. (4.22), the system of equations (4.13)–(4.16) become

$$\bar{\gamma}' = \frac{\bar{\gamma}\,(1-\bar{\gamma}^2)}{\sqrt{\bar{\gamma}+1}}\left[\frac{\bar{\gamma}^{\frac{1}{2}-q}\sqrt{3}}{x}\left(\frac{(1-\bar{\gamma})y^2}{(\bar{\gamma}+1)x^2}\right)^q\left(Mx^2-\Lambda y^2\right)+3\sqrt{\bar{\gamma}+1}z\right], \tag{4.24}$$

$$x' = \frac{\sqrt{3}}{2}\left[\bar{\gamma}(\bar{\gamma}+1)\right]^{\frac{1}{2}-q}\left[\frac{(1-\bar{\gamma})y^2}{x^2}\right]^q \Lambda y^2 + \frac{3xz}{2}\left[(\bar{\gamma}+1)(x^2-1)+\Omega_m(1+w_m)\right], \tag{4.25}$$

$$y' = -\frac{\sqrt{3}}{2}\left[\bar{\gamma}(\bar{\gamma}+1)\right]^{\frac{1}{2}-q}\left[\frac{(1-\bar{\gamma})y^2}{x^2}\right]^q \Lambda xy + \frac{3}{2}yz\left[x^2(1+\bar{\gamma})+\Omega_m(1+w_m)\right], \tag{4.26}$$

$$z' = \left(1-z^2\right)\left[1-\frac{3}{2}x^2\left(\bar{\gamma}+1\right)-\frac{3}{2}\Omega_m(1+w_m)\right]. \tag{4.27}$$

4.3.1 Stability analysis

We note that in the system, Eqs. (4.24), there are terms that could lead to singular fixed points. In an effort to avoid this[1], we find the fixed points for Eq. (4.24) and examine the dynamical system for each fix point case of $\bar{\gamma}$. The fixed points of Eq. (4.24) are

$$\bar{\gamma} = 0, \tag{4.28}$$

$$\bar{\gamma} = 1, \tag{4.29}$$

$$\frac{\bar{\gamma}^{\frac{1}{2}-q}\sqrt{3}}{x}\left(\frac{(1-\bar{\gamma})y^2}{(\bar{\gamma}+1)x^2}\right)^q\left(Mx^2-\Lambda y^2\right)+3\sqrt{\bar{\gamma}+1}z=0. \tag{4.30}$$

For each $\bar{\gamma}$ case, the fixed points of the reduced system and its stability is recorded in Tables 4.1 and 4.2.

Case I: Ultrarelativistic case ($\bar{\gamma} = 0$)

Recall $\bar{\gamma} = \gamma^{-1}$ where $\gamma \to \infty$ if $\bar{\gamma} = 0$. This case corresponds to an ultrarelativistic field. This implies that this is not a truly physical solution, since the solution asymptotically approaches $\gamma \to \infty$. To ensure that our dynamical system remains physical, we find a restriction on the parameter q. This condition also places a constraint on the potential and warp functions. The dynamical system for the ultrarelativistic case is

$$x' = \frac{3xz}{2}\left[(x^2-1)+\Omega_m(1+w_m)\right], \tag{4.31}$$

$$y' = \frac{3}{2}yz\left[x^2+\Omega_m(1+w_m)\right], \tag{4.32}$$

$$z' = \left(1-z^2\right)\left[1-\frac{3}{2}x^2-\frac{3}{2}\Omega_m(1+w_m)\right]. \tag{4.33}$$

In this case, we note that the system is independent of the parameter q and constants Λ and M. Therefore, the dynamical system for the ultrarelativistic case is independent of the specific choice of V and f.

[1]Fixed point solutions that result in 0/0 at the background level are also disregarded.

Our stability analysis confirms that only two sets of fixed points correspond to a bouncing solution, that is, when $z = 0$. For the parameter values $q \leq 1/2$, the solution has saddle stability around these fixed points. Panel P5 in Fig. 4.1 shows the stability around these fixed points for varied values of w_m and Ω_m when $q = 1/2$. A cosmological bounce in a radiation ($w_m = 1/3$) and pressureless matter-filled ($w_m = 0$) universe with $\Omega < 0.5$ and $\Omega_m < 0.65$, respectively, has a saddle stability. However, when $\Omega_m > 0.3$, where ultra-stiff matter dominates, there are no real fixed points. Cosmological solutions during the contracting epoch, i.e., when $z = -1$, are stable when 1. $x > 0$ and $y = 0$, that is, the velocity of the scalar field dominates the cosmological dynamics, in a radiation-filled universe with $\Omega < 0.7$ (Fig. 4.1 P1), and 2. $x = 0$ and $y = 0$, i.e., the universe is static and the scalar field rests in its true vacuum, where $\Omega_m = 1$. However, in this latter case, if it is dominated by radiation and $\Omega < 0.7$, its stability is unstable. During the cosmological expansion, i.e., $z = 1$, if the stability around the fixed points was stable or unstable during the contracting epoch, it is now unstable or stable, respectively. This is illustrated graphically in Fig. 4.1 where we see that the stability is swapped between P1 and P2, and between P3 and P4.

Case II: Standard quintessence ($\bar{\gamma} = 1$)

When $\bar{\gamma} = 1$, we can see Eq. (4.4) reduces to the general Klein-Gordon equation for a canonical scalar field. Therefore, when performing our numerical analysis, we will draw comparisons between the canonical and non-canonical scalar field, i.e., $\bar{\gamma} \neq 1$. In this canonical scenario, the dependence of the dynamical system on γ is removed provided that $q \neq 0$. This case, as in the ultrarelativistic case, also suffers from an ambiguity where the dynamical system is indeterminate. These cases are handled carefully, and the regular (non-divergent) solutions are summarized in Table 4.2. With these conditions,

the dynamical system becomes

$$x' = \frac{3xz}{2}\left[2(x^2-1)+\Omega_m(1+w_m)\right], \tag{4.34}$$

$$y' = \frac{3}{2}yz\left[2x^2+\Omega_m(1+w_m)\right], \tag{4.35}$$

$$z' = \left(1-z^2\right)\left[1-3x^2-\frac{3}{2}\Omega_m(1+w_m)\right]. \tag{4.36}$$

Our analyses recovers well known behavior in canonical scalar field cosmological dynamics. In Table 4.2, we recover the following solutions.

1. A solution corresponding to cosmic expansion ($z = 1$) and considering an energy density described by vacuum ($w_m = -1$), has the corresponding fixed points $x = 1$ and $y = 0$. This solution corresponds to the fixed points of a power law inflationary model [188].

2. In the limit $x \to 0$, where the scalar field's kinetic energy is subdominant, the dynamics lead to a quasi-de Sitter expansion.

3. When the dynamics result in a singular collapse due to a rapidly evolving scalar field, i.e., $x \to 1$, this case is identified as the Big Curnch.

Comparing the dynamical analysis of the ultrarelativistic case with the canonical scalar field, we notice that at the bounce $z = 0$ when $0 < q \leq 1/2$ the stability is the same, i.e., saddle stability. Figure 4.1 (P6) illustrates the stability around the bounce when $q = \frac{1}{2}$.

Case III: $0 < \bar{\gamma} < 1$

In this case, we consider the $\bar{\gamma}$ case of Eq. (4.30), where $\bar{\gamma}$ can take on constant values between 0 and 1. Rearranging Eq. (4.30) gives the relation

$$\sqrt{3}\left[\bar{\gamma}(\bar{\gamma}+1)\right]^{\frac{1}{2}-q}\left[\frac{(1-\bar{\gamma})y^2}{x^2}\right]^q = \frac{3xz\sqrt{\bar{\gamma}+1}}{(\Lambda y^2 - Mx^2)}, \tag{4.37}$$

where the dependence on the parameter q, provided $q \neq 0$, can be removed resulting in

$$x' = \frac{3}{2}\left[\frac{\sqrt{\bar{\gamma}+1}}{(\Lambda y^2 - M x^2)}\Lambda y^2 + (\bar{\gamma}+1)(x^2-1) + \Omega_m(1+w_m)\right] xz, \tag{4.38}$$

$$y' = \frac{3}{2}\left[-\frac{\sqrt{\bar{\gamma}+1}}{(\Lambda y^2 - M x^2)}\Lambda x^2 + (1+\bar{\gamma})x^2 + \Omega_m(1+w_m)\right] yz. \tag{4.39}$$

The z' equation is given by Eq. (4.27) and remains unchanged for this case. The stability analysis reveals the absence of stable fixed points for this scenario (see Table 4.2).

We perform a fixed-point analysis on the equation (4.27) to comment on the evolutionary behavior of the system. From Eq. (4.27), the cosmological dynamics is driven towards a contracting spacetime when the kinetic energy dominates, i.e., $x^2\,(\bar{\gamma}+1) > \frac{2}{3} - \Omega_m(1+w_m)$. Conversely, when the kinetic energy is $x^2\,(\bar{\gamma}+1) < \frac{2}{3} - \Omega_m(1+w_m)$, the dynamics is driven towards an expanding spacetime. Furthermore, the evolution of $\bar{\gamma}$, Eq. (4.24), results in contraction (expansion), which is the result of large (small) values of x^2 that drive $\bar{\gamma}$ to its submanifold at $\bar{\gamma} = 0$ ($\bar{\gamma} = 1$). This suggests that the system exhibits significant instability within the interval $0 < \bar{\gamma} < 1$.

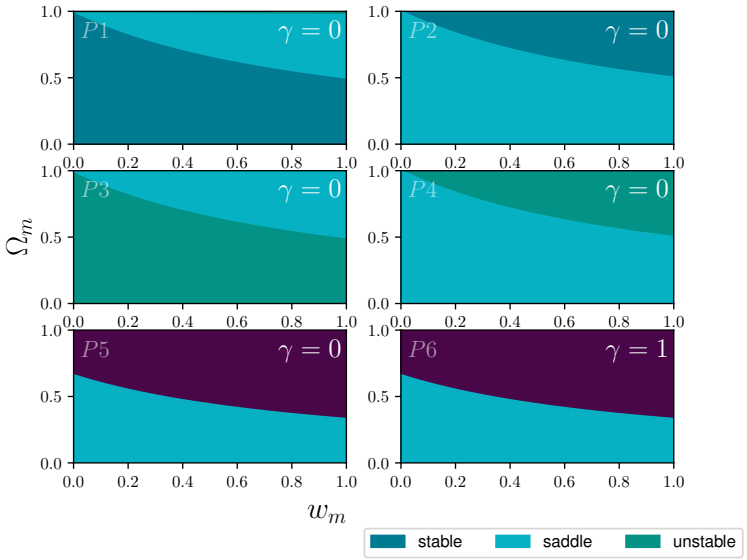

Figure 4.1: The fixed point stabilities, referenced in Tables 4.1 and 4.2, for a brane tension and scalar potential following a power law where $q = \frac{1}{2}$. In panels $P5$ and $P6$, the purple regions correspond to imaginary fixed points for combinations of Ω_m and w_m, and hence are excluded from the analysis.

$\bar{\gamma}$	x	y	z	Existence	Stability
0	$\pm\sqrt{\frac{2-3\Omega_m(1+w_m)}{3}}$	$\sqrt{\frac{1}{3}+\Omega_m w_m}$	0	$q \leq 1/2,\ \Omega_m(1+w_m) \leq 3/2$	Saddle
				$\Omega_m \in (0:1),\ w_m \in (0:1)$	Fig. 4.1, P5
0	$\pm\sqrt{1-\Omega_m(1+w_m)}$	0	-1	$q \leq 1/2,\ \Omega_m w_m = 0\ ,\ \Omega_m(1+w_m) \leq 1$	Stable
				$\Omega_m \in (0:1),\ w_m \in (0:1)$	Fig. 4.1, P1
0	$\pm\sqrt{1-\Omega_m(1+w_m)}$	0	1	$q \leq 1/2,\ \Omega_m w_m = 0\ ,\ \Omega_m(1+w_m) \leq 1$	Unstable
				$\Omega_m \in (0:1),\ w_m \in (0:1)$	Fig. 4.1, P2
0	0	$\sqrt{1-\Omega_m(1+w_m)}$	-1	$q \leq 1/2,\ \Omega_m w_m = 0\ ,\ \Omega_m(1+w_m) \leq 1$	Unstable
0	0	$\sqrt{1-\Omega_m(1+w_m)}$	1	$q \leq 1/2,\ \Omega_m w_m = 0\ ,\ \Omega_m(1+w_m) \leq 1$	Stable
0	0	0	-1	$q \leq 1/2,\ \Omega_m = 1,\ w_m > 0$	Stable
				$q \leq 1/2,\ \Omega_m = 1,\ w_m < 0$	Unstable
				$\Omega_m \in (0:1),\ w_m \in (0:1)$	Fig. 4.1, P3
0	0	0	1	$q \leq 1/2,\ \Omega_m = 1,\ w_m > 0$	Unstable
				$q \leq 1/2,\ \Omega_m = 1,\ w_m < 0$	Stable
				$\Omega_m \in (0:1),\ w_m \in (0:1)$	Fig. 4.1, P4

Table 4.1: This table lists all the physical fixed points for a power law brane tension and scalar potential when the ultrarelativistic case ($\bar{\gamma} = 0$) is considered. The corresponding stability is indicated and the conditions on the free parameters for existence.

4.4 Exponential brane tension and scalar potential

In this section, we consider the case in which both the brane tension and scalar potential depend on an exponential form of the scalar field,

$$V(\phi) = \sigma e^{-\lambda\phi}, \qquad f(\phi) = \nu e^{-\mu\phi}, \tag{4.40}$$

$\bar{\gamma}$	x	y	z	**Existence**	**Stability**
1	$\pm\sqrt{\frac{2-3\Omega_m(1+w_m)}{6}}$	$\sqrt{\frac{4-3\Omega_m(1-w_m)}{6}}$	0	$q>0\in\mathbb{R}$, $\Omega_m(1+w_m)\leq 2/3$	Saddle
				$\Omega_m\in(0:1)$, $w_m\in(0:1)$	Fig. 4.1, P6
1	$\pm\frac{\sqrt{2-\Omega_m(1+w_m)}}{\sqrt{2}}$	0	-1	$q>0,\ \Omega_m(1-w_m)=0,\ \Omega_m(1+w_m)\leq 2$	Stable
1	$\pm\frac{\sqrt{2-\Omega_m(1+w_m)}}{\sqrt{2}}$	0	1	$q>0,\ \Omega_m(1-w_m)=0,\ \Omega_m(1+w_m)\leq 2$	Unstable
1	0	$\sqrt{1-\Omega_m}$	1	$q>0,\ w_m=-1$	Stable
1	0	$\sqrt{1-\Omega_m}$	-1	$q>0,\ w_m=-1$	Unstable
1	0	0	-1	$q>0$, $\Omega_m=1$, $w_m=1$	Stable
				$q>0$, $\Omega_m=1$, $\lvert w_m\rvert<1$	Saddle
				$q>0$, $\Omega_m=1$, $w_m=-1$	Unstable
1	0	0	1	$q>0$, $\Omega_m=1$, $w_m=1$	Stable
				$q>0$, $\Omega_m=1$, $\lvert w_m\rvert<1$	Saddle
				$q>0$, $\Omega_m=1$, $w_m=-1$	Unstable
$\frac{1+3w_m\Omega_m}{3(\Omega_m-1)}$	$\pm\sqrt{1-\Omega_m}$	0	0	$q>0,\ w_m<0,\ \Omega_m>\frac{1}{3},\ \frac{2}{3}>\Omega_m(1+w_m)$	Unstable
$\frac{3-\Lambda^2(1-\Omega_m)}{3}$	0	$\sqrt{1-\Omega_m}$	±1	$q=-\frac{1}{2},\ \Lambda^2(1-\Omega_m)<3$	Unstable

Table 4.2: This table is a continuation of Table 4.1 when the brane tension and scalar potential follows a power law for a canonical scalar field ($\bar{\gamma}=1$) and when $0\leq\bar{\gamma}\leq 1$.

where λ, ν, σ, and μ constant parameters. This renders Eqs. (4.18) and (4.19) to zero where $\Lambda \to \lambda$ and $M \to \mu$. The exponential case is a special case of Sec. 4.3 when the power law parameters are $(p, r) \to \infty$. With the appropriate simplifications the dynamical system is given by Eqs. (4.13)–(4.16), and equivalently by Eqs. (4.24)–(4.27) when $q = 0$ for the power law case.

4.4.1 Stability analysis

The same approach is used to analyze the dynamical system as in the previous case in Sec. 4.3. Therefore, we begin by finding the roots of Eq. (4.13), which are

$$\bar{\gamma} = 0, \tag{4.41}$$

$$\bar{\gamma} = 1, \tag{4.42}$$

$$\bar{\gamma} = \frac{3x^2z^2}{(\mu x^2 - \lambda y^2)^2 - 3x^2z^2}. \tag{4.43}$$

A description of the stability of the system is given for each case of $\bar{\gamma}$ below.

Case I: Ultrarelativistic case ($\bar{\gamma} = 0$)

This case corresponds to the power law case with $q = 0$ and $\bar{\gamma} = 0$. Therefore, it is equivalent to the system given by Eqs. (4.31)–(4.33). Naturally, the same fixed points and stability are found for this case as in Table 4.1.

Case II: Standard quintessence ($\bar{\gamma} = 1$)

As discussed in Sec. 4.3, this case represents a canonical scalar field. This result yields an scalar potential characterized by an exponential function that is similar to those en-

countered in dark energy models [76]. The dynamical system for this case is,

$$x' = \frac{3}{2}xz\left[2(x^2-1)+\Omega_m(1+w_m)\right]+\sqrt{\frac{3}{2}}\lambda y^2, \tag{4.44}$$

$$y' = \frac{3yz}{2}\left[2x^2+\Omega_m(1+w_m)\right]-\sqrt{\frac{3}{2}}\lambda xy, \tag{4.45}$$

$$z' = (1-z^2)\left[1-3x^2-\frac{3}{2}\Omega_m(1+w_m)\right], \tag{4.46}$$

where the fixed points and stability are presented in Table 4.3. To draw similarities between this case and the power law case, the fixed points display the following:

1. The fixed point $y = 0$, which encodes the potential, only has a stable fixed point where cosmic evolution leads to a singular Big Crunch.

2. Assuming $y > 0$, the Universe generally evolves toward a quasi-de Sitter spacetime. However, in the absence of a scalar field, i.e., without dark energy or a vanishing potential, the Universe will eventually undergo collapse. This is consistent with the findings of Refs. [76, 77, 222].

It should be noted that these scenarios are not physically realistic, given the intrinsic behavior of exponential decay when $V > 0$ (i.e., $y \neq 0$).

Case III: $\bar{\gamma} = \frac{3x^2z^2}{-3x^2z^2+(\mu x^2-\lambda y^2)^2}$

Physically realistic fixed points for this case result in $z = 0$ or $x = 0$. This results in a repeated fixed point with $\bar{\gamma} = 0$.

4.5 A special case: $V \propto \phi^2$ and $f \propto \phi^{-4}$

In this section, we consider a quadratic potential and an inverse quartic brane tension. This case allows the field to behave like a canonical scalar field with $V \propto \phi^2$ (standard slow-roll inflation) at large ϕ, and causes the tension to dominate at small ϕ enforcing the speed limit Eq. (4.3). We perform a numerical analysis of our dynamical system for

$\bar{\gamma}$	x	y	z	Ω_m	**Existence**	**Stability**
1	-1	0	-1	0	$0 \leq w_m < 1$ and $0 \leq \lambda \leq \frac{6}{\sqrt{6}}$	Stable
					$0 \leq w_m \leq 1$ and $\lambda > \frac{6}{\sqrt{6}}$	Saddle
1	-1	0	1	0	$0 \leq w_m \leq 1$ and $\lambda > 0$	Unstable
1	0	0	-1	1	$0 \leq w_m < 1$ and $\lambda \in \mathbb{R}$	Saddle
					$w_m = 1$ and $\lambda \in \mathbb{R}$	Stable
1	0	0	1	1	$0 \leq w_m < 1$ and $\lambda \in \mathbb{R}$	Saddle
					$w_m = 1$ and $\lambda \in \mathbb{R}$	Unstable
1	1	0	-1	0	$0 \leq w_m \leq 1$ and $\lambda \in \mathbb{R}$	Stable
1	1	0	1	0	$0 \leq w_m \leq 1$ and $0 \leq \lambda < \frac{6}{\sqrt{6}}$	Unstable
1	$-\frac{1}{\sqrt{3}}$	$\sqrt{\frac{2}{3}}$	$-\frac{\lambda}{\sqrt{2}}$	0	$0 \leq w_m \leq 1$ and $\sqrt{\frac{6}{3}} < \lambda \leq \sqrt{\frac{8}{3}}$	Unstable
					$0 \leq w_m \leq 1$ and $0 < \lambda < \sqrt{2}$	Saddle
					$0 \leq w_m \leq 1$ and $\lambda > \sqrt{\frac{8}{3}}$	Unstable spiral
1	$\frac{1}{\sqrt{3}}$	$\sqrt{\frac{2}{3}}$	$\frac{\lambda}{\sqrt{2}}$	0	$0 \leq w_m \leq 1$ and $\sqrt{2} < \lambda \leq \sqrt{\frac{8}{3}}$	Stable
					$0 \leq w_m \leq 1$ and $0 < \lambda < \sqrt{2}$	Saddle
					$0 \leq w_m \leq 1$ and $\lambda > \sqrt{\frac{8}{3}}$	Unstable spiral

Table 4.3: This table lists all the physical fixed points for an exponential brane tension and scalar potential. The exponential case corresponds to the power law case when $q = 0$. This results in repeated fixed points for the ultrarelativistic ($\bar{\gamma} = 0$). The additional fixed points for this case is for a canonical scalar field ($\bar{\gamma}$), with its corresponding stability and the parameter region for existence.

the case $q = 1/2$. Several values of q were explored with an insignificant effect on the overall dynamics. We construct the 3-dimensional phase space in terms of the variables

$(\bar{\gamma}, x, z)$, since the behavior of the potential (y) provides little information and can be reconstructed from the Friedmann constraint. In Fig. 4.2, the submanifolds $\bar{\gamma} = 1$ and $\bar{\gamma} = 0$ exhibit comparable dynamics. The emergence of stable solutions $(x, z) = (0, 1)$ and $(y, z) = (0, -1)$, as identified in Tables 4.1 and 4.2, is evident in the phase space. We also see the saddle stability around $z = 0$, as depicted in Fig. 4.2 for $\bar{\gamma} = 1$ and $\bar{\gamma} = 0$.

In the region $0 < \bar{\gamma} < 1$, the stability is unstable around $z = 0$. This is not well represented in Fig. 4.2 given the choice of parameters, but the behavior at $\bar{\gamma} = 1/2$, as in the figure, is the same expanding across values of $\bar{\gamma}$ between 0 and 1. This might give an impression of cyclic behavior in the phase space, but it is an artifact of the transition between $z < 0$ flowing toward $\bar{\gamma} \to 0$ and $z > 0$ flowing toward $\bar{\gamma} \to 1$. However, trajectories in the cross-sectional region $0 < \bar{\gamma} < 1$, always lead to the ultrarelativistic case $(\bar{\gamma} = 0)$ or a canonical field $(\bar{\gamma} = 1)$. Therefore, the dynamics will always lead to a quasi-de Sitter Universe, corresponding to the stable solutions in Tables 4.1 and 4.2 for $z \to \pm z$.

The initial conditions and its effects that result in a bouncing cosmology are of common interest, so we study the initial conditions that admit a bounce, and the duration for the Universe to transition into a collapsing or expanding phase, as illustrated in Fig. 4.3. Each trajectory, distinguished by a unique color, represents the initial value of the kinetic energy of the field, x. We see that the evolution of the trajectories is significantly influenced by the initial value of x. This behavior resembles that of many bouncing models, where a Universe with dominant kinetic energy tends to evolve into expansion, while subdominant kinetic energy often leads to collapse. This trend is evident in Fig. 4.3, where the initial value of x varies with $\bar{\gamma}$. Table 4.3 highlights fixed points that possess stability corresponding to an unstable spiral. These fixed points exhibit cyclic behavior, eventually approaching either a singular collapse or a quasi-de Sitter phase. A comprehensive numerical analysis is needed to fully explore these solutions and is not presented in Fig. 4.3.

A particularly interesting result from this analysis is the frequency of trajectories resulting in a bounce scenario, where the trajectories evolve from a contracting to an

expanding spacetime for ultrarelativistic field, as compared to a canonical scalar field. We explore this further in the next section.

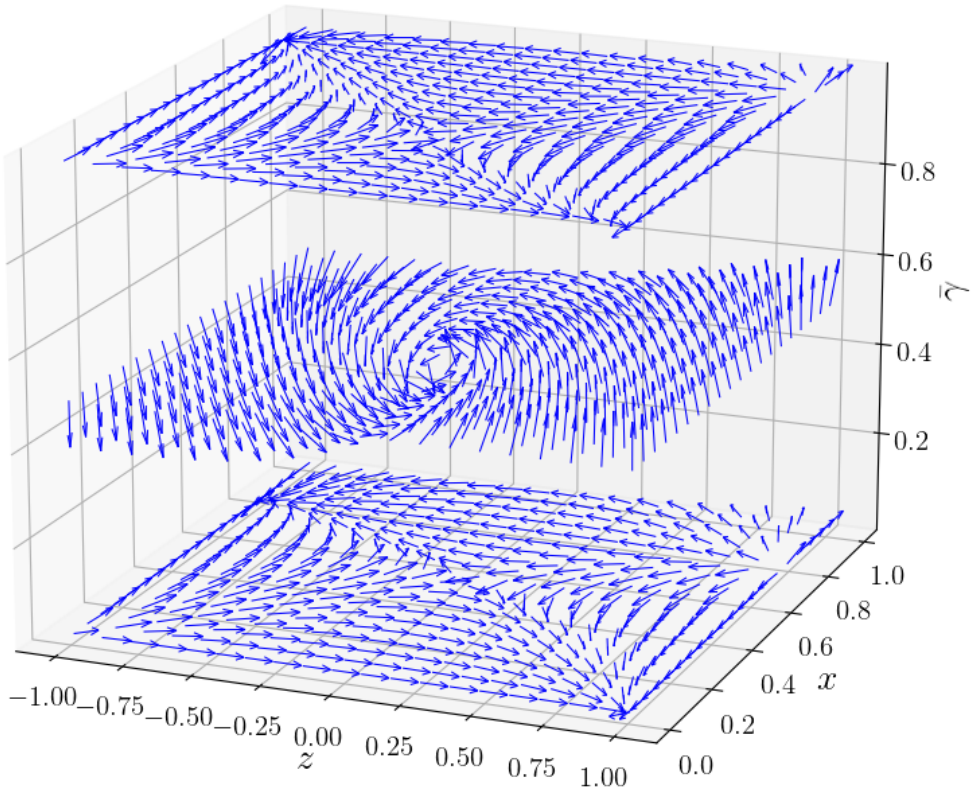

Figure 4.2: A vector plot illustrating the dynamical behavior for the power law case when $q = 1/2$, $M = \Lambda = 10^{-4}$, $w_m = 1/3$, and $\Omega_m = 0.2$. This graphically shows the bouncing solutions ($z = 0$), and trajectories in the $0 < \bar{\gamma} < 1$ region will either evolve towards the ultrarelativistic ($\bar{\gamma} = 0$) submanifold or the submanifold corresponding to a canonical scalar field ($\bar{\gamma} = 1$)

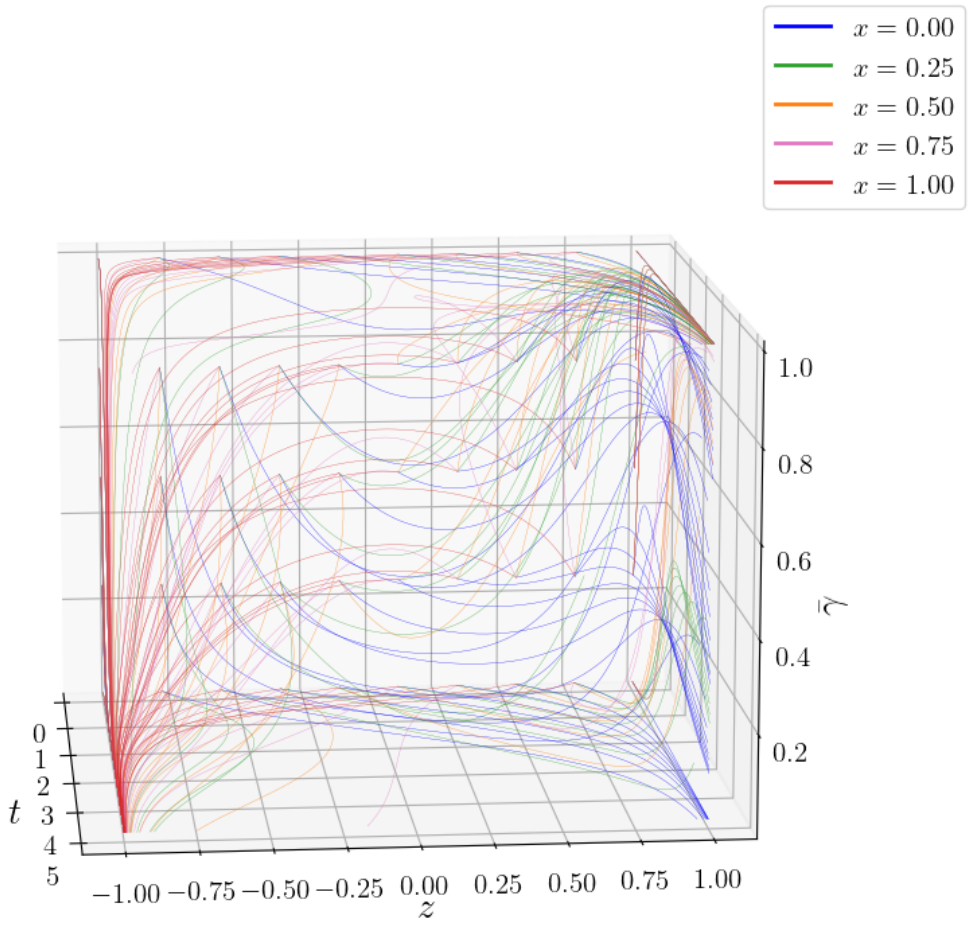

Figure 4.3: Trajectories in the phase space showing the effect of different initial values of x for a brane tension and scalar potential following a power law with $q = 1/2$, $M = \Lambda = 10^{-4}$, and $\Omega_m = 0$. For an integration time t, trajectories towards a contracting spacetime ($z = -1$) when $x \geq 0.5$ and towards an expanding spacetime ($z = 1$) when $x < 0.5$, for several values of $\bar{\gamma}$.

4.6 Bouncing cosmologies in the presence of a DBI field

Our stability analysis for a general power law, exponential model, and a particular model of the power law case has led to the conclusion that in the presence of a DBI field no stable cyclic solutions are present. We found that the field's unique deceleration mechanism assists in a larger range of initial conditions that lead to a bounce, compared to the

standard canonical scalar field ($\bar{\gamma} = 1$).

To further investigate, we numerically integrate the system, using initial conditions for z_i and x_i, with y_i determined by the Friedmann constraint, as in Fig. 4.3. This reveals how the initial conditions influence the dynamics leading to a bounce, and the following relation

$$r = \frac{A_{\bar{\gamma}} - A_{\bar{\gamma}=1}}{A_{\bar{\gamma}=1}}, \tag{4.47}$$

describes the percentage of initial conditions (r) that leads to a bounce in the presence of a DBI field, where $A_{\bar{\gamma}=1}$ is the area under the curve for a canonical scalar field ($\bar{\gamma} = 1$) and $A_{\bar{\gamma}}$ is the area under the curve for $0 \leq \bar{\gamma} \leq 1$. Figure 4.5 illustrates this, where the regions under the curves represent the sets of initial conditions that lead to a bounce ($z = 0$).

For an exponential brane tension and scalar potential, for which Fig. 4.5 is generated, there is a 69% increase in initial conditions leading to a bounce for the ultrarelativistic case ($\bar{\gamma} = 0$), and a 36% increase for $\bar{\gamma} = 1/2$ compared to the standard canonical scalar field. In the power law case with $q = 0.5$, the increase reaches 77% for the ultrarelativistic scenario, while for $\bar{\gamma} = 1/2$, there is a 41% increase relative to the canonical case, both leading to a bounce.

It is also noted that smaller z_i values correspond to slower contraction, allowing spatial curvature to dominate longer and thereby increasing the range of x_i values that lead to a bounce. Figure 4.5 shows that in the presence of a DBI field, excluding the canonical scalar field case, the range of initial conditions leading to a bounce increases as the initial value of $\bar{\gamma}$ increases towards the ultrarelativistic limit, $\bar{\gamma} = 0$.

4.6.1 Inducing a re-collapse

With the results of the analysis of Fig. 4.5, that a DBI field encourages bouncing behavior and as concluded in the previous section, that the dynamics result in quasi-de Sitter expansion ($z \to +1$) post-bounce, we include a negative cosmological constant to cause the dynamical evolution to re-collapse. This is motivated with the aim of witnessing cyclic

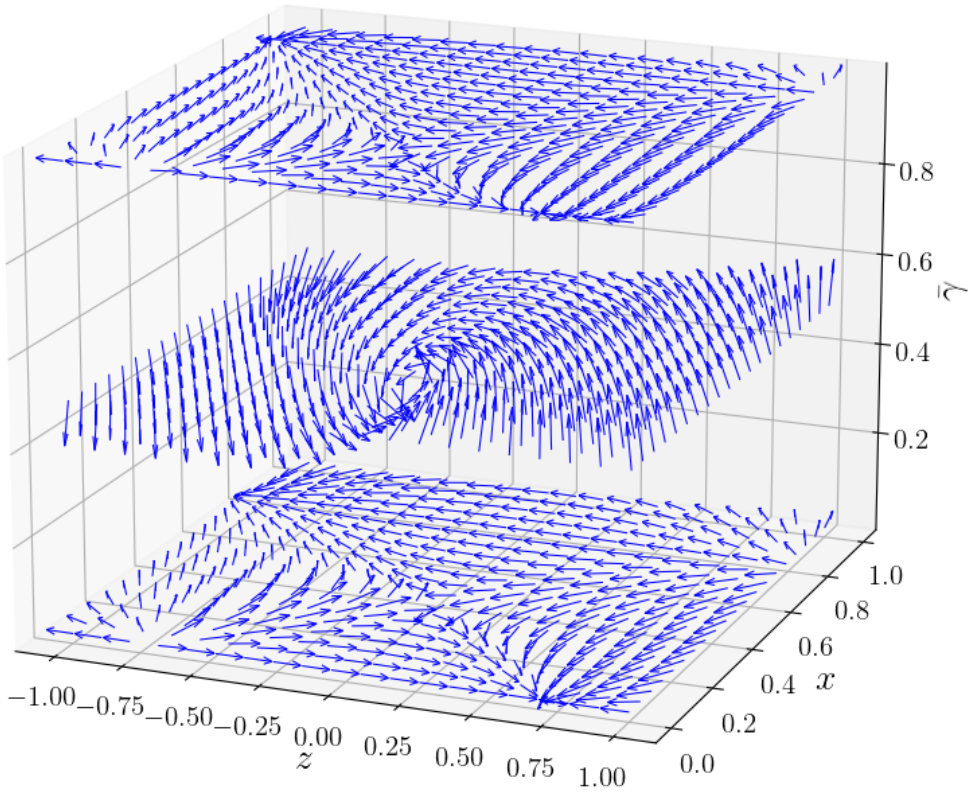

Figure 4.4: A vector plot illustrating the dynamical behavior for a power law model including a negative cosmological constant. The model parameter values are $q = 1/2$, $M = \Lambda = 10^{-4}$, and $\Omega_C = 0.3$.

behavior. The energy density of the cosmological constant is denoted by ρ_C where the corresponding equation of state is $w_C = -1$. The Friedmann equation is then,

$$3H^2 = \frac{\gamma^2\dot{\phi}^2}{\gamma+1} + V - 3\frac{K}{a^2} - \rho_C. \tag{4.48}$$

The effective Hubble parameter is redefined to include the cosmological constant, $\tilde{D}^2 = H^2 + \frac{K}{a^2} + \frac{\rho_C}{3}$. As explained before, this quantity aids in compactifying the $K > 0$ state space. Additionally, a new dimensionless variable $\Omega_C \equiv \frac{\rho_C}{3\tilde{D}^2}$ is defined. The equations

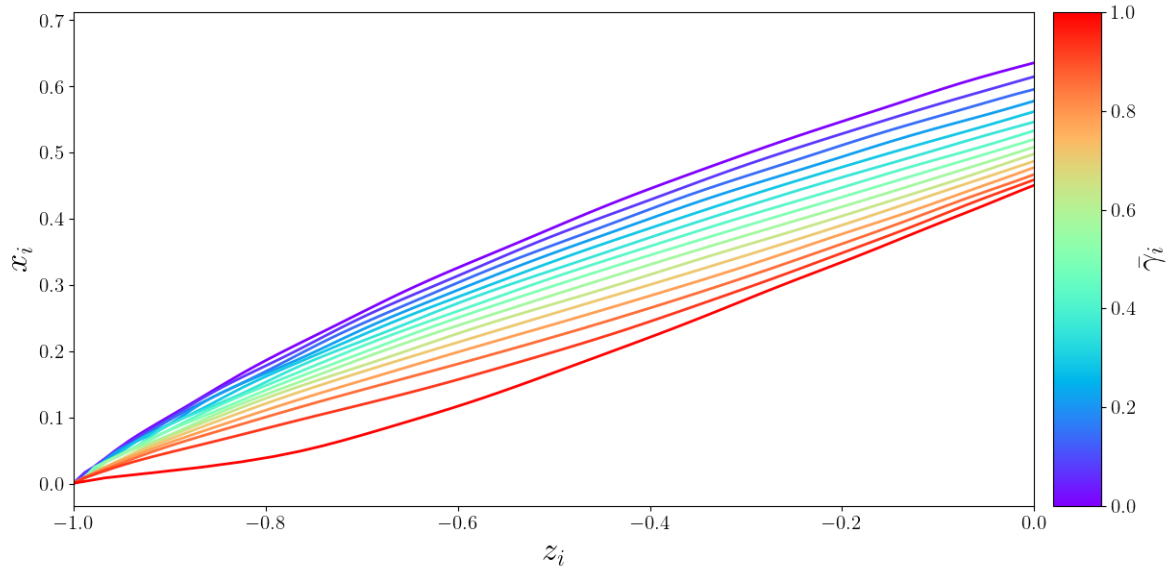

Figure 4.5: A plot indicating the area of the parameter space for initial values that result in a scenario where the spacetime experiences a bounce. Each curve encodes the maximum initial conditions that lead to an expanding spacetime i.e., $z > 0$ where each color indicates an initial value for $\bar{\gamma}$ denoted by $\bar{\gamma}_i$. The area under each curve then indicates the parameter space area (z_i, x_i) that leads to a bouncing universe for each $\bar{\gamma}_i$.

of motion including a negative cosmological constant is described by Eqs. (4.24)–(4.26), which remains unchanged, and

$$z' = (1 - z^2)\left[1 - \frac{3}{2}x^2(1 + \bar{\gamma})\right] - \Omega_C, \tag{4.49}$$

where in this case $' \equiv \tilde{D}^{-1}\frac{d}{dt}$. Equivalently, this analysis can be performed by choosing $w_m = -1$, removing the dependence of Ω_m from Eqs. (4.24)–(4.27). The system Eqs. (4.24)–(4.26) and Eq. (4.49) is preferred, since it explicitly shows the dependence on Ω_C. The fixed point analysis is performed for the power law case when $q = 1/2$, and is tabulated in Table 4.4.

As shown in Fig. 4.4, our analysis leads to two noteworthy results,

1. An increase in the range of 'x' values resulting in a collapsing universe, as compared to the previous scenarios omitting a negative cosmological constant. This is a result of the downward shift of the saddle point of the submanifolds $\bar{\gamma} = 0$ and $\bar{\gamma} = 1$,

$\bar{\gamma}$	x	y	z	**Existence**	**Stability**
0	0	$\pm\sqrt{1-\Omega_m}$	$-\sqrt{\frac{2(\Omega_C-1)+3\Omega_m(1+w)}{-2+3(1+w_m)}}$	$\Omega_m(1+w_m)\geq\frac{2}{3}$	Stable
0	0	$\pm\sqrt{1-\Omega_m}$	$\sqrt{\frac{2(\Omega_C-1)+3\Omega_m(1+w_m)}{-2+3(1+w_m)}}$	$\Omega_m(1+w_m)\geq\frac{2}{3}$	Unstable
0	$\pm\sqrt{\frac{2(1-\Omega_C)-3\Omega_m(1+w_m)}{3}}$	$\sqrt{\frac{1+2\Omega_C+3\Omega_m w_m}{3}}$	0	$\Omega_m(1+w_m)\leq\frac{2}{3}(1-\Omega_C)$	Saddle
1	0	$\pm\sqrt{1-\Omega_m}$	$-\sqrt{\frac{2(\Omega_C-1)+3\Omega_m(1+w_m)}{-2+3(1+w_m)}}$	$\Omega_m(1+w_m)\geq\frac{2}{3}$	Stable
1	0	$\pm\sqrt{1-\Omega_m}$	$\sqrt{\frac{2(\Omega_C-1)+3\Omega_m(1+w_m)}{-2+3(1+w_m)}}$	$\Omega_m(1+w_m)\geq\frac{2}{3}$	Unstable
1	$\pm\sqrt{\frac{2(1-\Omega_C)-\Omega_m(1+w_m)}{6}}$	$\sqrt{\frac{4+2\Omega_C+3\Omega_m(w_m-1)}{6}}$	0	$\Omega_m(1+w_m)\leq 2(1-\Omega_C)$	Saddle
$\frac{1+w_m\Omega_m}{3(\Omega_m-1)}$	$\pm\sqrt{\frac{2(1-\Omega_C)-3\Omega_m(1+w_m)}{2-3\Omega_m(1+w_m)}}$	$\sqrt{\frac{2(1-\Omega_m)\Omega_C}{2-3\Omega_m(1+w_m)}}$	0	$w_m<0,\ \Omega_m>\frac{1}{3}$, $\frac{2}{3}>\Omega_m(1+w_m)$	Unstable

Table 4.4: A tabulation of the fixed points, the parameter intervals for existence, and its stability for the power law case with $q = 1/2$ and the inclusion of a negative cosmological constant. We choose the dimensionless cosmological constant parameter to lie in the interval $0 < \Omega_C < 1$ and exclude conditions that require $\Omega_C = 0$ since this repeats the result in Tables 4.1 and 4.2.

relative to its 'x' position. This change can also be seen in Table 4.4.

2. In the limiting cases $\bar{\gamma} = 0$ and $\bar{\gamma} = 1$, the fixed points no longer correspond to quasi-de Sitter asymptotic solutions during contraction ($z = -1$) and expansion ($z = 1$). This can be seen in Fig. 4.4 and Table 4.4.

The saddle point shift, toward lower values of x, in this case minimizes the parameter space that allows bouncing solutions compared to the power law case in Sec. 4.3.

To identify cyclicity through a dynamical systems analysis, the fixed points of the system should be of the form: $(x,\ y,\ z) = (A_1 i,\ A_2 i,\ 0)$, where A_1 and A_2 are expressions of the cosmological parameter constants, and i signifies an imaginary number ($i \equiv \sqrt{-1}$). Fixed points of this kind show closed orbits in the phase-space diagram, indicating evidence of cyclic behavior where the evolutionary orbits will follow expansion after a bounce ($z = 0$) and undergo contraction post re-collapse ($z = 0$) on return. The $z = 0$ entries in Table 4.4 show that cyclic orbits would not be possible in a DBI field with a negative cosmological constant if we apply the condition that the expressions in the square roots

for x and y should be negative. For example, focusing on the y component for the entries 3, 6 and 7 in Table 4.4, and using the current observational measurements $\Omega_m \simeq 0.3$ and $\Omega_C \simeq 0.7$, we find that $w_m < -2.7$, $w_m < -3.86$, and $\Omega_m > 1$ respectively. This suggests that only matter crossing the phantom barrier would exhibit cyclic behavior, and demands physics beyond the standard model.

We can conclude that the inclusion of a negative cosmological constant, additional features and advantages emerge, but it does not encourage cyclic behavior in a DBI field.

A realization of cyclicity in this DBI model would involve extensions that support bounce solutions with attractors. For example, a hybrid DBI-ekpyrotic setup could support true cyclicity if a steep negative potential were considered. As in the ekpyrotic scenario, this could act as a contraction attractor, and the DBI brane tension $f(\phi)$ could allow a safe approach to the negative potential since γ suppresses gradients. Another modification to consider is to adopt higher-order curvature corrections to the field equations. These add new fixed points in the dynamical system which can act as centers (closed orbits). For instance, $R + R^2$ gravity creates oscillatory solutions in the scale factor $a(t)$, creating stable limit cycles in the (a, H) phase space. Below, in Table 4.5, is a comparative analysis of our model with other cyclic cosmology frameworks.

Model	Bounce Mechanism	Cyclic Attractor?	Why DBI Differs
Our DBI model	Curvature + DBI speed-limit suppression.	No (bounce is a saddle).	No restoring force in phase space; $\bar{\gamma} \to 0$ or 1; $V > 0$ eliminates ekpyrotic-type attractors.
Conformal Cyclic Cosmology (CCC)	Conformal matching between aeons, no FLRW bounce.	Yes (geometric identification).	Not a dynamical scalar-field bounce; cyclicity emerges from conformal rescaling, not from limit cycles in (a, H).
Ekpyrotic / Cyclic brane models	Steep negative potential + extra-dimensional brane collision.	Yes.	Require $V < 0$ and ultra-stiff $w \gg 1$ attractor; single-field DBI with $V > 0$ lacks a contraction attractor.
Loop Quantum Cosmology (LQC)	Quantum gravity correction: $H^2 = \frac{\rho}{3}(1 - \rho/\rho_c)$.	Yes.	Bounce arises from modified gravity; not reproducible in GR + DBI without quantum corrections.
DBI + extra fields	Multi-field dynamics, angular momentum in field space.	Potentially.	Extra degrees of freedom produce centers/limit cycles; single-field DBI phase space is too simple to support this.

Table 4.5: Comparison of cyclic mechanisms across cosmological models with a single-field DBI model.

CHAPTER 5

SUMMARY OF PART II

Extending the analysis of Copeland et al. [78], we investigated the dynamics of a DBI field with a positive spatial curvature, where we explored the stability of the additional fixed points, particularly around $z = H/D = 0$ where the spacetime experiences a bounce. We performed a comprehensive dynamical systems analysis for a general power law and exponential brane tension and scalar potential, respectively. In addition, we focused our numerical analysis on the special case: $V \propto \phi^2$ and $f \propto \phi^{-4}$. A summary of our analysis is as follows:

1. The exponential case is a subset of the power law case where its fixed-point analysis is repeated.

2. In both the ultrarelativistic case and the canonical scalar field case, the stability around the fixed point $z = 0$, corresponding to a bouncing cosmology, is an unstable saddle.

3. In the region $0 < \tilde{\gamma} < 1$, the system is unstable and the dynamics is driven either towards the ultrarelativistic submanifold or the canonical scalar field submanifold, as shown in Fig. 4.2. A bounce is still present in this region of $\tilde{\gamma}$, but does not

exhibit any cyclic behavior.

4. As the dynamics evolves from a canonical scalar field toward the ultrarelativistic limit, the number of initial conditions leading to a bounce increases, as shown in Fig. 4.5.

5. An additional degree of freedom is realized through a negative cosmological constant so that a re-collapse is induced and does not facilitate cyclic behavior. This addition increases the range of points that result in a collapse. However, the initial conditions leading to a bounce are constrained by the saddle point, and the x-value, which encodes the velocity of the ϕ-field, is less than in the cases omitting a negative cosmological constant.

In constructing cyclic cosmological models, the unique deceleration mechanism of the DBI field facilitates the occurrence of a bounce. The parameter space of initial conditions that lead to a bounce is enlarged when the field approaches the ultrarelativistic limit. However, generic cyclic behavior cannot be achieved through a negative cosmological constant alone; an additional exotic degree of freedom is required.

Recent DESI data indicate a preference for dynamical dark energy over a cosmological constant [5]. The inclusion of a decaying dark energy term could potentially induce recollapse and lead to a bounce or cyclical behavior in the phase space, as demonstrated by Ellis et al. in the context of a chaotic inflationary model [113]. Future research directions include considering multi-field extensions, analyzing linear cosmological perturbations, and extending the analysis to the nonlinear regime, for example, by calculating the bispectrum or trispectrum, which could reveal observable signatures that distinguish DBI cosmologies from canonical inflation.

Part III:

Relativistic stars in fourth-order gravity

> Science has material and non-material appliances to bore into the interior, and I have chosen to devote this address to what may be described as analytical boring devices –absit omen!.
>
> A. S. Eddington, *The Internal Constitution of the Stars.*

CHAPTER 6

INTRODUCTION

The mathematical formulation underpinning the study of relativistic stars, particularly neutron stars, was significantly advanced by Oppenheimer and Volkoff's investigation of the stability of neutron cores [219]. Building on the static, spherically symmetric solutions to Einstein's field equations developed by Tolman [267], Oppenheimer and Volkoff provided a physical interpretation of stellar interiors by modeling matter as a degenerate Fermi gas governed by an appropriate equation of state. Their work led to the development of an algorithm for determining interior solutions to spherically symmetric configurations of stellar matter within the framework of general relativity.

This formulation, now known as the Tolman–Oppenheimer–Volkoff (TOV) approach, has become foundational in the study of relativistic stellar structures, both in GR and in extended theories of gravity. These alternative theories often introduce additional degrees of freedom beyond those present in GR, and compact objects like neutron stars, due to their extreme densities and strong gravitational fields, serve as ideal astrophysical laboratories for testing and constraining such modifications. As such, the study of neutron stars provides a critical pathway toward identifying a gravitational theory capable of consistently describing both the universe on cosmological scales and the compact astrophysical

phenomena it contains.

The framework used to study and analyze relativistic stellar solutions in gravity has predominantly been performed using the (1+3) decomposition. The following chapters will present new stellar solutions in the context of $f(R)$ theories using the (1+1+2) covariant formalism. The pedagogical motivation for using the (1+1+2) formalism in the study of relativistic stars is that the underlying spacetime geometry possesses a natural preferred spatial direction: the radial direction. Both static and dynamical stellar models exhibit a spherical or locally rotationally symmetric (LRS) structure, in which all angular directions are equivalent and the only physically distinct spatial direction is the one pointing outward from the centee. This feature makes the (1+1+2) covariant formalism especially well suited for stellar physics.

The (1+1+2) approach is a refinement of the standard (1+3) decomposition used throughout general relativity. In the (1+3) split, spacetime is divided into temporal evolution along a chosen four-velocity field and spatial quantities orthogonal to it. The (1+1+2) formalism proceeds one step further, decomposing the three-dimensional spatial sector into:

1. one preferred spatial direction (the radial unit vector), and

2. two-dimensional sheets orthogonal to both the time direction and this radial vector.

This "time + radial + angular" split mirrors the natural geometry of a relativistic star. As a result, the field equations, kinematical quantities, and curvature variables separate into scalars, vectors, and tensors defined on the two-sheets, with many components vanishing identically in spherically symmetric or LRS spacetimes.

The formalism offers several pedagogical and practical benefits for the study of relativistic stars:

- **Symmetry is incorporated from the start.** The decomposition builds spherical symmetry directly into the variables. Unlike coordinate-based methods, no special

coordinate choices are needed to enforce symmetry, eliminating coordinate artifacts, and making the physical content of each variable transparent.

- **Significant reduction in complexity.** In spherically symmetric spacetimes, many vector and tensor components on the two-sheets vanish automatically. The remaining degrees of freedom reduce to a small, closed set of scalar equations. This simplifies the Einstein field equations and aids in the analysis of static stars or dynamical collapse.

- **Clear physical interpretation of variables.** Geometric and dynamical quantities, such as expansion, shear, acceleration, and the Weyl curvature take on simple and intuitive forms in the (1+1+2) split. This helps connect the mathematics directly to the physics of stellar structure, stability, anisotropy, or collapse.

- **Coordinate-free description of stellar interiors.** Because the formalism is fully covariant, results are independent of coordinates. This is advantageous when comparing stellar models or matching interior solutions to exterior spacetimes, where coordinate systems may differ.

- **Natural framework for perturbations of stars.** When studying oscillations, quasi-normal modes, or gauge-invariant perturbations of spherically symmetric spacetimes, the angular structure built into the (1+1+2) framework allows scalar, vector, and tensor perturbations to decouple cleanly. This greatly simplifies mode analysis and stability studies.

For these reasons, the 1+1+2 formalism is not only computationally efficient but also pedagogically valuable: it reveals the geometric and physical structure of stellar configurations in gravity in a particularly transparent way.

This part comprises six chapters. Chapter 7 presents the mathematical formulation of the Tolman–Oppenheimer–Volkoff (TOV) equations within the standard framework of GR. Chapter 8 introduces the (1+1+2) covariant formalism used to describe Locally

Rotationally Symmetric (LRS) class II spacetimes. In Chapter 9, compact objects are modeled as two-fluid systems, and the dimensionless form of the TOV equations is derived in the context of $f(R)$ gravity theories. Chapter 10 outlines the boundary and energy conditions necessary to obtain solutions that are physically relevant. Chapter 11 demonstrates the implementation of the developed scheme, yielding new solutions to the TOV equations within this modified gravity setting [53]. Finally, Chapter 12 summarizes the key results.

The notation for the parameters and variables used in the following chapters is consistent with that of our article [53], and is self-contained within this part of the thesis.

CHAPTER 7

TOLMAN-OPPENHEIMER-VOLKOFF EQUATIONS

Oppenheimer and Volkoff developed the algorithm for finding solutions to static spherically symmetric spheres given an equation of state in order to link Tolman's more classical approach to a physically relevant case and its implications in studying stellar objects [219, 267].

A review of Tolman's methodology for finding new static solutions to spheres of fluid is presented in this chapter, since our mathematical scheme for finding two-fluid solutions to relativistic stars in Chs. 9 and 11 are analogous to the Tolman approach.

Following the Misner-Thorne-Wheeler metric convention, a static spherically symmetric distribution of matter is described by the line element[1]

$$ds^2 = -e^{\nu(r)}dt^2 + e^{\lambda(r)}dr^2 + r^2 d\theta^2 + r^2 \sin^2\theta d\phi^2. \tag{7.1}$$

Deriving the field equations for Eq. (7.1), which takes the form

$$T_{\mu\nu} = R_{\mu\nu} - \frac{1}{2}Rg_{\mu\nu} + \Lambda g_{\mu\nu}, \tag{7.2}$$

[1] In Tolman's seminal paper he uses the $(+---)$ metric convention [267].

and considering the energy momentum tensor is of the form of a perfect fluid

$$T^{\mu\nu} = (\rho + p)u^{\mu}u^{\nu} + g^{\mu\nu}p, \tag{7.3}$$

where ρ is the energy density and p is the isotropic pressure, the remaining components of the energy momentum tensor (EMT) yields

$$p = e^{-\lambda}\left(\frac{\nu'}{r} + \frac{1}{r^2}\right) - \frac{1}{r^2} + \Lambda, \tag{7.4}$$

$$p = e^{-\lambda}\left(\frac{\nu''}{2} - \frac{\lambda'\nu'}{4} + \frac{\nu'^2}{4} + \frac{\nu' - \lambda'}{2r}\right) + \Lambda, \tag{7.5}$$

$$\rho = e^{-\lambda}\left(\frac{\lambda'}{r} - \frac{1}{r^2}\right) + \frac{1}{r^2} - \Lambda. \tag{7.6}$$

This connects the properties of the fluid in terms of its energy density and pressure via the gravitational potentials in Eq. (7.1). To ensure solubility in the search for explicit analytical solutions, the system Eqs. (7.4)–(7.6) is re-expressed in a form that ascertains the conditions on λ and ν. This can be immediately seen by equating Eq. (7.4) and Eq. (7.5) and then rewriting it in a form that is nearly integrable. By doing so, the equivalent system to Eqs. (7.4)–(7.6) is

$$\frac{d}{dr}\left(\frac{e^{-\lambda} - 1}{r^2} + \frac{d}{dr}\left(\frac{e^{-\lambda}\nu'}{2r}\right) + e^{\lambda-\nu}\frac{d}{dr}\left(\frac{e^{\nu}\nu'}{2r}\right)\right) = 0, \tag{7.7}$$

$$p = e^{-\lambda}\left(\frac{\nu'}{r} + \frac{1}{r^2}\right) - \frac{1}{r^2} + \Lambda, \tag{7.8}$$

$$\rho = e^{-\lambda}\left(\frac{\lambda'}{r} - \frac{1}{r^2}\right) + \frac{1}{r^2} - \Lambda. \tag{7.9}$$

As a simple example to illustrate a specific solution, we will consider the static Einstein universe which is described by a matter distribution with uniform energy density and pressure. First, Tolman assumed the following form for the gravitational potential: $e^{\nu} = \text{constant}$.

One can immediately see that the last two terms of Eq. (7.7) drop out making it straight-

forward to integrate. This results in the solution

$$e^{\lambda} = \left(1 - \frac{r^2}{R_0^2}\right)^{-1}, \quad e^{\nu} = c_0^2, \tag{7.10}$$

$$\rho = \frac{3}{R_0^2} - \Lambda, \quad p = -\frac{1}{R_0^2} + \Lambda, \tag{7.11}$$

where the cosmological constant is constrained by the interval $3/R_0^2 > \Lambda > 1/R_0^2$ and R_0 is an integration constant. To illustrate the reproducibility of previously known results, Tolman calculated the energy and pressure distributions for the Schwarschild-de Sitter solution and the interior Schwarzschild solution. Since the interior Schwarzschild solution and Tolman's solutions are used as an example in the implementation of our new scheme to find analytical solutions to the TOV equations in the context of $f(R)$ theories of gravity, we provide details of the solutions as follows:

Interior Schwarzschild

The assumed form for the gravitational potential in Eq. (7.1) is

$$e^{-\lambda} = 1 - \frac{r^2}{R_0^2}. \tag{7.12}$$

Using Eqs. (7.7)–(7.9) to find the complete solution:

$$e^{\lambda} = \left(1 - \frac{r^2}{R_0^2}\right)^{-1}, \quad e^{\nu} = \left[A - B\left(1 - \frac{r^2}{R_0^2}\right)^{\frac{1}{2}}\right]^2, \tag{7.13}$$

$$\rho = \frac{3}{R_0^2} - \Lambda, \tag{7.14}$$

$$p = \frac{1}{R_0^2}\left(\frac{3B\left(1 - \frac{r^2}{R_0^2}\right)^{\frac{1}{2}} - A}{A - B\left(1 - \frac{r^2}{R_0^2}\right)^{\frac{1}{2}}}\right) + \Lambda, \tag{7.15}$$

where A and B are integration constants. This solution describes a static spherically symmetric distribution of matter that has a uniform constant energy density and a pressure that decreases with increasing radius.

Tolman's seminal paper also contains his new solutions which is now more commonly referred as the Tolman IV, Tolman V, Tolamn VI, Tolman VII and Tolman VIII in the literature. In this thesis we will focus specifically on the Tolman IV solution where Tolman assumes $e^{\nu}\nu'/2r$ = constant in Eq. (7.7). The solutions to the gravitational potentials, the energy density and pressure are as follows.

Tolman IV

An assumed form for the last term in Eq. (7.7), to ease integrability, is

$$\frac{e^{\nu}\nu'}{2r} = \text{constant}. \tag{7.16}$$

Following the same procedure as before, Tolman finds the first of his new solutions:

$$e^{\lambda} = \frac{1+2\frac{r^2}{A^2}}{\left(1-\frac{r^2}{R_0^2}\right)\left(1+\frac{r^2}{A^2}\right)}, \tag{7.17}$$

$$e^{\nu} = B^2\left(1+\frac{r^2}{A^2}\right), \tag{7.18}$$

$$\rho = \frac{1}{A^2}\frac{1+3\frac{A^2}{R_0^2}+3\frac{r^2}{R_0^2}}{1+2\frac{r^2}{A^2}} + \frac{2}{A^2}\frac{1-\frac{r^2}{R_0^2}}{\left(1+2\frac{r^2}{A^2}\right)^2} - \Lambda, \tag{7.19}$$

$$p = \frac{1}{A^2}\frac{1-\frac{A^2}{R_0^2}-3\frac{r^2}{R_0^2}}{1+2\frac{r^2}{A^2}} + \Lambda, \tag{7.20}$$

where, again, A and B are integration constants. For suitable values of A and R_0 this solution describes a static sphere of fluid with a compressible matter distribution and a pressure that drops to zero at the boundary of the sphere. In the more limiting cases of the parameter values, if $R_0^2 > A^2$, the energy density and pressure would fall from their central values to their boundary values where the energy density remains positive throughout. If we define the sound speed to be $c^2 \equiv \frac{\partial p}{\partial \rho} = \frac{dp}{dr}/\frac{d\rho}{dr}$, then the squared sound

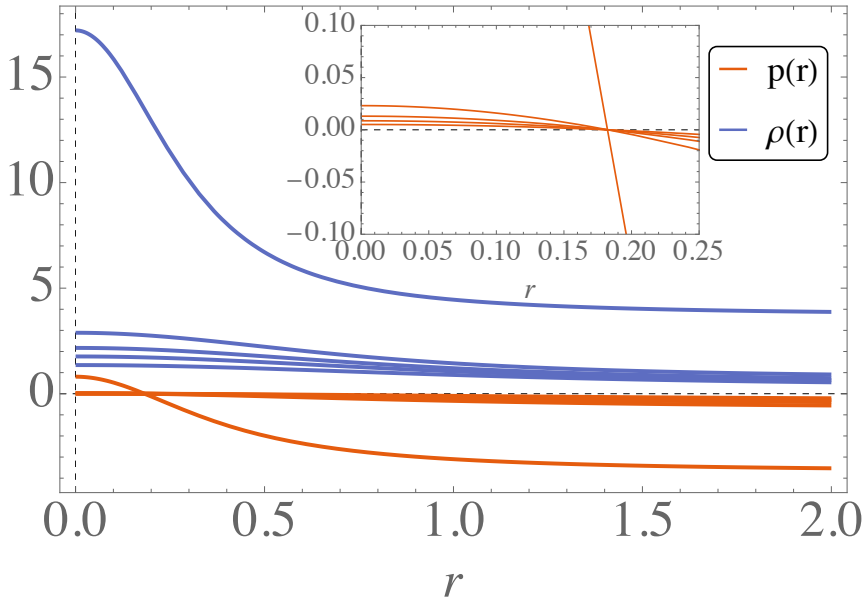

Figure 7.1: Various solutions to the energy density and pressure, Eqs. (7.19) and (7.20) when $\Lambda = 0$, using the parameter values corresponding to Table 7.1, for the Tolman IV metric description. We notice that for smaller values of R_0^2 and A^2, the energy density and pressure are larger at the core than at increased parameter values. The energy density remains positive throughout, in fact, $\rho \to \frac{3}{2R_0^2}$ for $r \to \infty$.

speed for the Tolman IV solution is

$$c^2 = \frac{A^2 + 2r^2}{5A^2 + 2r^2}.$$

So the sound speed throughout this fluid sphere obeys the causal limit $0 \leq c^2 \leq 1$, behaving like standard matter, and as $r \to \infty$ the square-speed-of-sound approaches $c^2 \to 1$. This means that as the fluid sphere expands in size, standard matter becomes more compressed.

R_0^2	2.81617	4.47183	0.405665	3.44953	2.12928
A^2	2.71617	4.37183	0.305665	3.34953	2.02928

Table 7.1: Parameter values for the Tolman IV solution obeying the $R_0^2 > A^2$ condition. The corresponding figure for which these parameter values are used for is Fig. 7.1.

Summarizing:

Tolman presented a new methodology for finding exact static, spherically symmetric perfect-fluid solutions to Einstein's field equations. He found five new exact solutions, and his method also reproduced the well-known Einstein universe, Schwarzschild-de Sitter, and Interior Schwarzschild solutions. Following the same method as described above, the solutions found by Tolman and the other well-known solutions are summarized, in Table (7.2), by the assumptions made on the terms in Eq. (7.7).

Eq. (7.7): $\frac{d}{dr}\left(\frac{e^{-\lambda}-1}{r^2}+\frac{d}{dr}\left(\frac{e^{-\lambda}\nu'}{2r}\right)+e^{-\lambda-\nu}\frac{d}{dr}\left(\frac{e^{\nu}\nu'}{2r}\right)\right)=0$

Spacetime	**Assumption**
Interior Schwarzschild	$e^{-\lambda}=1-\frac{r^2}{R_0^2}$
Tolman VI	$e^{-\lambda}=$ constant
Tolman VII	$e^{-\lambda}=1-\frac{r^2}{R_0^2}+\frac{4r^4}{A^4}$
Tolman VIII	$e^{-\lambda}=$ constant $\cdot\, r^{-2b}e^{\nu}$
Schwarzschild-de Sitter	$e^{-\lambda-\nu}=$ constant
Einstein Universe	$e^{\nu}=$ constant
Tolman V	$e^{\nu}=$ constant $\cdot\, r^{2n}$
Tolman IV	$\frac{e^{\nu}\nu'}{2r}=$ constant

Table 7.2: List of the solutions presented in Tolman's seminal paper in 1939 [267] and the assumptions to the integrability condition to determine the new and recover other well known static, spherically symmetric metric solutions.

Inspired by his interests in the stability of neutron cores and its possible implementation for military purposes with the newly discovered neutron fission process in 1938, Oppenheimer together with Volkoff (O-V) found a way to transform the general relativis-

tic description of a fluid sphere to a description of a stellar structure by using a realistic equation of state and its physical implications [219].

(O-V) started with the same metric and fluid source assumptions as Tolman and wrote down what would become known as the TOV equations, which is (with $\Lambda = 0$) Eq. (7.4), Eq. (7.6), and

$$\frac{dp}{dr} = -\frac{p+\rho}{2}\nu', \tag{7.21}$$

together with the equation of state of the interior fluid $\rho = \rho(p)$ closes the system. This reformulation of Tolman's approach gives a new physical interpretation to single fluid spheres, that is, by using the equation of state it determines the mechanical equilibrium of the matter distribution inside the sphere. In Tolman's seminal paper, he addressed the use of an equation of state and its natural introduction to Eqs. (7.4)–(7.6) from a physical point of view. However, because of the non-linear form of Eqs. (7.4)–(7.6) an analytical solution would not be guaranteed. Instead, for mathematical convenience, and to avoid not finding a physically interesting or physically possible solution, the equation of state can be introduced after the fact as a relation connecting λ or ν or both with r.

In the next chapter, we discuss LRS II spacetimes in the (1+1+2) covariant formalism. This is the foundational aspect of our new scheme for finding exact solutions to a dimensionless form of the TOV equations in the context of $f(R)$ theories of gravity using the covariant approach.

CHAPTER 8

LRS II SPACETIMES

The study of locally rotationally symmetric (LRS) spacetimes has often been employed to investigate problems involving highly symmetric configurations. A key advantage of LRS spacetimes is that, under the (1+3) spacetime decomposition, the dynamical equations reduce to a set of differential relations involving only scalar quantities [272]. This simplification makes LRS spacetimes a powerful and attractive framework for modeling complex astrophysical scenarios [39, 128, 264], as it facilitates both analytical and numerical treatments.

In the classification of cosmological symmetries [110, 272], LRS has a one-dimensional isotropy group and a multiply-transitive isomotry group. It possesses the following symmetries:

1. The kinematical quantities are rotationally symmetric about a preferred spatial direction.

2. Observations at every general point are rotationally symmetric about that point.

3. In the case of a perfect fluid and dust, all the metrics are known.

The fundamental quantities describing a spacetime are constructed upon the intro-

duction of a vector field which represents the observers' congruence, its threading and projection of all vectors and tensors orthogonal to the vector fluid. The (1+3) formalism is a time-like threading of a vector field u^a, with the property $u^a u_a = -1$. Upon the introduction of this vector field, a projection tensor is introduced and defined as

$$h_a{}^b \equiv g_a{}^b + u^a u_b. \tag{8.1}$$

The use of this projection tensor one may split any four-vector and second-rank tensor into scalar, three-vector, and projected, symmetric, trace-free (PSTF) three-tensor parts. The (1+1+2) decomposition follows the same procedure as the (1+3) threading, introducing another vector field, e^a, orthogonal to u^a, where

$$e^a e_a = 1, \quad u^a e_a = 0. \tag{8.2}$$

Then performing another split of the (1+3) quantities using the projection tensor

$$N_a{}^b \equiv h_a{}^b - e_a e^b = g_a{}^b + u_a u^b - e_a e^b, \quad N_a{}^a = 2, \tag{8.3}$$

we can project vectors and tensors orthogonal to e^a and u^a, i.e., $e^a N_{ab} = 0 = u^a N_{ab}$. In this way, we can project onto the 2-surfaces referred to as the *sheet*, and we obtain a three-vector and a PSTF three-tensor as

$$\psi^a = \Psi e^a\,, \quad \Psi \equiv \psi^a e_a\,, \quad \Psi^a \equiv N^{ab}\psi_b\,, \tag{8.4}$$

$$\psi_{ab} = \psi_{\langle ab\rangle} = \Psi\left(e_a e_b - \frac{1}{2}N_{ab}\right). \tag{8.5}$$

As illustrated above, the (1+1+2) threading picks a preferred spatial direction and projects all the quantities describing the spacetime onto 2-surfaces. Therefore, the (1+1+2) covariant formalism is uniquely adapted for LRS spacetimes.

Since in this part, we are considering astrophysical objects that possess spherical symmetry, we limit our study to a subclass of LRS spacetimes: LRS class II. This class is rotation-free and is described by the following set of scalar quantities in the (1+1+2) covariant formalism:

$$\text{LRS class II: } \{\mathcal{A}, \Theta, \phi, \Sigma, \mathcal{E}, \mu, p, Q, \Pi\}. \tag{8.6}$$

This is the advantage of using the (1+1+2) formalism in this subclass of spacetimes: the quantities describing this spacetime is symmetric about a preferred spatial direction, and this renders all the background quantities to scalars, and the vector and tensor quantities of this background to vanish. In our case of spherical symmetry, the preferred spatial direction in this formalism is the areal radius.

For us to describe the propagation of the quantities, Eq. (8.6), we need to define the derivatives in this formalism. The derivative D_a is defined in the space of stationary observers

$$D_c\psi_{a\ldots b} \equiv h_c{}^d h_a{}^e \ldots h_b{}^f \nabla_d \psi_{e\ldots f}. \tag{8.7}$$

With this, we define the derivative along the vector 2-surfaces (orthogonal to u^a), the projected derivative onto the 2-surfaces respectfully:

$$\hat{\psi}_{a..b}{}^{c..d} \equiv e^f D_f \psi_{a..b}{}^{c..d} \ , \tag{8.8}$$

$$\delta_f \psi_{a..b}{}^{c..d} \equiv N_a{}^f \ldots N_b{}^g N_h{}^c .. N_i{}^d N_f{}^j D_j \psi_{f..g}{}^{i..j} \ . \tag{8.9}$$

The covariant derivative is

$$\mathrm{D}_a e_b = e_a a_b + \frac{1}{2}\phi N_{ab}, \tag{8.10}$$

where

$$a_a \equiv e^c D_c e_a = \hat{e}_a \qquad \text{acceleration of the sheet,} \tag{8.11}$$

$$\phi \equiv \delta_a e^a \qquad \text{sheet expansion along } e^a. \tag{8.12}$$

The other derivative is the change of e^a along u^a,

$$\dot{e}_a = \mathcal{A} u_a + \alpha_a, \qquad \alpha_a \equiv \dot{n}_{\bar{a}}, \quad \mathcal{A} = e^a \dot{u}_a. \tag{8.13}$$

where the scalar quantity that forms part of the description of an LRS spacetime in the (1+1+2) formalism, $\mathcal{A}$, is interpreted as the acceleration of the preferred spatial direction and more specifically in our case the acceleration of the areal radius.
The quantities a_a, ϕ and α_a are the fundamental objects of the spacetime in this formalism where their dynamics provides information about the spacetime geometry. The rest of the (1+1+2) scalar quantities are defined as

$$\Theta \equiv D_a u^a, \quad \Sigma \equiv \sigma^{ab}\left(e_a e_b - \frac{1}{2}N_{ab}\right), \quad \mathcal{E} \equiv C_{acbd} u^c u^d e^a e^b, \tag{8.14}$$

$$\mu \equiv T_{ab} u^a u^b, \quad p \equiv \frac{1}{3} T_{ab}\left(e^a e^b + N_{ab}\right), \quad Q \equiv \frac{1}{2} T_{ab} e^a u^b, \quad \Pi \equiv \frac{1}{2} T_{ab}(2e^a e^b - N^{ab}), \tag{8.15}$$

where they, respectfully, represent the expansion of the spacetime, shear, electric Weyl scalar, energy density, isotropic pressure, heat flux, and the ansisotropic stress/ pressure.

The propagation and constraint equations for an LRS class II spacetime are

Propagation equations

$$\hat{\phi} = -\frac{1}{2}\phi^2 + \left(\frac{1}{3}\Theta + \Sigma\right)\left(\frac{2}{3}\Theta - \Sigma\right) - \frac{2}{3}\mu - \frac{1}{2}\Pi - \mathcal{E}\,, \tag{8.16}$$

$$\hat{\Sigma} - \frac{2}{3}\hat{\Theta} = -\frac{3}{2}\phi\Sigma - Q, \tag{8.17}$$

$$\hat{\mathcal{E}} - \frac{1}{3}\hat{\mu} + \frac{1}{2}\hat{\Pi} = -\frac{3}{2}\phi\left(\mathcal{E} + \frac{1}{2}\Pi\right) + \left(\frac{1}{2}\Sigma - \frac{1}{3}\Theta\right)Q. \tag{8.18}$$

Evolution equations

$$\dot{\phi} = -\left(\Sigma - \frac{2}{3}\Theta\right)\left(\mathcal{A} - \frac{1}{2}\phi\right) + Q, \tag{8.19}$$

$$\dot{\Sigma} - \frac{2}{3}\dot{\Theta} = -\mathcal{A}\phi + 2\left(\frac{1}{3}\Theta - \frac{1}{2}\Sigma\right)^2 + \frac{1}{3}(\mu + 3p) - \mathcal{E} + \frac{1}{2}\Pi, \tag{8.20}$$

$$\dot{\mathcal{E}} - \frac{1}{3}\dot{\mu} + \frac{1}{2}\dot{\Pi} = \left(\frac{3}{2}\Sigma - \Theta\right)\mathcal{E} + \frac{1}{4}\left(\Sigma - \frac{2}{3}\Theta\right)\Pi + \frac{1}{2}\phi Q - \frac{1}{2}(\mu + p)\left(\Sigma - \frac{2}{3}\Theta\right). \tag{8.21}$$

Propagation/Evolution Equations

$$\dot{\mu} + \hat{Q} = -\Theta(\mu + p) - (\phi + 2\mathcal{A})Q - \frac{3}{2}\Sigma\Pi, \tag{8.22}$$

$$\dot{Q} + \hat{p} + \hat{\Pi} = -\left(\frac{3}{2}\phi + \mathcal{A}\right)\Pi - \left(\frac{4}{3}\Theta + \Sigma\right)Q - (\mu + p)\mathcal{A}, \tag{8.23}$$

$$\hat{\mathcal{A}} - \dot{\Theta} = -(\mathcal{A} + \phi)\mathcal{A} + \frac{1}{3}\Theta^2 + \frac{3}{2}\Sigma^2 + \frac{1}{2}(\mu + 3p)\,. \tag{8.24}$$

8.1 Including extra fluids

The Einstein field equations are nonlinear due to the structure of the Einstein tensor $G_{\mu\nu}$, which includes terms that depend nonlinearly on the metric and its derivatives. However, linear superposition applies to the energy-momentum tensor $T_{\mu\nu}$, which means that contributions from different matter or energy sources simply add together. The nonlinearity of gravity arises not from $T_{\mu\nu}$, but from the way spacetime curvature, represented by $G_{\mu\nu}$,

responds to these sources. If a fluid only interacts gravitationally, e.g., cold-dark matter and baryons, they have to be independently conserved. However, as we will see in the following chapters when considering higher-order curvature corrections to GR, the *curvature* fluid does not have to be independently conserved, as long as the total effective fluid is conserved. In our study, we limit ourselves to a non-interacting two-fluid configuration to maintain simplicity, and these are also sufficient to describe realistic approximations of the global structure of neutron stars, as concluded in [171]. However, strong interactions which occur in neutron stars usually require modeling multifluid components as a single entity with an equation of state that accounts for all the microphysics, and our reconstruction technique to finding relativistic star solutions in the context of $f(R)$ gravity is motivated by this. In the following chapters, we focus on the static, rotation-free LRS-II subclass to model non-rotating relativistic stars. The multifluid source and propagation equations for a static LRS II spacetime is

$$T^{\mathbf{tot}}_{ab} = \mu^{\mathbf{tot}} u_a u_b + (p^{\mathbf{tot}} + \Pi^{\mathbf{tot}}) e_a e_b + \left(p^{\mathbf{tot}} - \frac{1}{2}\Pi^{\mathbf{tot}} \right) N_{ab} + 2Q^{\mathbf{tot}} e_{(a} u_{b)}, \tag{8.25}$$

where in the case of staticity, $Q^{\mathbf{tot}} = 0$, the propagation equations are

$$\hat{\phi} = -\frac{1}{2}\phi^2 - \frac{2}{3}\mu^{\mathbf{tot}} - \frac{1}{2}\Pi^{\mathbf{tot}} - \mathcal{E} \ , \tag{8.26}$$

$$\hat{\mathcal{E}} - \frac{1}{3}\hat{\mu}^{\mathbf{tot}} + \frac{1}{2}\hat{\Pi}^{\mathbf{tot}} = -\frac{3}{2}\phi \left(\mathcal{E} + \frac{1}{2}\Pi^{\mathbf{tot}} \right) \ , \tag{8.27}$$

$$0 = -\mathcal{A}\phi + \frac{1}{3}\left(\mu^{\mathbf{tot}} + 3p^{\mathbf{tot}}\right) - \mathcal{E} + \frac{1}{2}\Pi^{\mathbf{tot}} \ , \tag{8.28}$$

$$\hat{p}^{\mathbf{tot}} + \hat{\Pi}^{\mathbf{tot}} = -\left(\frac{3}{2}\phi + \mathcal{A} \right) \Pi^{\mathbf{tot}} - \left(\mu^{\mathbf{tot}} + p^{\mathbf{tot}}\right) \mathcal{A} \ , \tag{8.29}$$

$$\hat{\mathcal{A}} = -\left(A + \phi\right) \mathcal{A} + \frac{1}{2}\left(\mu^{\mathbf{tot}} + 3p^{\mathbf{tot}}\right) \ , \tag{8.30}$$

and the Gaussian curvature is expressed as

$$K = \frac{1}{3}\mu^{\mathbf{tot}} - \mathcal{E} - \frac{1}{2}\Pi^{\mathbf{tot}} + \frac{1}{4}\phi^2. \tag{8.31}$$

The total energy density is denoted by $\mu^{\mathbf{tot}}$, the total isotropic pressure by $p^{\mathbf{tot}}$, the total energy flux by $q_a^{\mathbf{tot}}$, and the total PSTF anisotropic stress by $\pi_{ab}^{\mathbf{tot}}$. The superscript "**tot**" signifies that, in the presence of multiple fluid sources, each quantity represents the sum over all individual fluids. For example, for two fluids, $\mu^{\mathbf{tot}} = \mu_1 + \mu_2$, $p^{\mathbf{tot}} = p_1 + p_2$, and $\Pi^{\mathbf{tot}} = \Pi_1 + \Pi_2$.

Now that we have all the fundamental quantities describing our spacetime in the (1+1+2) covariant formalism, along with the propagation of the fluid sources and their kinematical quantities, we can write down the TOV equations governing the interior of a static, spherically symmetric spacetime containing a two-fluid source in the (1+1+2) covariant framework. This will be addressed in the next chapter.

CHAPTER 9

TOV EQUATIONS IN THE (1+1+2) THREADING

In this chapter, we construct a new dimensionless form of the TOV equations for a generalized $f(R)$ theory of gravity in the (1+1+2) covariant framework. This is the first representation of the TOV equations in this form for a generalized $f(R)$ theory of gravity [53]. Given that anisotropy naturally arises in $f(R)$ gravity, we maintain this generality for our fluid sources. This choice is also motivated by the relative ease of finding solutions with more general matter forms, as will be demonstrated in the forthcoming chapters. Previous research has highlighted the significant role of anisotropies in $f(R)$ gravity. For instance, in the context of $f(R)$ models of gravity, De Felice and Tsujikawa [85] studied anisotropy in charged or rotating black holes, while Nashed and Capozziello showed that anisotropic compact stars in these theories can model observationally consistent astrophysical objects in particular pulsars [208].

The physical origin of anisotropy in stellar configurations in gravity has been attributed to strong electromagnetic fields, exotic phase transitions and pion condensation [146] (and references therein), and the mixture of two gases (e.g., monatomic hydrogen, or ionized hydrogen and electrons) [176].

9.1 TOV equations in fourth-order gravity

A key advantage of $f(R)$ gravity theories is that their field equations can be reformulated to resemble those of General Relativity (GR) with an effective two-fluid source: one fluid representing non-minimally coupled matter and the other an effective *curvature* fluid [18–20, 59].

More generally, fourth-order gravity theories extend the Einstein-Hilbert action, Eq. (1.3), by including additional curvature invariants such as R, $R_{ab}R^{ab}$, and $R_{abcd}R^{abcd}$. A simple yet general form of such theories in highly symmetric four-dimensional spacetimes is defined by the action [35, 278]

$$\mathbb{A} = \frac{1}{2}\int d^4x\sqrt{-g}\left[f(R) + 2\mathcal{L}_m\right] \ , \tag{9.1}$$

where the Lagrangian $\mathcal{L}_m$ describes the matter field.

The general modified field equations are obtained by varying Eq. (9.1) with respect to the metric g_{ab}:

$$f'R_{ab} - \frac{1}{2}f g_{ab} - \nabla_b\nabla_a f' + g_{ab}\nabla_c\nabla^c f' = T^m_{ab}, \tag{9.2}$$

where $f \equiv f(R)$, and T^m_{ab} denotes the stress-energy tensor of the matter content. The above equation can be recast as

$$G_{ab} = T^{\mathbf{eff}}_{ab} = \tilde{T}^m_{ab} + T^R_{ab}, \tag{9.3}$$

where

$$T^R_{ab} \equiv \frac{1}{f'}\left[\frac{1}{2}(f - Rf')g_{ab} + \nabla_b\nabla_a f' - g_{ab}\nabla_c\nabla^c f'\right], \tag{9.4}$$

and

$$\tilde{T}^m_{ab} \equiv T^m_{ab}/f'. \tag{9.5}$$

Rearranging Eq. (9.2) to resemble Eq. (9.3), the higher-order corrections to Einstein's equations can be interpreted as an effective fluid. This reformulation allows the use of GR-based methods (e.g., [205, 206]) to derive analytical descriptions of the interior of a relativistic compact object containing a two-fluid source.

The trace of the field equations, Eq. (9.3), is given by

$$\begin{aligned} R =& \frac{1}{f'}(3p^m - \mu^m) + \frac{2f}{f'} - 3\frac{f'''}{f'}\nabla^a R \nabla_a R - 3\frac{f''}{f'}\nabla^2 R + 3\Theta\dot{R}\frac{f''}{f'} + \\ &+ 3\frac{f''}{f'}\ddot{R} + 3\frac{f'''}{f'}\dot{R}^2 - 3\dot{u}^c\frac{(\nabla_c f')}{f'}, \end{aligned} \tag{9.6}$$

and plays a crucial role in formulating the modified Tolman–Oppenheimer–Volkoff (TOV) equations, since it encapsulate the dynamics of the extra scalar degree of freedom that is intrinsic to $f(R)$ description of gravity.

The divergence of the Einstein tensor in Eq. (9.3) vanishes as a consequence of the twice contracted Bianchi identities. As a result, the divergence of the energy-momentum tensor must also vanish, implying that $T^{\mathbf{eff}}_{ab}$ is conserved. This leads to a key implication: if baryonic matter is conserved, then the total fluid is conserved as well. However, this does not necessarily mean that each individual fluid component is conserved independently[1], i.e.,

$$\nabla^b\left(\frac{T^m_{ab}}{f'}\right) = -\nabla^b T^R_{ab} = -\frac{f''}{f'^2}T^m_{ab}\nabla^b R. \tag{9.7}$$

We also emphasize that both T^R_{ab} and $\tilde{T}^m_{ab}$ in Eq. (9.3) represent *effective* fluids. As such, they may exhibit properties that would be nonphysical for a baryonic matter fluid. Analyzing the solutions presented in the following sections, we ensure that T^m_{ab} satisfies a set of conditions that guarantee the physical viability of the source fluid.

Consequently, our scheme parallels the two-fluid equations in the (1+1+2) framework,

[1]The field equations can be written in following form where the individual fluids are conserved: $G_{ab} = T^m_{ab} + f'\ T^R_{ab} + (1 - f')G_{ab}$.

discussed in Ch. 8, and is derived by merely setting

$$T_{ab}^{\mathbf{tot}} = T_{ab}^{\mathrm{eff}} \tag{9.8}$$

in Eqs. (8.26-8.30), or, equivalently, by choosing

$$\mu^{\mathbf{tot}} = T_{ab}^{\mathbf{eff}} u^a u^b = \frac{\mu^m}{f'} + \mu^R, \tag{9.9}$$

$$p^{\mathbf{tot}} = \frac{1}{3} T_{ab}^{\mathbf{eff}} \left(e^a e^b + 2N^{ab}\right) = \frac{p^m}{f'} + p^R, \tag{9.10}$$

$$\Pi^{\mathbf{tot}} = \frac{2}{3} T_{ab}^{\mathbf{eff}} \left(e^a e^b - N^{ab}\right) = \frac{\Pi_{ab}^m}{f'} + \Pi_{ab}^R, \tag{9.11}$$

$$Q^{\mathbf{tot}} = -\frac{1}{2} T_{bc}^{\mathbf{eff}} u^c e^b = -\frac{Q^m}{f'} + Q^R, \tag{9.12}$$

where the thermodynamical properties of the curvature fluid are defined as

$$\mu^R = \frac{1}{f'}\left(\frac{1}{2}(Rf' - f) + f''\hat{X} + f''X\phi + f'''X^2\right), \tag{9.13}$$

$$p^R = \frac{1}{f'}\left(\frac{1}{2}(f - Rf') - \frac{2}{3}f''\hat{X} - \frac{2}{3}f''X\phi - \frac{2}{3}f'''X^2 - \mathcal{A}f''X\right), \tag{9.14}$$

$$\Pi^R = \frac{1}{f'}\left(\frac{2}{3}f''\hat{X} + \frac{2}{3}f'''X^2 - \frac{1}{3}f''X\phi\right), \tag{9.15}$$

$$Q^R = -\frac{1}{f'}\left(f'''\dot{R}X + f''(\dot{X} - \mathcal{A}\dot{R})\right), \tag{9.16}$$

the hat-derivative of the Ricci scalar as $\hat{R} \equiv X$, and in the case of staticity $Q^R = 0$. Applying the covariant description and the previously defined variables, Eq. (9.6) takes the form $Rf = 3p^{\mathbf{eff}} - \mu^{\mathbf{eff}}$ or

$$Rf' - 2f = 3p^m - \mu^m - 3f''\hat{X} - 3f''X\phi + -3f'''X^2 - 3\mathcal{A}f''X\ . \tag{9.17}$$

For our purposes, a more useful form of the trace equation is

$$\hat{X} = \frac{p^m}{f''} - \frac{1}{3}\frac{\mu^m}{f''} - \frac{1}{3}\frac{f'}{f''}R + \frac{2}{3}\frac{f}{f''} - \frac{f'''}{f''}X^2 - X(\phi + \mathcal{A}). \tag{9.18}$$

When $f(R) = R$, the propagation equations, fluid quantities, and the field equations reduce to those of GR.

We have now established the mathematical framework to obtain a covariant description of the fundamental equations governing the interior of a compact relativistic object within $f(R)$ theories of gravity. The mathematical formulation is analogous to the Tolman–Oppenheimer–Volkoff (TOV) equations presented in [219, 267]. To facilitate both the analysis of their mathematical structure and the development of solution methods, they are expressed in terms of normalized variables.

We begin by defining a dimensionless radial coordinate, introducing the parameter ρ such that

$$\hat{X} = \phi X_{,\rho}. \tag{9.19}$$

To support the physical interpretation of our results, we relate the parameter ρ to the area radius r,

$$\rho = 2\ln\left(\frac{r}{r_0}\right), \tag{9.20}$$

where r_0 is an integration constant and it is set to $r_0 = 1$. In the following analysis, we perform calculations using ρ, but present the results in terms of r to facilitate comparison with what exists in the current literature.

The normalized variables are now introduced:

$$\Xi = \frac{\phi_{,\rho}}{\phi}, \qquad Y = \frac{\mathcal{A}}{\phi}, \qquad \frac{X}{\phi} \equiv \mathbb{X}, \qquad \mathcal{K} = \frac{K}{\phi^2}, \qquad E = \frac{\varepsilon}{\phi^2}, \tag{9.21}$$

$$\tilde{\mathbb{M}}^m = \frac{\tilde{\mu}^m}{\phi^2}, \qquad \tilde{P}^m = \frac{\tilde{p}^m}{\phi^2}, \qquad \tilde{\mathbb{P}}^m = \frac{\tilde{\Pi}^m}{\phi^2}, \tag{9.22}$$

$$\mathbb{M}^R = \frac{\mu^R}{\phi^2}, \qquad P^R = \frac{p^R}{\phi^2}, \qquad \mathbb{P}^R = \frac{\Pi^R}{\phi^2}. \tag{9.23}$$

Employing Eqs. (8.26)–(8.30), the modified (1+1+2) TOV equations for a two-fluid source

in the context of $f(R)$ theories of gravity are given by

$$\mathbb{X}_{,\rho} + \mathbb{X}\Xi = \frac{P^m}{f''} - \frac{\mathbb{M}^m}{3f''} - \frac{f'}{3f''}\frac{R}{\phi^2} + \frac{2}{3}\frac{f}{f''\phi^2} - \frac{f'''}{f''}\mathbb{X} - \mathbb{X}(1+Y), \tag{9.24}$$

$$P^{\rm tot}_{,\rho} + \mathbb{P}^{\rm tot}_{,\rho} = -Y\left(\mathbb{M}^{\rm tot} + P^{\rm tot}\right) - \mathbb{P}^{\rm tot}\left(2\Xi + Y + \frac{3}{2}\right) - 2\Xi P^{\rm tot}, \tag{9.25}$$

$$Y_{,\rho} = -Y\left(\Xi + Y + 1\right) + \frac{1}{2}\left(\tilde{\mathbb{M}}^m + \mathbb{M}^R\right) + \frac{3}{2}\left(\tilde{P}^m + P^R\right), \tag{9.26}$$

$$\mathcal{K}_{,\rho} = -\mathcal{K}(1+2\Xi), \tag{9.27}$$

with the following constraints

$$1 + 4Y - 4\mathcal{K} - 4(\tilde{P}^m + P^R) - 4(\tilde{\mathbb{P}}^m + \mathbb{P}^R) = 0, \tag{9.28}$$

$$1 + 2\Xi - 2Y + 2(\tilde{\mathbb{M}}^m + \mathbb{M}^R) + 2(\tilde{P}^m + P^R) + 2(\tilde{\mathbb{P}}^m + \mathbb{P}^R) = 0, \tag{9.29}$$

$$2(\tilde{\mathbb{M}}^m + \mathbb{M}^R) - 6Y - 6E + 6(\tilde{P}^m + P^R) + 3(\tilde{\mathbb{P}}^m + \mathbb{P}^R) = 0. \tag{9.30}$$

A general metric satisfying the TOV equations takes the form of [205]

$$ds^2 = -k_1(\rho)dt^2 + k_2(\rho)d\rho^2 + k_3(\rho)d\Omega^2, \tag{9.31}$$

where

$$k_3(\rho) = K_0 e^{\rho}, \tag{9.32}$$

$$d\Omega^2 = d\theta^2 + \sin^2\theta d\phi^2, \tag{9.33}$$

and K_0 is a constant. The (1+1+2) kinematical quantities in our spacetime configuration

corresponding to the static LRS-II class are

$$\phi = \frac{1}{\sqrt{k_2}}\,, \qquad Y = \frac{k_{1,\rho}}{2k_1}, \quad \Xi = -\frac{k_{2,\rho}}{k_2}, \tag{9.34}$$

$$\mathcal{A} = \frac{k_{1,\rho}}{2k_1\sqrt{k_2}}, \quad \mathcal{K} = \frac{k_2}{K_0 e^{\rho}}. \tag{9.35}$$

The metric coefficients of (9.31), in terms of the area radius, r, are

$$k_1(\rho) = k_1(r), \qquad k_2(\rho) = \frac{r^2}{4}k_2(r), \qquad r^2(\rho) = K_0 e^{\rho}. \tag{9.36}$$

To obtain realistic solutions to the TOV equations, we must define and impose the physical and boundary conditions appropriate for our two-fluid compact stellar model. This will be addressed in the next chapter.

CHAPTER 10

THE BOUNDARY AND ENERGY CONDITIONS

Not all solutions to the TOV equations correspond to physically realistic relativistic stars, as discussed by Delgaty and Lake in [89]. To describe stellar objects within a gravitational framework, it is necessary to define the thermodynamic properties throughout the stellar interior, as well as the conditions imposed at the surface, referred to as the junction conditions. Tolman, Oppenheimer, and Volkoff outlined the essential criteria for modeling a physical stellar structure and provided a general classification of the distinct regions a star should possess. In this chapter, we first summarize the general features of these regions, followed by a discussion of the energy and boundary conditions required in an $f(R)$ theory of gravity, extended to the (1+1+2) covariant formalism.

10.0.1 Vacuum exterior ($r > r_b$):

When the areal radius r is greater than the radius of the boundary of the matter distribution r_b, there is no spherically symmetric distribution of matter, i.e., $p = \rho = 0$. This is described by the most general spherically symmetric solution in empty space, the

Schwarzschild-de Sitter solution, which has the following metric potentials:

$$e^{-\lambda(r)} = 1 + \frac{A}{r}, \quad \text{and} \quad e^{\nu(r)} = B\left(1 + \frac{A}{r}\right). \tag{10.1}$$

The constants A and B are integration constants fixed by the weak field limit ($B = 1$ and $A = -2m$), and m is the total Newtonian mass of the matter distribution as measured by a distant observer.

10.0.2 Stellar interior ($r < r_b$):

In the case $r < r_b$ the fluid pressure has to be $p > 0$ and the energy density $\rho > 0$. (O-V) provides another condition that the solution depends on the equation of state of the fluid connecting p and ρ in terms of the areal radius r since there exist equations of state with a *sharp* boundary at a finite value of r_b.

10.0.3 Boundary ($r = r_b$):

The boundary is defined where the pressure vanishes, $p = 0$, at the finite radius $r = r_b$ and the energy density is still finite. This will describe a sphere that contains a quantified pressure and energy density with a definite boundary r_b. In addition, an assumption is made about the coordinate system of the matching surfaces. For mathematical simplicity, it is assumed that the spacetimes describing the interior and the exterior separately share the same coordinate system. This choice does not impose a physical restriction but instead facilitates a transparent implementation of the junction conditions, since no non-trivial coordinate transformation is required at the matching surface. It also has a motivation rooted in the physical meaning of a solution, that is, at $r = r_b$ for both solutions that describe the exterior and interior of a sphere, the physical measurements lead to the same results. Identifying the coordinate systems across the boundary ensures that observers located on the surface $r = r_b$ agree on invariant quantities such as proper time, circumferential radius, and radial distance. Thus, the boundary is not merely a

mathematical construction but a physical interface where both geometries describe the same measurable reality, and the continuity of the induced metric is implemented in the most direct and physically transparent way.

As mentioned, most TOV solutions do not correspond to any meaningful matter spacetime configuration. The article [89] lists the criteria for a static spherically symmetric interior solution of a single fluid in GR to be physically acceptable. A list of physically acceptable solutions in GR is tabulated in 10.1 and 10.2. The interior Schwarzschild solution is not listed since its constant energy density results in a sound speed that is undefined.

Tolman IV	$-B^2\left(1+\frac{r^2}{A^2}\right)dt^2+\frac{1+2\frac{r^2}{A^2}}{\left(1-\frac{r^2}{R^2}\right)\left(1+\frac{r^2}{A^2}\right)}dr^2+r^2d\Omega^2$
Wyman IIa $n\neq 2$ and $n\neq\sqrt{2}$	$\left(Ar^{1-n}-Br^{1+n}\right)^2dt^2+\left.\frac{1}{2-n^2}+ar^b\left[A(2-n)-B(2+n)r^{2n}\right]^c\right)^{-1}dr^2+r^2d\Omega^2$ here $b=2\frac{n^2-2}{n-2}$, $c=2\frac{2-n^2}{n^2-4}$
Buch1	$-A\left[(1+Cr^2)^{3/2}+B\sqrt{2-Cr^2}\,(5+2Cr^2)\right]^2dt^2+\frac{2\left(1+Cr^2\right)}{2-Cr^2}dr^2+r^2d\Omega^2$
Heint IIa	$-A^2\left(1+ar^2\right)^3dt^2+\left(1-\frac{3ar^2}{2}\frac{1+C\left(1+4ar^2\right)^{-\frac{1}{2}}}{1+ar^2}\right)^{-1}dr^2+r^2d\Omega^2$
Whitman II	$-\left(A^2\left(1+a\frac{r^2}{R^2}\right)+B\frac{r}{R\sqrt{2a}}\sinh\beta\left[1+\frac{R^2+2aa^2}{2ar^2}\times\left(1-\sqrt{10a}\frac{r}{\sqrt{R^2+2ar^2}}\coth\beta\right)\right]\right)dt^2$ $+B^2\left(1+2a\frac{r^2}{R^2}\right)\left(A^2\left(1+a\frac{r^2}{R^2}\right)+B\frac{r}{R\sqrt{2a}}\sinh\beta\right.$ $\left.\times\left[1+\frac{R^2+2ar^2}{2ar^2}\left(1-\sqrt{10a}\frac{r}{\sqrt{R^2+2ar^2}}\coth\beta\right)\right]\right)^{-1}dr^2+r^2d\Omega^2$ where $\beta=\sqrt{5}\,\mathrm{arcsinh}\sqrt{\frac{R^2}{2ar^2}}$
Whitman IV	$-fdt^2+\frac{a}{f}\left(1-b\frac{r^2}{R^2}\right)^3dr^2+r^2d\Omega^2$, where $f=\frac{r^2}{R^2}(g_p+g_h)$, $g_p=\frac{aR^2}{r^2}\left(1-\frac{3}{8}\frac{br^2}{R^2}-\frac{3}{4}\frac{b^2r^4}{R^4}+\frac{1}{2}\frac{b^3r^6}{R^6}\right)$, $g_h=C\left(1-\frac{br^2}{R^2}\right)^{3/2}\left[\frac{3}{4}\frac{\cos\beta}{\left(1-b\frac{r^2}{R^2}\right)^{3/2}}-\frac{3}{2}\sqrt{\frac{3}{b}}\frac{R\sin\beta}{r\left(1-b\frac{r^2}{R^2}\right)}-3R^2\frac{\cos\beta}{br^2\sqrt{1-b\frac{r^2}{R^2}}}+\frac{\sqrt{3}}{2}\frac{\sin\beta}{\left(\frac{br^2}{R^2}\right)^{3/2}}\right]$, and $\beta=2\sqrt{3}\arcsin\sqrt{\frac{br^2}{R^2}}$.
F-S	$-D^2\left(\left(B-A\sqrt{1+Cr^2}\right)\cos\sqrt{1+Cr^2}+\left(A+B\sqrt{1+Cr^2}\right)\sin\sqrt{1+Cr^2}\right)^2dt^2+$ $\left(1+Cr^2\right)dr^2+r^2d\Omega^2$

Table 10.1: Spherically symmetric static single fluid solutions in General Relativity that obeys all the physical criteria set by [89].

In the following section, we present the conditions on the thermodynamical quantities of a stellar object comprising baryonic matter. When modeling our system in the context

of $f(R)$ theories, by considering it as a two-fluid configuration, we note that the conditions on the baryonic matter fluid would not apply to the curvature fluid, since it is constructed as an *effective fluid*. Therefore, the thermodynamical quantities of the effective fluid can violate the energy conditions without compromising its interpretation of the solutions.

Given the inherently anisotropic nature of $f(R)$ models, we analyze these stellar configurations as anisotropic compact objects. To facilitate the physical interpretation of our solutions, we introduce two additional thermodynamic quantities: the radial and orthogonal pressures, expressed as

$$p_r = p + \Pi, \quad p_\perp = p - \frac{1}{2}\Pi. \tag{10.2}$$

Equation (10.2) allow us to establish the two essential sets of conditions required for modeling a physically consistent relativistic compact object, namely the energy and boundary conditions.

10.1 The energy conditions

To establish the physical validity of a solution to the TOV equations, we first impose constraints on the thermodynamic quantities. Specifically, for a physically relevant description of a relativistic stellar object, the thermodynamical quantities must remain positive at all points within the stellar interior. These conditions ensure that the solution adheres to fundamental physical requirements. Explicitly, they are

$$\mu^m \geq 0, \quad p_r^m \geq 0, \quad p_\perp^m \geq 0. \tag{10.3}$$

Consequently, these conditions guarantee that weak energy condition is always obeyed,

$$\mu^m + p_r^m \geq 0. \tag{10.4}$$

In general relativity, relativistic stellar models typically require that the gradients of thermodynamic quantities be negative throughout the interior. However, this condition does not necessarily hold in the cases we will explore. Nevertheless, a critical constraint remains: the sound speed within the matter sources must adhere to causal limits, ensuring that the propagation of sound waves do not exceed the speed of light, i.e.,

$$0 \leq c^2_{m,r} = \frac{\partial p^m_{,r}}{\partial \mu^m} \leq 1, \qquad 0 \leq c^2_{m,\perp} = \frac{\partial p^m_{,\perp}}{\partial \mu^m} \leq 1. \tag{10.5}$$

In the following section, we examine the boundary conditions which are pivotal in defining the star's structure and its transition to the external spacetime.

10.2 Junction Conditions

In relativistic astrophysics, it is customary to assume that compact stellar objects possess a "hard" boundary, meaning that matter is confined within a well-defined volume surrounded by a vacuum. A convenient way to model this configuration is to smoothly join the interior spacetime, describing the matter distribution, with an exterior vacuum spacetime. To achieve this matching in a general and covariant manner, we rely on a set of conditions developed by Israel [156], which provide the necessary framework for connecting two distinct spacetimes. These conditions are essential for ensuring the physical consistency of the star's boundary and its transition to the external vacuum.

In our context, we assume that the boundary's normal n_a is parallel to the vector field e_a. The Israel conditions are then:

$$[\gamma_{ab}]^+_- = 0\,, \tag{10.6}$$

$$[K_{ab}]^+_- - \gamma_{ab}[K]^+_- = -S_{ab}\,, \tag{10.7}$$

where the induced metric on the separation surface is given by $\gamma_{ab} = N_{ab} + u_a u_b$, the extrinsic curvature is denoted by K_{ab}, S_{ab} signifies the energy-momentum tensor of a

structure within the boundary surface $\mathcal{S}$ described by a shell. The quantities defined on the boundary surface $\mathcal{S}$ are referred to as the *jump of* χ, for example. Therefore, we introduce the notation $[\chi]^+_- = \chi^+ - \chi^-$, which will denote a *jump*. For algebraic simplicity, another parenthetical quantity is defined

$$\{\chi\} = \frac{1}{2}(\chi^+ + \chi^-). \tag{10.8}$$

These geometric conditions can be translated to conditions on the thermodynamical potentials of baryonic matter. In fact, Einstein's field equations become

$$S_{ab}\{K^{ab}\} + [T_{ab}e^a e^b]^+_- = 0, \tag{10.9}$$

by imposing the Israel junction conditions. This implies that on the boundary surface, the jump of the radial pressure has to obey the following condition:

$$[p_r]^+_- = 0. \tag{10.10}$$

When considering $f(R)$ theories of gravity an additional degree of freedom arises from the higher-order curvature terms. Therefore, to account for the additional scalar degree of freedom obtained, the Israel junction conditions must be generalized. Junction conditions in $f(R)$ theories of gravity were first explored in [90] and further expanded in [251, 252]. For a general review of junction conditions in theories with extra scalar degrees of freedom, see [243]. The general junction conditions for $f(R)$ models of gravity, in four dimensions,

are

$$[\gamma_{ab}]^+_- = 0\,, \tag{10.11}$$

$$[K]^+_- = 0\,, \tag{10.12}$$

$$[R]^+_- = 0\,, \tag{10.13}$$

$$f'(R)[K^*_{ab}]^+_- = -S^*_{ab}\,, \tag{10.14}$$

$$3f''(R)[e^a\nabla_a R]^+_- = S\,, \tag{10.15}$$

where

$$K^*_{ab} = K_{ab} - \frac{1}{3}\gamma_{ab}K, \tag{10.16}$$

$$S^*_{ab} = S_{ab} - \frac{1}{3}\gamma_{ab}S. \tag{10.17}$$

Our framework adopts an effective fluid interpretation of the field equations, therefore, following the approach usually performed in GR, it is worth translating the above into conditions on the thermodynamical quantities. Since the description of the interior of our stellar structure is equivalent to the two-fluid case in GR, the Israel junction conditions on the field equations are

$$S_{ab}\{K^{ab}\} + [T^{\rm tot}_{ab}e^a e^b]^+_- = 0. \tag{10.18}$$

In the absence of a shell within the boundary surface $\mathcal{S}$, i.e., $S^*_{ab} = 0$, this leads to

$$[T^{\rm eff}_{ab}e^a e^b]^+_- = [p^{\rm eff}_r]^+_- = 0. \tag{10.19}$$

From the definition of $p^{\rm eff}_r$, we have

$$\left[\frac{p^m_r}{f'} + p^R_r\right]^+_- = \left[\frac{p^m_r}{f'}\right]^+_- + \left[p^R_r\right]^+_- = 0. \tag{10.20}$$

By virtue of Eq. (10.13), $[f]^+_-$, $[f']^+_-$, and higher derivatives of f with respect to R vanish, assuming f contains no terms other than the cosmological constant. Consequently, we can expand the expression of the jump of p^R_r as

$$\begin{aligned}[p^R_r]^+_- &= \left[p^R + \Pi^R\right]^+_- \\ &= \left[\frac{f}{2f'}\right]^+_- - \left[\frac{f''}{f'}\right]^+_- \{X\}\{\phi\} - \left[\frac{f''}{f'}\right]^+_- \{X\}\{\mathcal{A}\},\end{aligned} \tag{10.21}$$

and using Eqs. (10.11-10.15), we find the condition $[p^R_r]^+_- = 0$. To ensure a smooth junction, we require that

$$[p^m_r]^+_- = [p^m + \Pi^m]^+_- = 0. \tag{10.22}$$

We find that this is consistent with the results in [251, 252]. However, unlike in general relativity (GR), this is not the sole constraint on the matter fluid. Since the trace of the field equations can be expressed as

$$R = 3p^{\rm tot} - \mu^{\rm tot}, \tag{10.23}$$

the jump of R, Eq. (10.13), implies that

$$\begin{aligned}0 = [R]^+_- &= \left[\frac{3p^m - \mu^m}{f'} - \frac{f''}{f'}\hat{X}\right]^+_- \\ &= [3p^m - \mu^m]^+_- - \frac{f''}{f'}\left[\hat{X}\right]^+_-,\end{aligned} \tag{10.24}$$

must hold at the boundary. As a result, a constraint on the energy density and isotropic pressure at the boundary is imposed via this relation.

The junction conditions analyzed so far imply that a mismatch is allowed across the extrinsic curvature or in the derivative of the Ricci scalar, provided the boundary $\mathcal{S}$ supports the matter distribution described by the tensor S_{ab}. When this mismatch occurs, it implies that a shell is present within the boundary surface. Given the extrinsic curvature

of $\mathcal{S}$ is

$$\begin{aligned} K_{ab} &= \gamma_a{}^c \gamma_b{}^d \nabla_c e_d \\ &= (N_a{}^c + u_a u^c)(N_b{}^d + u_b u^d)\nabla_c e_d, \end{aligned} \tag{10.25}$$

and the jump of the extrinsic curvature in the presence of spherical symmetry is

$$[K_{ab}]^+_- = \left[\frac{1}{2}\phi N_{ab} - u_a u_b \mathcal{A}\right]^+_-. \tag{10.26}$$

Equations (10.14) and (10.15) gives the stress-energy tensor on the boundary as

$$\begin{aligned} S_{ab} &= (N_{ab} + u_a u_b) f''[X]^+_- - f'[K_{ab}]^+_- \\ &= u_a u_b \left(f'[\mathcal{A}]^+_- + f''[X]^+_-\right) + N_{ab}\left(f''[X]^+_- - \frac{f'}{2}[\phi]^+_-\right). \end{aligned} \tag{10.27}$$

When Eq. (10.27) is non-zero, a shell is present with an energy density and orthogonal pressure given by

$$\mu^{\mathcal{S}} = S_{ab} u^a u^b, \tag{10.28}$$

$$p^{\mathcal{S}}_{\perp} = \frac{1}{2} S_{ab} N^{ab}. \tag{10.29}$$

In the case of staticity along with spherical symmetry, the radial pressure at the boundary surface $\mathcal{S}$ is zero, i.e., $p^{\mathcal{S}}_r = S_{ab} e^a e^b = 0$. To ensure that the shell represents a physical structure, the usual criterion is $\mu^{\mathcal{S}} \geq 0$ and $p^{\mathcal{S}}_{\perp} \geq 0$. However, given that the weak energy condition is obeyed, the orthogonal pressure is allowed to have negative values, i.e., $p^{\mathcal{S}}_{\perp} < 0$. In this case, a negative orthogonal pressure describes a tension on the shell.

As discussed by Senovilla in [251, 252], shells in theories of $f(R)$ gravity can possess what is called a *double layer*. In theories with $f'''(R) = 0$, such structures arise when Eq. (10.13) is not satisfied. On the boundary surface, the energy-momentum tensor becomes more complex, with several normal components emerging that depend on $[R]^+_-$.

In our case, the total energy-momentum tensor, taking the double layer into account, is

$$\bar{S}_{ab} + \bar{\varsigma}_{ab} = S_{ab} + \varsigma_{ab} + \varsigma_a e_b + \varsigma e_a e_b + \bar{\varsigma}_{ab}, \tag{10.30}$$

where

$$\varsigma_{ab} = f'' \{K_{ab}\} [R]^+_- , \tag{10.31}$$

$$\varsigma_a = f'' \left(N^b{}_a + u^b u_a\right) \nabla_b [R]^+_- , \tag{10.32}$$

$$\varsigma = f'' \{K\} [R]^+_- . \tag{10.33}$$

The term $\bar{\varsigma}_{ab}$ represents the energy-momentum tensor of the double layer, and its physical interpretation is analogous to a dipole distribution,

$$\bar{\varsigma}_{ab} = f'' \nabla_\rho \left[[R]^+_- \gamma_{ab} e^\rho \delta^\Sigma \right] = f'' \Delta_{ab}, \tag{10.34}$$

where δ^Σ is a scalar distribution (Dirac delta) with support on the hypersurface Σ (see Fig. 10.1 and [252]), Δ_{ab} describes the distribution of the double layer, and f'' is a constant in Starobinsky gravity. We also note that the terms ς_a and ς in Eq. (10.35) require the presence of $\bar{\varsigma}_{ab}$, however, the converse is not necessarily true.

Performing a decomposition of the stress-energy tensor of the shell $\bar{S}_{ab}$ along u^a, e^a and N_{ab} gives

$$\bar{S}_{ab} = \bar{\mu}^S u_a u_b + \bar{p}^S_r e_a e_b + \bar{p}^S_\perp N_{ab} + 2\bar{Q}^S u_{(a} e_{b)} + \bar{Q}^S_{(a} e_{b)}, \tag{10.35}$$

where the thermodynamical description of the shell in terms of the geometrical quantities

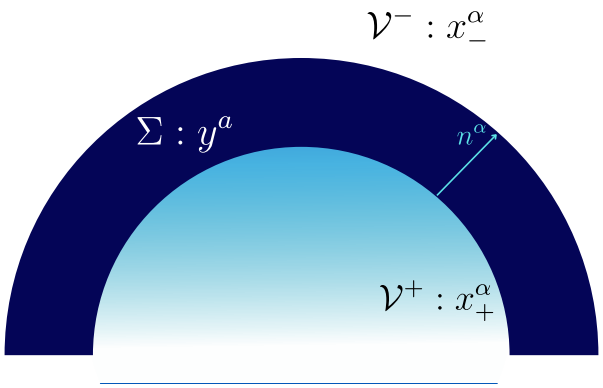

Figure 10.1: We define conditions on the matching hypersurface Σ to ensure a smooth matching between the spacetimes $\mathcal{V}^-$ and $\mathcal{V}^+$.We assume that the regions $\mathcal{V}^\pm$ share the same coordinate system and choose the unit normal n^α to the hypersurface Σ, to point from $\mathcal{V}^-$ to $\mathcal{V}^+$.

is given by

$$\bar{\mu}^{\mathcal{S}} = f'[\mathcal{A}]^+_- + f''[X]^+_- - f''\{\mathcal{A}\}[R]^+_-, \tag{10.36}$$

$$\bar{p}^{\mathcal{S}}_r = f''\{K\}[R]^+_-, \tag{10.37}$$

$$\bar{p}^{\mathcal{S}}_\perp = -\frac{1}{2}f'\,[\phi]^+_- + f''[X]^+_- + f''\{\phi\}[R]^+_-, \tag{10.38}$$

$$\bar{Q}^S = f''\left(u^b\nabla_b[R]^+_-\right)u_a, \tag{10.39}$$

$$\bar{Q}^S_a = f''\delta_a[R]^+_-. \tag{10.40}$$

In the static case, the scalar and vector heat flux, Eqs. (10.39) and (10.40) are zero. The decomposition of the energy-momentum tensor of the double layer $\bar{\varsigma}_{ab}$ is given by

$$\bar{\varsigma}_{ab} = f''\left(\Delta_u u_a u_b + \frac{1}{2}\Delta_N N_{ab}\right), \tag{10.41}$$

where $\Delta_u = \Delta_{ab}u^a u^b$ and $\Delta_N = \Delta_{ab}N^{ab}$.

A summary of the energy requirements and boundary conditions is provided in Tables 10.3 and 10.4, respectively.

Tolman VII	$-B^2 \sin^2 \ln \sqrt{\frac{1}{C}\left(\sqrt{1-\frac{r^2}{R^2}+4\frac{r^4}{A^4}}+2\frac{r^2}{A^2}-\frac{1}{4}\frac{A^2}{R^2}\right)}dt^2 + \left(1-\frac{r^2}{R^2}+4\frac{r^4}{A^4}\right)^{-1}dr^2 + r^2 d\Omega^2$
P-V IIa $b > c$	$-\left[A\cos\left(\frac{1}{2}\operatorname{arcsinh}\left(\frac{b^2r^2-c}{\sqrt{b^2-c^2}}\right)+d\right)+B\sin\left(\frac{1}{2}\operatorname{arcsinh}\left(\frac{b^2r^2-c}{\sqrt{b^2-c^2}}\right)+d\right)\right]^2 dt^2 + \left(b^2r^4-2cr^2+1\right)^{-1}dr^2 + r^2 d\Omega^2$
Nariai IV	$-A\cos^2\left(a-\frac{\sqrt{2}M}{4}r^2\right)\cos^{-2}\left(b+\frac{M}{4}r^2\right)dt^2 + A\cos^{-2}\left(b+\frac{M}{4}r^2\right)\left(dr^2+r^2d\Omega^2\right)$
Mehra	$-\left[\sqrt{1-\frac{16\pi a^2\rho_c}{15}}\cos\left(\frac{z_1-z}{2}\right)-\frac{2a}{3}\sqrt{\frac{2\pi\rho_c}{5}}\sin\left(\frac{z_1-z}{2}\right)\right]^2 dt^2 + \left[1-\frac{8\pi\rho_c}{15}\left(5r^2-\frac{3r^4}{a^2}\right)\right]^{-1}dr^2 + r^2d\Omega^2,$ where $a^2 < \frac{9}{10\pi\rho_c}$, $z = \ln\left(\frac{r^2}{a^2}-\frac{5}{6}+\sqrt{\frac{r^4}{a^4}-\frac{5r^2}{3a^2}+\frac{5}{8\pi a^2\rho_c}}\right)$, and $z_1 = \ln\left(\frac{1}{6}+\sqrt{\frac{5}{8\pi a^2\rho_c}-\frac{2}{3}}\right)$.
Kuch2 III	$-Be^{\frac{Ar^2}{2}}dt^2 + \left\{1+r^2e^{-\frac{1}{2}Ar^2}\left[C-\frac{A}{2e}\mathrm{Ei}\left(1+\frac{Ar^2}{2}\right)\right]\right\}^{-1}dr^2 + r^2d\Omega^2$
Gold III	$-A\left(\frac{g-1}{g+1}\right)dt^2 + B\left(1+\frac{1}{g}\right)^2\left(dr^2+r^2d\Omega^2\right),$ where $g = \cosh(a+br^2)$.
M-W I	$-\left(1+a\frac{r^2}{R^2}\right)\left(A\sin z + B\cos z\right)^2 dt^2 + \left(1+2a\frac{r^2}{R^2}\right)dr^2 + r^2d\Omega^2,$ where $z = \sqrt{1+2a\frac{r^2}{R^2}} - \tan^{-1}\sqrt{1+2a\frac{r^2}{R^2}}$.
Durg IV	$-A\left(1+Cr^2\right)^4 dt^2 + \left(\frac{7-10Cr^2-C^2r^4}{7(1+Cr^2)^2}+\frac{KCr^2}{(1+Cr^2)^2(1+5Cr^2)^{\frac{5}{2}}}\right)^{-1}dr^2 + r^2d\Omega^2$
Durg V	$-A\left(1+Cr^2\right)^5 dt^2 + \left(\frac{1-\frac{Cr^2(309+54Cr^2+8C^2r^4)}{112}+\frac{KCr^2}{\sqrt[3]{1+6Cr^2}}}{(1+Cr^2)^3}\right)^{-1}dr^2 + r^2d\Omega^2$

Table 10.2: Spherically symmetric single fluid solutions in GR obeying the physical criteria set in [89]. These solutions have a sound speed (c_s^2) that is monotonically decreasing as the radius increases.

Energy Condition	**Mathematical form**	**Meaning**
Positivity	$\mu^m \geq 0,\ p_r^m \geq 0,\ p_\perp^m \geq 0,$ Eq. (10.3).	Physical energy density and pressures inside the star must be non-negative.
Weak energy condition (WEC)	$\mu^m + p_r^m \geq 0$, Eq. (10.4).	Ensures physically meaningful matter; implied when the above positivity conditions hold.
Causality	$0 \leq c_{m,r}^2 \leq 1,\ 0 \leq c_{m,\perp}^2 \leq 1,$ Eq. (10.5).	Ensures propagation of perturbations does not exceed the speed of light.
Shell ($S_{ab} \neq 0$)	$\mu^{\mathcal{S}} \geq 0,\ p_\perp^{\mathcal{S}} \geq 0,\ p_r^{\mathcal{S}} = 0,$ Eqs. (10.28) and (10.29).	The radial pressure on the shell only vanishes in static spherically symmetric spacetimes.
When WEC obeyed	$p_\perp^{\mathcal{S}} \leq 0$	Represents a tension on the shell.

Table 10.3: A summary of the required energy conditions of the stellar interior and on the shell.

Boundary Condition	**Mathematical form**	**Meaning**
Continuity of induced metric.	$[\gamma_{ab}]^+_- = 0$, Eq. (10.6).	Geometry of the boundary surface must be the same from both sides. This condition is the same in GR and $f(R)$.
Extrinsic curvature jump gives shell-stress energy.	$[K_{ab}]^+_- - \gamma_{ab}[K]^+_- = -S_{ab}$, Eq. (10.7).	GR: $[K_{ab}]^+_- \neq 0$ allows a surface layer of matter. No shell: $S_{ab} = 0$.
Traceless part of extrinsic curvature jump.	$f'(R)[K^*_{ab}]^+_- = -S^*_{ab}$, Eq. (10.14).	Shell stress tensor is modified by $f'(R)$. No shell: $S^*_{ab} = 0$.
Trace of extrinsic curvature continuous.	$[K] = 0$, Eq. (10.12).	Extra requirement from higher-order field equations.
Ricci scalar continuous.	$[R] = 0$, Eq. (10.13).	Eliminates certain singular layers unless double layer structures are present.
Derivative of R jump condition.	$3f''(R)[e^a\nabla_a R]^+_- = S$, Eq. (10.15).	Scalar degree of freedom introduces new shell terms. No shell: $S = 0$.
Effective radial pressure continuity.	$[p_r^{\text{eff}}]^+_- = 0$, Eq. (10.19).	No discontinuity in the radial pressure unless shells exists. Generalization of the GR pressure condition.
Radial pressure continuity.	$[p_r^R]^+_- = 0$, $[p_r^m]^+_- = 0$, Eq. (10.22).	Ensures a smooth junction in $f(R)$ theories.
Constraint from trace equation.	$[3p^m - \mu^m]^+_- - \frac{f''}{f'}\left[\hat{X}\right]^+_- = 0$, Eq. (10.24).	Additional matter constraint at the boundary due to R continuity.
Ricci scalar does not match across the boundary.	$[R]^+_- \neq 0$.	Double layer appears, but only when $f'''(R) = 0$. This structure is unique to $f(R)$ gravity. GR has no distributional dipole layers.

Table 10.4: A summary of the boundary conditions.

CHAPTER 11

ANALYTICAL DESCRIPTIONS OF INTERIOR STELLAR STRUCTURES IN QUADRATIC GRAVITY

In this chapter, the new solutions we obtained in [53] are presented. The framework for finding new exact solutions to the modified TOV equations is outlined, and to illustrate its implementation we consider a quadratic model of gravity for two cases of the single fluid metric anzats: 1) an interior Schwarzschild-Tolman IV (IS-TIV) metric, and 2) a generic spherically symmetric metric that recovers the Newtonian limit but with a quartic radial correction.

11.1 The model and fluid description

Among the various possible forms of the function $f(R)$, a natural extension of GR is including a quadratic correction in the Ricci scalar to the Einstein-Hilbert action. Minimally coupled to matter, the gravitational action is given by

$$\mathcal{S}_R = \frac{1}{2}\int d^4x\sqrt{-g}\left[R + \alpha R^2 + 2\mathcal{L}_m\right] \ . \tag{11.1}$$

When the constant parameter α is positive, this is known as the *Starobinsky model* [262]. Originally, it was introduced as an effective action capturing quantum corrections to the matter content of spacetime. In a cosmological context, Starobinsky demonstrated that his model can produce an inflationary phase without requiring an additional scalar field [262]. Furthermore, in Part I, we showed that Starobinsky inflation can follow a cosmological bounce.

A key feature of this model, relevant to our study, is that the Schwarzschild solution is the only static, spherically symmetric, asymptotically flat solution with a regular horizon [198]. As such, it serves as an ideal description of the exterior spacetime of a compact object and has been widely investigated within the context of spherically symmetric spacetimes in modified gravity theories [22, 27, 120, 127, 285].

In the next section, the reconstruction method will require a specific form for the function f. A quadratic form is chosen based on three main motivations: (i) its established significance within cosmology and quantum field theory in a curved spacetime setting, (ii) the simplicity of its mathematical structure, which, as will be demonstrated, aids in obtaining exact solutions, and (iii) that the Starobinsky model represents the simplest extended theory of gravity that enables the study of double layers.

11.2 Reconstruction algorithm

In this section, building on the results presented in [205, 206] and employing the modified TOV equations, Eqs. (9.25–9.30), we develop a reconstruction method that enables the generation of new exact solutions to interior compact stellar objects.

Once the function f is specified, the next step in the reconstruction algorithm is to choose a base metric. A natural choice is to choose the metric coefficients from two known static spherically symmetric single-fluid solutions in general relativity and combine them to construct a new static spherically symmetric metric. One benefit of this approach is that it increases the likelihood of obtaining physically meaningful results. In particular,

the mismatch between the two metrics naturally introduces an anisotropic contribution, also a general feature of $f(R)$ theories of gravity. Nonetheless, this is not always the most suitable approach to adopt. Therefore, we will also consider an entirely general form for the starting metric.

Assuming a specific form for the metric tensor determines the quantities Y and $\mathcal{K}$, as they are directly related to the metric components via Eqs. (9.34)–(9.35). With these quantities, the Ricci scalar can be computed explicitly. This, in turn, allows us to express the thermodynamical quantities of the effective curvature fluid directly in terms of the metric coefficients.

Considering Eqs. (9.26), (9.27), (9.28) and (9.29), we can find new solutions to the baryonic matter fluid from quantities that are constructed from the metric alone:

$$R = \frac{\phi^2\left(\mathcal{K}\left(4\mathcal{K} - 4Y_{,\rho} - 2Y(2Y+1) - 1\right) + 2(Y+1)\mathcal{K}_{,\rho}\right)}{2\mathcal{K}}, \tag{11.2}$$

$$\widetilde{\mathbb{M}}^m = -\frac{-2\mathcal{K}_{,\rho} - 4\mathcal{K}^2 + \mathcal{K} + 4\mathcal{K}\mathbb{M}_R}{4\mathcal{K}}, \tag{11.3}$$

$$\widetilde{P}^m = -\frac{2\mathcal{K}_{,\rho} + 4\mathcal{K}^2 - \mathcal{K} + 12\mathcal{K}P_R - 8\mathcal{K}Y_{,\rho} + 4Y\mathcal{K}_{,\rho} - 8\mathcal{K}Y^2 - 4\mathcal{K}Y}{12\mathcal{K}}, \tag{11.4}$$

$$\widetilde{\mathbb{P}}^m = -\frac{6\mathbb{P}_R\mathcal{K} - \mathcal{K}_{,\rho} + 4\mathcal{K}^2 - \mathcal{K} + 4\mathcal{K}Y_{,\rho} - 2Y\mathcal{K}_{,\rho} + 4\mathcal{K}Y^2 - 4\mathcal{K}Y}{6\mathcal{K}}, \tag{11.5}$$

where

$$\mathbb{M}^R = \frac{R}{2\phi^2} + \frac{f''}{f'}\left(R_{,\rho\rho} + R_{,\rho} + \Xi R_{,\rho}\right) - \frac{1}{2\phi^2}\frac{f}{f'}, \tag{11.6}$$

$$P^R = -\frac{R}{2\phi^2} - \frac{2}{3}\frac{f''}{f'}\left(R_{,\rho\rho} + R_{,\rho} + \Xi R_{,\rho} + \frac{3}{2}YR_{,\rho}\right) + \frac{1}{2\phi^2}\frac{f}{f'}, \tag{11.7}$$

$$\mathbb{P}^R = \frac{2}{3}\frac{f''}{f'}\left(R_{,\rho\rho} - \frac{1}{2}R_{,\rho} + \Xi R_{,\rho}\right). \tag{11.8}$$

Equations (11.3–11.5) satisfy the constraints given by Eqs. (9.28–9.30) and, as a result, naturally fulfill the TOV equations. Although Eqs. (11.3–11.5) represent an infinite family of solutions, not all of them correspond to physically meaningful configurations. In particular, to model physically consistent stellar objects in $f(R)$ theories of gravity, it

is crucial that the junction and energy conditions outlined in Chapter 10 are satisfied.

11.3 Reconstruction of quadratic gravity models using the Interior Schwarzschild-Tolamn IV metric

We consider a combination of two of the simplest interior solutions for relativistic stars: the interior Schwarzschild and Tolman IV metrics. Specifically, we take the metric component k_1 to correspond to that of the Interior Schwarzschild solution, while the component k_2 is chosen to match the Tolman IV solution, both expressed in terms of the area radius

$$k_1(r) = a_0(c_1 + z)^2, \qquad k_2(r) = \frac{\mathcal{R}^2(A^2 + 2r^2)}{(\mathcal{R}^2 - r^2)(A^2 + r^2)}, \tag{11.9}$$

where $z = \sqrt{3 - \mu_1 r^2}$ and a_0, c_1, μ_1, A and R are constants. It is important to note that, in the original solution, μ_1 is a constant associated with the uniform density of the source. In our context, however, it is treated merely as an additional parameter.

The kinematical quantities defined in Eq. (9.21)-(9.23), in terms of the metric coefficients for this spacetime configuration and the parameter ρ, are

$$Y_{\rm IS} = \frac{\mu_1 e^{\rho}}{2\mu_1 e^{\rho} - 2c_1\sqrt{3 - \mu_1 e^{\rho}} - 6}, \tag{11.10}$$

$$\mathcal{K}_{\rm TIV} = \frac{-\mathcal{R}^2(A^2 + 2e^{\rho})}{4(A^2 + e^{\rho})(e^{\rho} - \mathcal{R}^2)}, \tag{11.11}$$

$$\phi = \frac{e^{-\frac{\rho}{2}}}{\sqrt{\mathcal{K}_{\rm TIV}}}. \tag{11.12}$$

As previously noted, the main difficulty in obtaining physically viable solutions lies in satisfying stringent boundary and thermodynamical conditions. In particular, we must ensure the existence of parameter sets that meet the criteria outlined in Chapter 10. Additionally, the interior solution is matched to an exterior Schwarzschild geometry.

With the ansatz given by Eqs. (11.10–11.11), the Ricci scalar R, as expressed in

Eq. (11.2), turns out to be independent of the Starobinsky parameter α. We were only able to find solutions consistent with physical constraints for the specific choice $\alpha = 0.001$. As shown in Part I, this value also preserves the stability of the model, allowing Starobinsky inflation to follow a cosmological bounce. In natural units, this corresponds to $\alpha \sim 10^2$ cm^2, which is consistent with the bounds reported in [23].

With the chosen parameters in Figs. 11.1–11.5, our solution exhibits a shell featuring a double layer. This arises because the radial pressure and the Ricci scalar, R, of the matter do not vanish at the stellar boundary simultaneously. Using the results of Chapter 10, we can determine the physical characteristics of the matter that makes up this shell. The total fluid thermodynamics on the boundary surface $\mathcal{S}$, accounting for both the shell and the double layer strength, are given by

$$\bar{\mu}^{\mathcal{S}} = 2\alpha[X]^+_- + (1+2\alpha R)[\mathcal{A}]^+_- - 2\alpha\{\mathcal{A}\}[R]^+_-, \tag{11.13}$$

$$\bar{p}^{\mathcal{S}}_r = 2\alpha\left(\{\phi\} + \{\mathcal{A}\}\right)[R]^+_-, \tag{11.14}$$

$$\bar{p}^{\mathcal{S}}_\perp = 2\alpha[X]^+_- - \frac{1}{2}(1+2\alpha R)[\phi]^+_- + f''\{\phi\}[R]^+_-. \tag{11.15}$$

Using the parameter values in Figs. 11.1–11.5 the energy density along the surface $\mathcal{S}$ is $\bar{\mu}^{\mathcal{S}} > 0$. This satisfies the weak energy condition and indicates that the shell is made of non-exotic material. However, the orthogonal pressure along the surface $\mathcal{S}$, is negative, i.e., $\bar{p}^{\mathcal{S}}_\perp < 0$, while $\bar{p}^{\mathcal{S}}_r > 0$. The negative orthogonal pressure means that the surface pulls inwards onto itself, like a taut membrane, a signature of surface tension, while the positive radial pressure prevents the shell from collapsing radially inwards. As, $\bar{\mu}^{\mathcal{S}} + \bar{p}^{\mathcal{S}}_r > 0$, the weak energy condition holds, and we deduce that the shell signifies a tension on the boundary surface. The complete expressions for the jump quantities in Eqs. (11.13)–(11.15), the Ricci scalar, and the total thermodynamical quantities is in Appendix A.1.

To further clarify the physical picture of the shell and its accompanying double-layer structure, it is useful to draw an analogy with electrostatics and familiar real-world scenarios. The shell behaves as a membrane with finite, nonzero surface density and pressure,

similar to a soap bubble whose thin surface layer possesses its own energy density and tension, distinct from the interior and exterior media. The double layer structure plays the role of a gravitational analog to an electrostatic dipole layer: just as a surface charge produces a discontinuity in the electric potential and a dipole layer produces a discontinuity in the electric field (the derivative of the potential), the gravitational double layer induces a discontinuity in the Ricci scalar, which depends on derivatives of the metric across the boundary. This double layer introduces the shell with an intrinsic dipole moment, giving it an internal structure. Consequently, the shell is not merely a membrane with tension; rather, the double layer actively maintains the orthogonal tension by resisting deformations that would modify the surface curvature.

Altogether, the physical interpretation of our solution is that the star's outer boundary forms a stable, tension-supported membrane arising from the interplay between the interior $f(R)$ geometry and the exterior Schwarzschild vacuum.

Identifying a particular solution that meets the conditions outlined in Ch. 10 is insufficient to support the proposed solution. It is also essential to demonstrate that there exists a broader region in the parameter space where the conditions in Ch. 10 are met. To this end, we employ computational techniques, specifically, a parameter space analysis. The sampling method of the model parameters, μ, A, $\mathcal{R}$, and c_1 used in Fig. 11.5 are described in Appendix B.

Given that the most stringent physical constraint is the causality condition on the matter fluid, we performed a conditional check to test this requirement across the parameter combinations. Parameter sets that satisfy this condition were recorded and plotted, allowing us to identify clusters within the parameter space. These clusters help narrow the parameter ranges and increase the likelihood of identifying solutions that fulfill the conditions outlined in Eq. (10.3). Solutions satisfying the physical criteria from Ch. 10 are shown in Figs. 11.1–11.3.

As previously emphasized, the curvature fluid is an effective construct and therefore

is not subject to the same physical constraints as baryonic matter. Nevertheless, we can assess its impact on the thermodynamics of the baryonic fluid. Notably, the energy density, as well as the radial and orthogonal pressures of the curvature fluid (see Fig. 11.4), are significantly smaller than those of the baryonic matter fluid (see Fig. 11.2).

While this behavior could be attributed to the chosen value of the Starobinsky parameter, $\alpha = 0.001$, it is not solely dependent on it. In fact, in the next section, we explore cases with even smaller values of α that still yield comparable thermodynamical contributions from both the curvature and baryonic matter fluids. This outcome is a manifestation of the theory's inherent nonlinearity: even minor deviations from the Einstein-Hilbert action can lead to solutions that differ significantly from those in General Relativity.

Figure 11.5 demonstrates the likelihood of identifying parameter sets that satisfy the causal condition for the radial baryonic matter fluid alone, by slightly perturbing the parameters from those of a physically consistent solution. In Figures 11.6, 11.7, 11.8, and 11.9, we show the fluid properties of both the matter and the effective curvature fluids for different values of α.

We observe that the parameter α influences the slope of the energy density (Fig. 11.6) and the pressures, especially those of the baryonic matter fluid, near the core ($r = 0$) of the stellar object (Fig. 11.7). Specifically, as α increases, the squared radial and orthogonal sound speeds, $c^2_{m,r}$ and $c^2_{\perp,r}$, tend to become negative close to the center. Interestingly, regardless of the value of α, the energy density of matter converges to the same value near the boundary of the star.

By comparing the orthogonal and radial pressures, we find that, for these parameter values, the solution describes a "quasi-isotropic object," similar to those identified in [57] for a single-fluid scenario. Such objects arise when the radial and orthogonal pressures behave similarly, although anisotropies still affect other physical parameters. This can be seen for the radial and orthogonal sound speeds, where they show relatively distinct behaviors. In particular, the orthogonal sound speed reaches a minimum near the star's

center, corresponding to a peak in anisotropy.

The effective fluid arising from curvature invariants has an energy density and pressure significantly lower than those of baryonic matter, indicating that the solution primarily represents a baryonic matter object with a structure different from its GR counterpart. Furthermore, the curvature fluid shows positive energy density and pressure (see Fig. 11.4). As α increases, the pressure of the curvature fluid increases alongside the energy density of the baryonic matter, while the pressures of the baryonic matter fluid tend to decrease overall (see Figs. 11.6 and 11.7). Interestingly, near the center of the star, the matter sound speeds change drastically, becoming rapidly negative (see Fig. 11.8).

In the next section, we carry out the reconstruction beginning with a fully general metric defined by polynomial and rational functions.

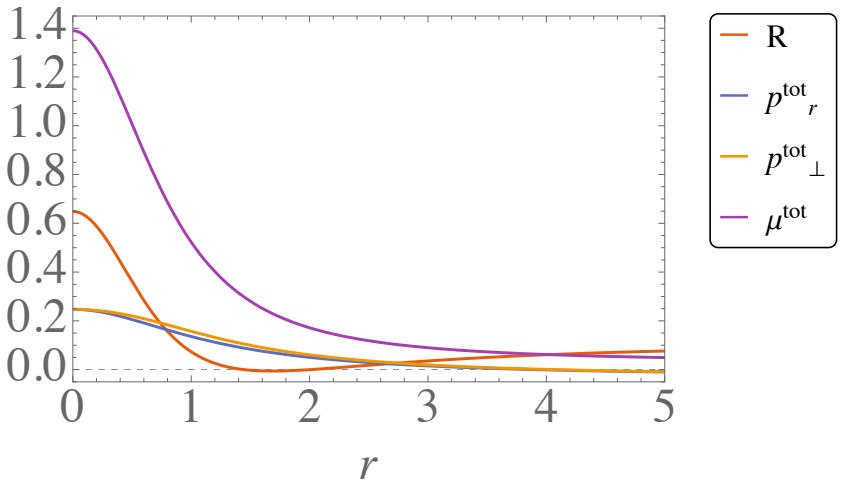

Figure 11.1: Solution for Starobinsky gravity where $\alpha = 0.001$, applied to the interior Schwarzschild–Tolman IV (IS-TIV) metric as discussed in Sec. 11.3. The parameter values used in this solution are: $\mu_1 = -1.25$, $\mathcal{R} = 7.3$, $c_1 = 0.3$, and $A = 1.5$. The radial coordinate r is shown in normalized units, defined by r/r_0 with $r_0 = 1$.

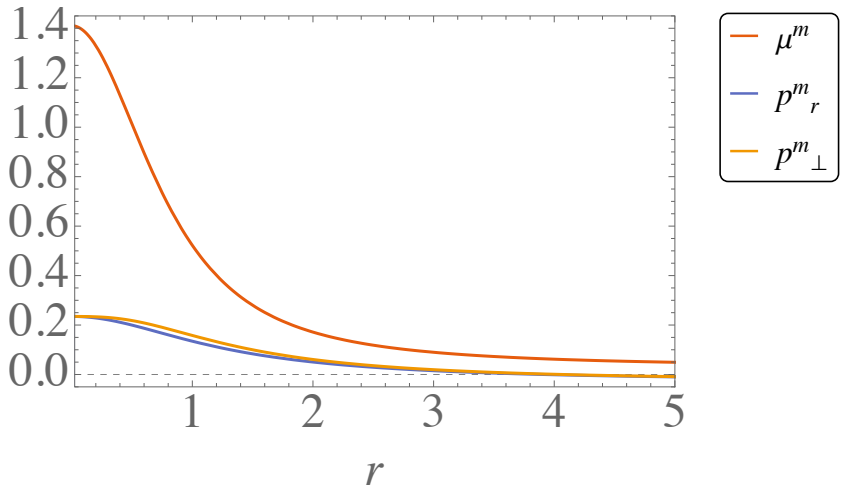

Figure 11.2: Baryonic matter fluid profiles corresponding to the (IS-TIV) metric discussed in Sec. 11.3. The energy density, radial pressure, and orthogonal pressure satisfy the energy conditions outlined in Sec. 10.1. The parameter values used are: $\alpha = 0.001$, $\mu_1 = -1.25$, $\mathcal{R} = 7.3$, $c_1 = 0.3$, and $A = 1.5$. The radial coordinate r is normalized such that r/r_0 with $r_0 = 1$.

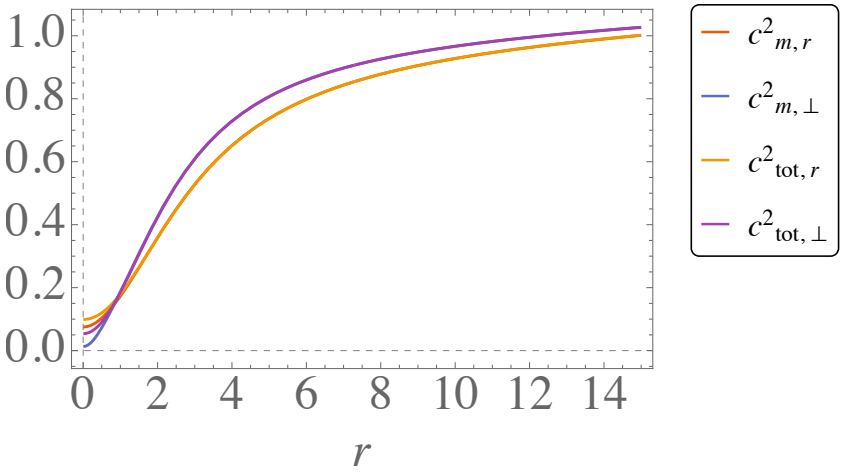

Figure 11.3: The sounds speeds for the orthogonal and radial components of the baryonic fluid and the total fluid source, for the (IS-TIV) metric discussed in Sec. 11.3. All causal conditions specified in Sec. 10.1 are satisfied. The parameter values are: $\alpha = 0.001$, $\mu_1 = -1.25$, $\mathcal{R} = 7.3$, $c_1 = 0.3$, and $A = 1.5$. The radial coordinate r is normalized such that r/r_0 with $r_0 = 1$.

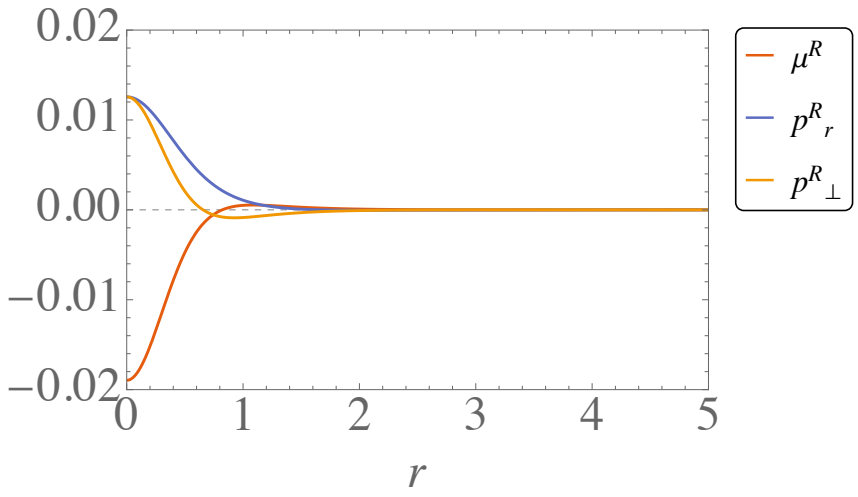

Figure 11.4: Curvature fluid solutions for the (IS-TIV) metric discussed in Sec. 11.3. The parameter values are: $\alpha = 0.001$, $\mu_1 = -1.25$, $\mathcal{R} = 7.3$, $c_1 = 0.3$, and $A = 1.5$. The radial coordinate r is normalized, i.e., r/r_0 where $r_0 = 1$.

11.4 Reconstruction of quadratic gravity models using a generic interior metric

In this section, we apply the reconstruction method using a general metric ansatz. We consider the component k_1 of the metric such that the first two terms recover the Newtonian limit that generates a gravitational potential that matches the one of an interior describing a classical spherical matter distribution with a uniform density. This is the same anzats of the Tolman IV solution. Therefore, we extend the potential by including a quartic term in r. The component k_2 of the metric is chosen to be a rational function, maintaining a high level of generality. This choice provides a flexible set of parameters while helping to limit the increased complexity of the TOV equations. The line element is of the form Eq. (9.31) with the following metric coefficients

$$k_1(r) = 1 + \mathfrak{D}_1 r^2 + \mathfrak{D}_2 r^4, \qquad k_2(r) = \frac{1 + \mathfrak{D}_3 r^2}{1 + \mathfrak{D}_4 r^2 + \mathfrak{D}_5 r^4}. \tag{11.16}$$

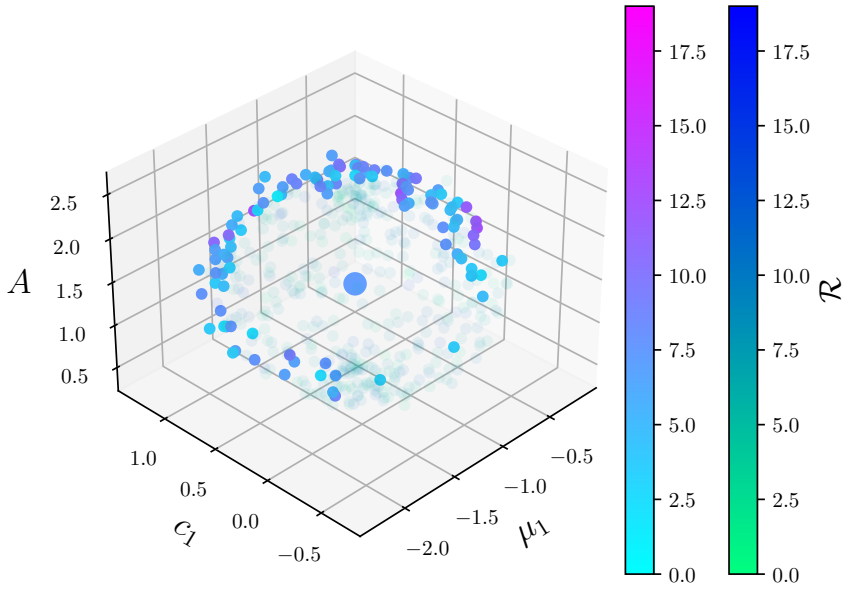

(a) Parameter space plot of the squared radial sound speed for the baryonic fluid.

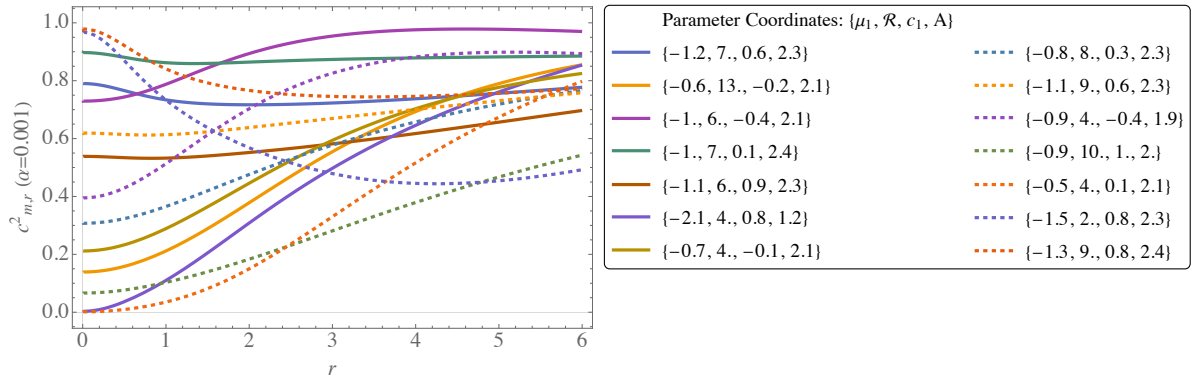

(b) The general envelope for $c^2_{m,r}$ solutions where the parameter values satisfy the causal condition as shown in Fig. 11.5a. Here, r is the normalized radius, i.e., r/r_0 with $r_0 = 1$.

Figure 11.5: A parameter perturbation from the values used in Fig. 11.1 (the central point) is illustrated in Figure 11.5a. The faint points represent 500 randomly generated parameter sets, each shifted radially by 0.05 and confined to a sphere of radius 1. The darker points, which make up 21% of the total, satisfy the causal condition $0 < c^2_{m,r} \leq 1$. This analysis applies to the (IS-TIV) metric discussed in Sec. 11.3. Figure 11.5b displays the overall envelope of the radial sound speed $c^2_{m,r}$ for the parameter sets that meet the causal condition shown in Fig. 11.5a.

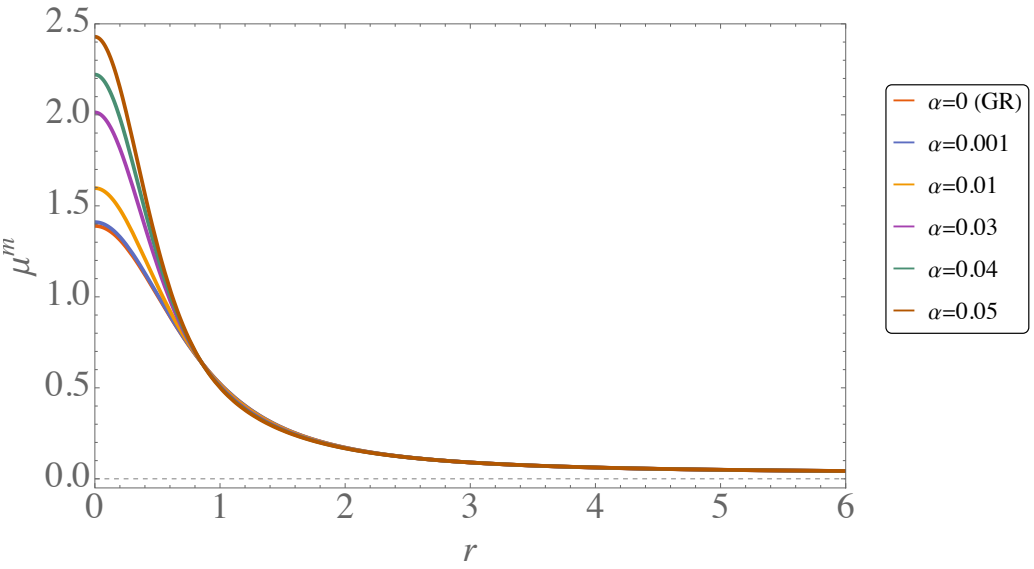

Figure 11.6: Baryonic matter fluid energy density profiles are shown for various values of α, using the same parameter set as in Fig. 11.1, for the (IS-TIV) metric discussed in Sec. 11.3. The radial coordinate r is normalized by r_0, with $r_0 = 1$.

The general total fluid quantities, in terms of the metric coefficients, are

$$\mu^{\text{tot}} = \frac{rk_2'(r) + k_2(r)2 - k_2(r)}{r^2 k_2(r)^2}, \tag{11.17}$$

$$p_r^{\text{tot}} = \frac{rk_1'(r) - k_1(r)k_2(r) + k_1(r)}{r^2 k_1(r)k_2(r)}, \tag{11.18}$$

$$p_\perp^{\text{tot}} = \frac{k_1''(r)}{2k_1(r)k_2(r)} - \frac{k_1'(r)k_2'(r)}{4k_1(r)k_2(r)^2} - \frac{k_1'(r)^2}{4k_1(r)^2k_2(r)} - \frac{k_2'(r)}{2rk_2(r)^2} + \frac{k_1'(r)}{2rk_1(r)k_2(r)}. \tag{11.19}$$

The complete expressions for the total fluid quantities in terms of the parameters are given in the Appendix A.2, including a link to the GitHub repository which contains the Mathematica notebooks with the complete expressions for the fluid sources.

To obtain physically viable solutions, we impose the junction conditions by requiring that

$$R(r_b) = \hat{R}(r_b) = p_r^{\text{tot}}(r_b) = 0,$$

where r_b denotes the boundary of the star. This approach enables the elimination and constraint of certain parameter dependencies.

Applying these junction conditions to ensure a smooth matching reduces the number

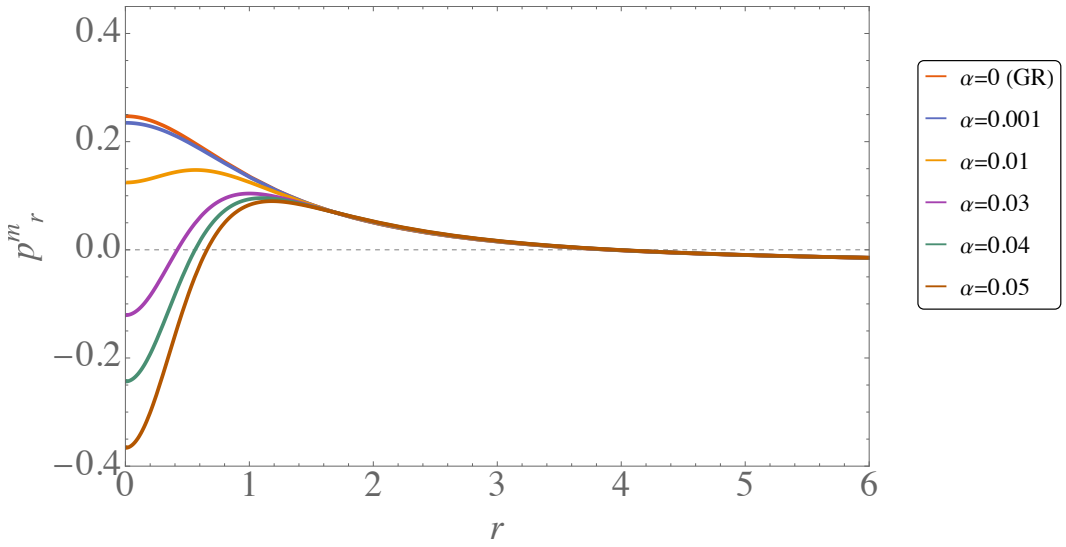

(a) Radial pressure of the baryonic matter fluid for different values of α using the (IS-TIV) metric in Sec. 11.3.

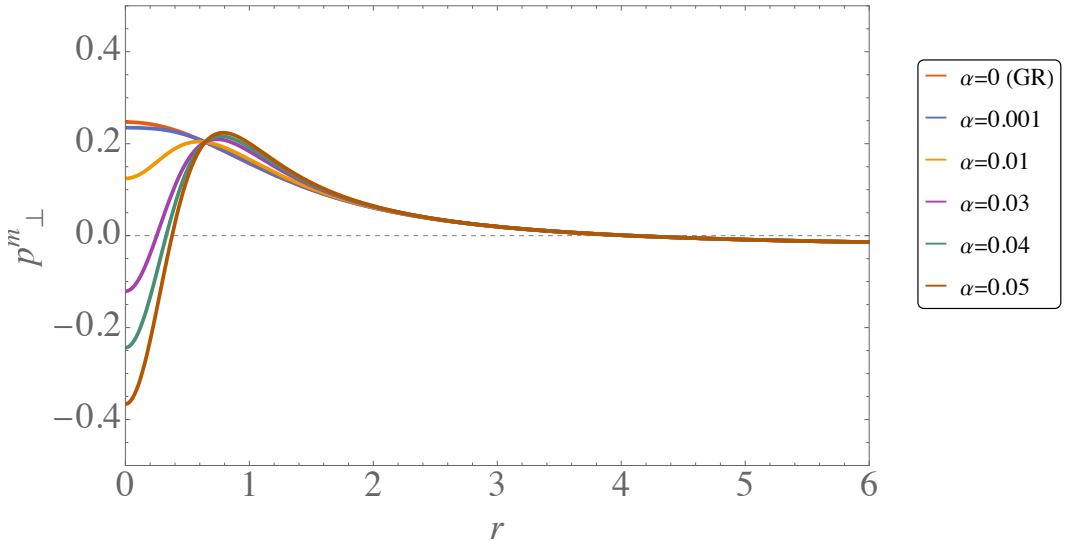

(b) The orthogonal pressure of the baryonic matter fluid for different values of α using the (IS-TIV) metric in Sec. 11.3.

Figure 11.7: Baryonic matter fluid solutions for different values of α, using the same parameter set as in Fig. 11.1. These solutions correspond to the (IS-TIV) metric described in Sec. 11.3. The radius r is normalized by r_0, where $r_0 = 1$.

of independent parameters to just three: $\mathfrak{D}_1$, $\mathfrak{D}_2$, and α. We adopt the same strategy used to solve the TOV equations as described in Sec. 11.3. The complete expressions for the thermodynamic variables in terms of the metric components are provided in Appendix A.2.

Figures 11.10 and 11.11 illustrate the radial profiles of baryonic matter for specific

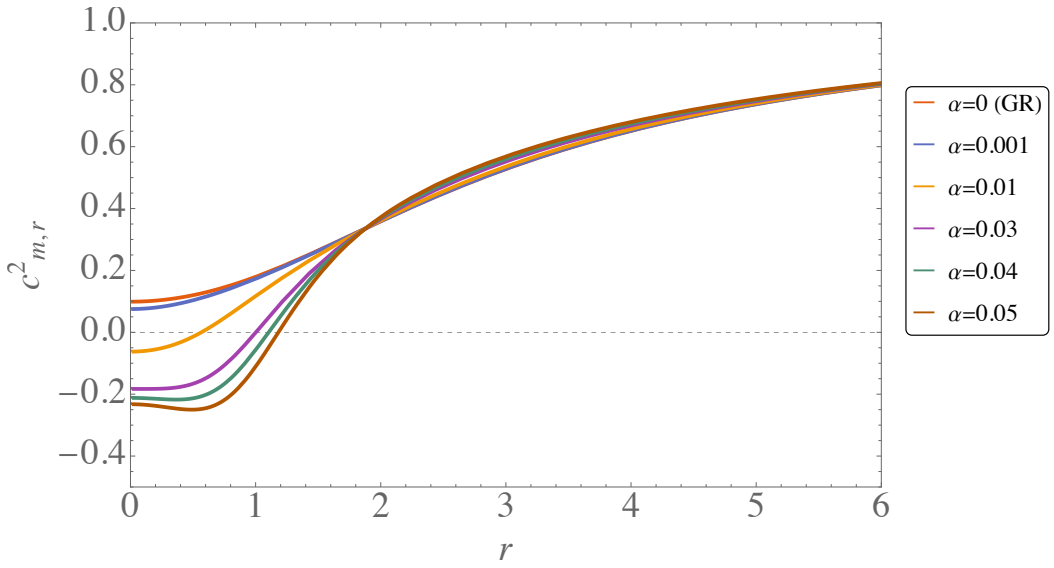

(a) The radial sound speed of the baryonic matter fluid for different values of α using the (IS-TIV) metric in Sec. 11.3.

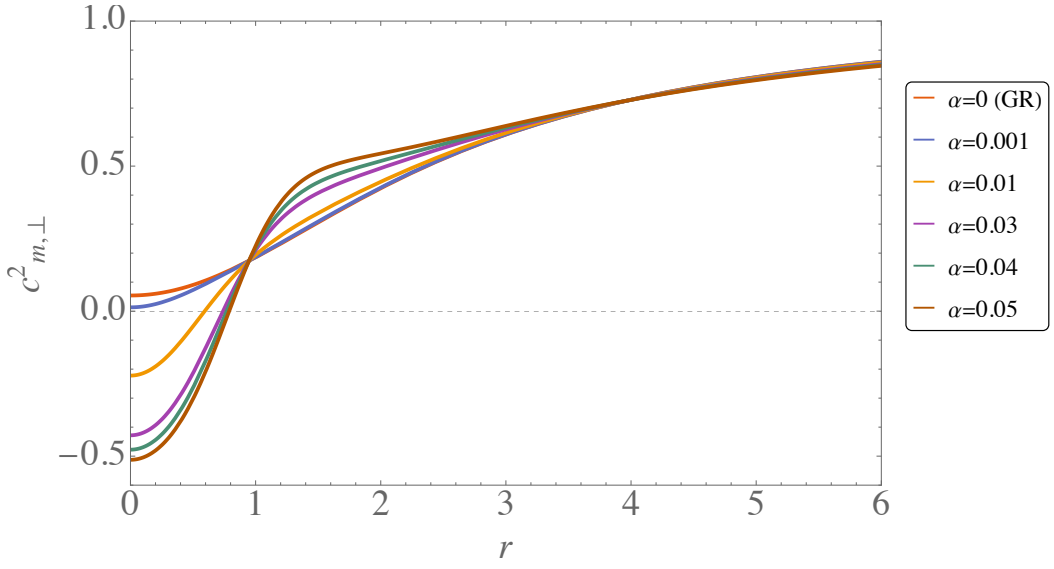

(b) The orthogonal sound speed of the baryonic matter fluid for different values of α using the (IS-TIV) metric in Sec. 11.3.

Figure 11.8: The sound speeds of the orthogonal and radial components for the baryonic fluid are shown for various values of α, using the same parameter set as in Fig. 11.1. These results correspond to the (IS-TIV) metric discussed in Sec. 11.3. The radius r is normalized by r_0, where $r_0 = 1$.

parameter values. This yields a solution that meets the physical requirements outlined in Sec. 10.1 and allows for a smooth matching to the exterior, consistent with a quadratic $f(R)$ model featuring a positive α value, $\alpha = 0.0001$ (corresponding to $\alpha \sim 10^6$ cm^2, in agreement with the constraints reported in [23]).

The behavior of baryonic matter closely resembles typical solutions to the TOV equations: the energy density, pressures, and sound speed profiles decrease monotonically with radius. However, in comparison to the previous solution, Fig. 11.11 reveals a stellar structure with a more compact core, characterized by a central sound speed $c^2_{m,r}(r = 0) \simeq 0.8$.

Examining the relative magnitudes of the baryonic and effective curvature fluid quantities provides interesting insights. In this case (see Fig. 11.12), the effective curvature contributions are smaller yet still comparable to the matter quantities, unlike the case discussed in Sec. 11.3, where the curvature fluid quantities are significantly subdominant. This highlights an important insight: even a small fourth-order modification to the gravitational action can lead to non-negligible deviations from GR in the resulting physical observables.

Figure 11.13 shows that a small deviation from the particular solution in Fig. 11.10 results in only about 1% of the sampled sets satisfying the causal condition, $c^2_{m,r} > 0$. Among those, as seen in Fig. 11.14, the baryonic matter sound speeds often exhibit oscillatory behavior. These oscillations may signal potential instabilities in the solution, where confirming this would require a dedicated perturbative analysis. Additionally, the orthogonal sound speed is not always well-behaved: Fig. 11.11 shows parameter sets for which this quantity exceeds the causal limit, violating physical constraints.

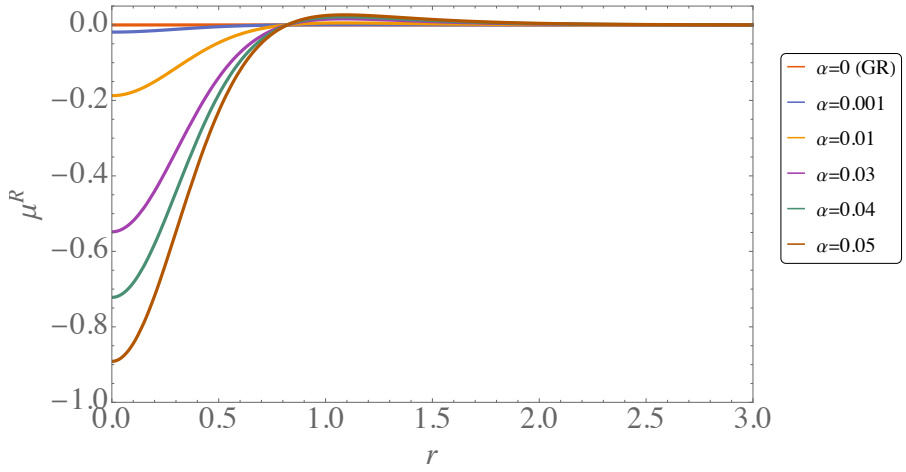

(a) Energy density of the curvature fluid for different values of α.

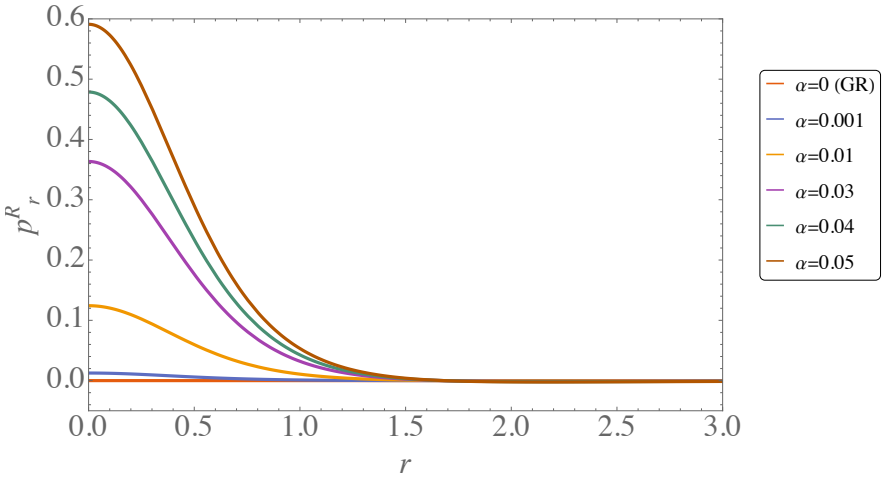

(b) Radial pressure of the curvature fluid for different values of α.

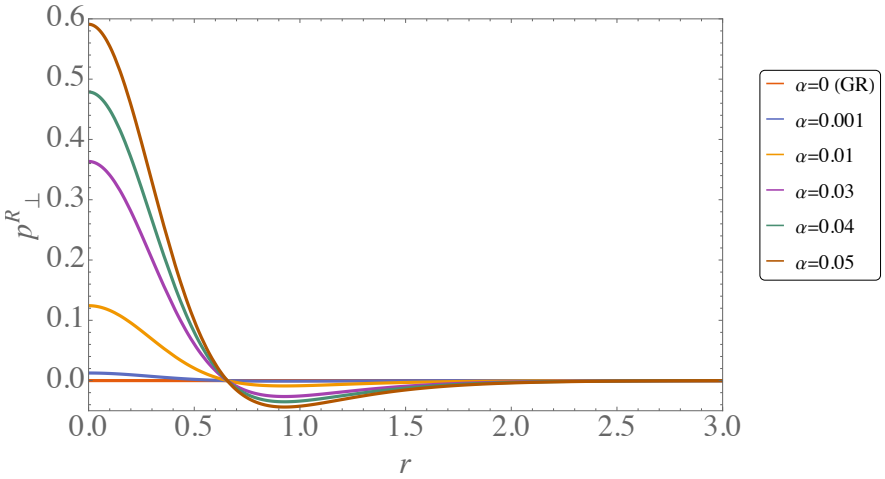

(c) The orthogonal pressure of the curvature fluid for different values of α.

Figure 11.9: Curvature fluid solutions are shown for different values of α, using the same parameter set as in Fig. 11.1. These correspond to the (IS-TIV) metric described in Sec. 11.3. The radius r is normalized by r_0, where $r_0 = 1$.

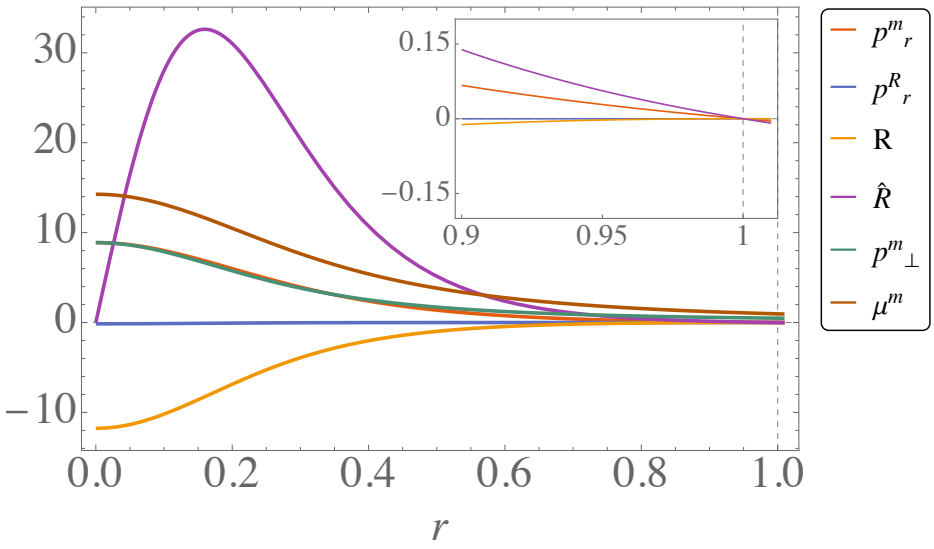

Figure 11.10: Baryonic fluid solutions for Starobinsky gravity using the following parameter values: $\alpha = 0.0001$, $\mathfrak{D}_1 = 6.8$, and $\mathfrak{D}_2 = 10$. The star's boundary is located at $r = r_b = 1$, where r is the normalized radius (i.e., r/r_0 with $r_0 = 1$). This solution exhibits smooth matching as described in Sec. 10.2 and corresponds to the case studied in Sec. 11.4.

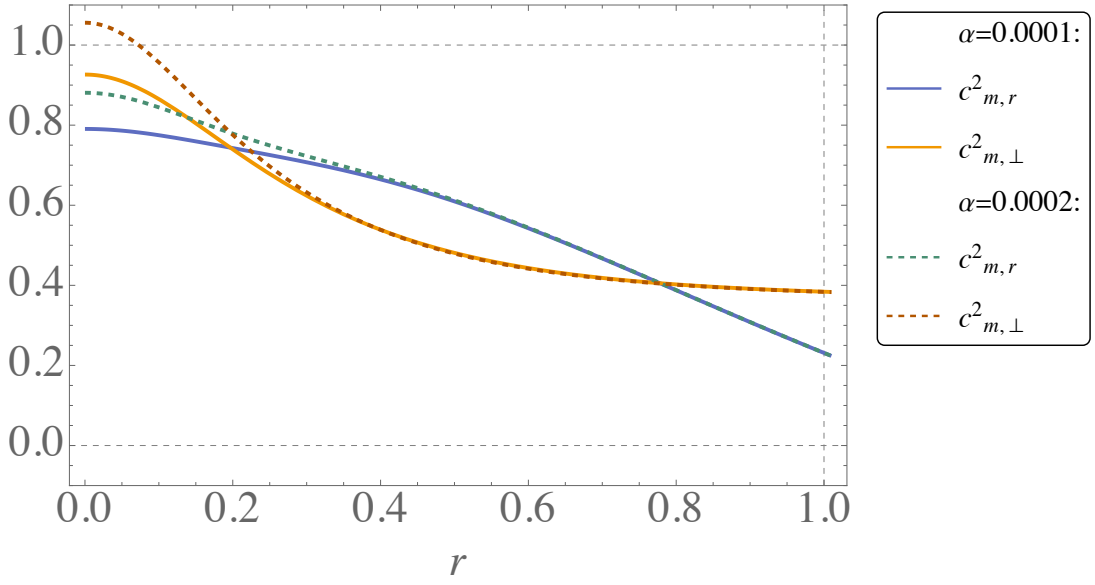

Figure 11.11: The sound speeds of the orthogonal and radial components for the baryonic fluid. These solutions correspond to the a generic interior metric case, as discussed in Sec. 11.4. This configuration describes a stellar object with a highly compact core at $r = 0$, where $c^2_{m,r} \simeq 0.8$. A small variation in the parameter α is included to demonstrate the sensitivity of the sound speed to changes in α, consistent with the observations in Sec. 11.3. Notably, for values $\alpha > 0.00015$, $c^2_{m,\perp} > 1$ at the stellar center.

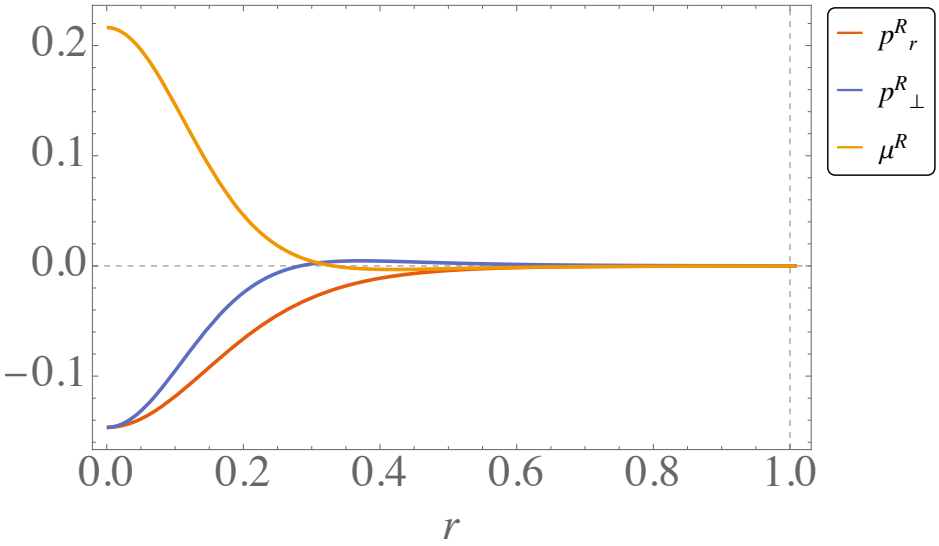

Figure 11.12: The radial, orthogonal pressures, and the energy density of the curvature fluid corresponding to the generic interior metric case, as presented in Sec. 11.4, for a quadratic form for $f(R)$. The parameter values used are $\alpha = 0.0001$, $\mathfrak{D}_1 = 6.8$, and $\mathfrak{D}_2 = 10$. The stellar boundary is located at $r = r_b = 1$, with r representing the normalized radial coordinate, i.e., r/r_0 with $r_0 = 1$.

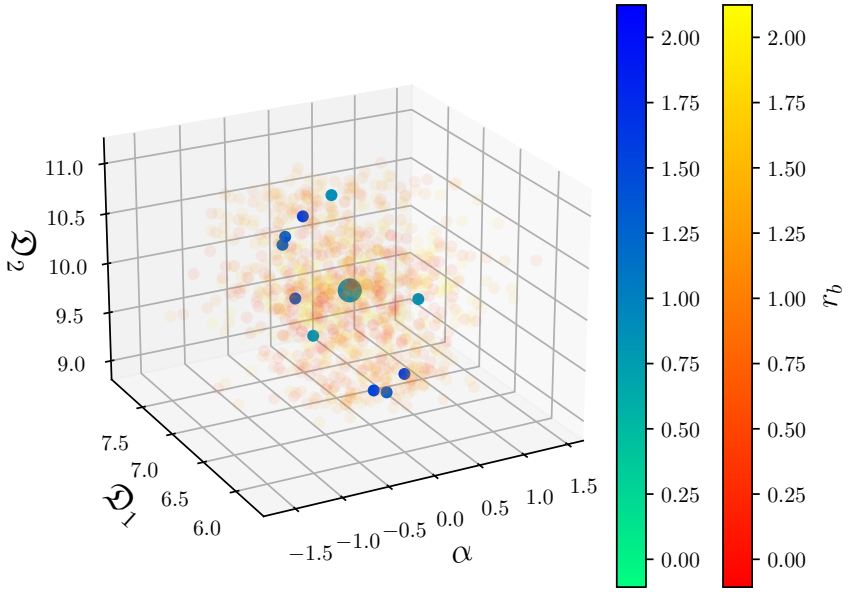

Figure 11.13: Parameter space of the squared radial sound speed for baryonic matter, based on the generic interior metric in Sec. 11.4. The faint points indicate randomly sampled parameter sets, while the darker green points correspond to combinations that satisfy the causal condition $0 \leq c^2_{m,r} \leq 1$. Here, the number of random parameter sets has been doubled compared to Fig. 11.5, yet only 1% meet the causality criterion for $c^2_{m,r}$.

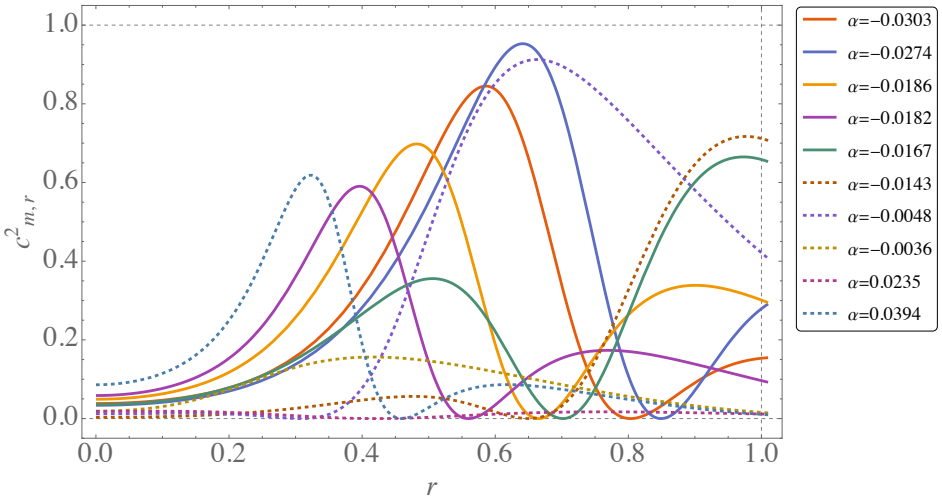

Figure 11.14: The sound speeds of the radial component for baryonic matter. The parameter sets from Fig. 11.13 that satisfy the causal condition are used. The boundary lies at $r = r_b = 1$, with r normalized by $r_0 = 1$. These results correspond to the generic interior metric in Sec. 11.4.

CHAPTER 12

SUMMARY OF PART III

Extending the work of Carloni et al. for a single fluid and the two-fluid approach in general relativity [57, 58, 205, 206], exact solutions were found by considering a quadratic form for $f(R)$ using the (1+1+2) covariant approach [53]. The advantages of using this formalism are that it renders all the background quantities to scalars and is suitably adapted to LRS II spacetimes, i.e., a spacetime with spherical symmetry since the (1+1+2) threading picks a preferred spatial direction.

Considering a quadratic form for $f(R)$, we found two physically viable solutions that describe (1) a quasi-isotropic stellar object with a shell and double layer and (2) a configuration characterized by a quartic correction to a quadratic Newtonian potential with smooth matching of the boundary surface. The first solution, which contains a double layer, is interpreted as a structure with a shell that has a tension on the surface. Double layers are not well understood in the literature since they are a mathematical consequence when investigating junction conditions in fourth-order gravity and are unique to Starobinsky models [240]. Our work shows the first explicit example of a stellar object describing a double layer.

The overall findings of this work indicate that analytical approaches can effectively

describe astrophysical phenomena in the context of extended theories of gravity. Furthermore, the structural and compositional distinctions observed in these relativistic stars compared to standard general relativity suggest measurable differences that could emerge with future observational advances.

Future directions for this work include improving our understanding of the properties of the obtained solutions, with particular emphasis on observable features that could serve as signatures for testing higher-order corrections to the gravitational action in relativistic stars. In particular, the mass–radius relation and the maximum mass limit of these solutions warrant further investigation. Exploring alternative functional forms of $f(R)$ gravity, such as the Hu–Sawicki model [148] and the R^n model, where perturbative effects can be studied by setting $n = 1 + \delta$ [68], would also be valuable.

One direct observational prospect for testing our models is the construction of a buffer region between the matter boundary and the exterior spacetime. Constructing buffer metrics for a class of $f(R)$ theories involves imposing the Israel–Darmois junction conditions on a general static, spherically symmetric metric, ensuring smooth matching to Schwarzschild and maintaining physical consistency. By characterizing the buffer region, we can analyze its gravitational lensing effects. The lensing analysis will follow the covariant approach of [216], deriving the null geodesic equations within the $(1+1+2)$ threading and calculating the bending-angle integral for our specific buffer metric. This work could identify unique observational signatures, such as Einstein-ring shifts and time delays, that distinguish modified gravity from GR. The existence of a detectable buffer metric, with its specific lensing properties, would provide direct evidence for physics beyond Einstein's theory in the strong-field regime.

Another direction involves finding isotropic stellar solutions within the framework of $f(R)$ gravity. The motivation is to model stellar objects that resemble stars composed of baryonic matter in GR externally, but with an interior governed by an $f(R)$ description. Additionally, studying the lensing effects of the solutions and extending the models to include magnetism, enabling the description of magnetars, within both GR and modified

gravity using the (1+1+2) covariant formalism would be a compelling avenue for future research.

The framework we have outlined for finding exact solutions to relativistic stars in extended gravity theories provides a solid foundation for constructing more realistic stellar models that satisfy stringent physical and boundary conditions. In particular, this work underscores the importance of carefully defining and applying such conditions in $f(R)$ gravity to ensure the physical viability of the solutions. For example, in the attempt to model a more realistic stellar system by matching a spherically symmetric vacuum solution to an expanding Friedmann–Lemaître–Robertson–Walker (FLRW) background, Clifton et al. showed that, for $f(R) = R^n$ models, such a matching is not possible [69, 72].

CHAPTER 13

CONCLUSIONS

This chapter summarizes the principal findings of this thesis, which investigated bouncing cosmologies and relativistic stellar solutions within extended theories of gravity. The key results are grouped according to the structure of the thesis and is discussed below.

Considering a spatially closed FLRW spacetime, we analyzed the initial conditions that induced a bounce in a canonical $f(\phi, R)$ model and a non-canonical single scalar field model, in Parts I and II.

In Part I, we determined the initial conditions necessary for a bounce to occur during the contracting period by displacing the ϕ field in its false vacuum and demanding that the R^2 term remain subdominant during this phase. The bounce and its conditions then depended only on the ϕ field. However, during this phase, it was crucial that the evolution of the scalaron (R^2 term) followed the ϕ field, and as ϕ decayed, the scalaron dominated and drove inflation. We found that sufficient inflation could occur following a bounce, and our perturbative analysis indicated that our model was stable.

In Part II, we performed a detailed dynamical system analysis for the DBI field, in particular, the bounce solutions it exhibited. DBI fields have a unique feature in that they possess a deceleration mechanism that can facilitate bounce behavior. Our study

was the first to investigate this behavior for a DBI model [52]. Considering a power-law and exponential function for the potential and the brane tension, our analysis of the dynamical system revealed that the fixed point $z = 0$ corresponding to the bounce in the submanifolds $\bar{\gamma} = 0$ (ultrarelativistic) and $\bar{\gamma} = 1$ (canonical scalar field) was an unstable saddle. In addition, for $0 < \bar{\gamma} < 1$, the system was unstable, and the dynamics were driven towards the $\bar{\gamma} = 0$ or $\bar{\gamma} = 1$ submanifold. With further analysis, we found that the number of initial conditions leading to a bounce solution increased as the dynamical system approached the ultrarelativistic case. Motivated by this finding, we sought to determine whether a DBI field could exhibit cyclic behavior in its phase space. This would require inducing a re-collapse following the bounce. We achieved this by including a negative cosmological constant. Interestingly, this did not result in cyclical behavior; in fact, it reduced the number of bouncing solutions as the system evolved towards the ultrarelativistic limit. This indicated that a more exotic degree of freedom would be required to find cyclic solutions in the phase space of a bouncing cosmology with a DBI field.

In light of the announcement of the DESI result supporting a dynamical dark energy model [5], these models could be used to explore the effect of a dynamical dark energy component on the system and its stability. For instance, in a chaotic inflationary model, Ellis et al. showed that cyclic behavior appeared in the phase space by incorporating a decaying dark energy model [113]. Other future directions include incorporating a reheating mechanism to realize a more realistic early universe model, and investigating the power spectrum of curvature perturbations. Studying the latter provides insight into how inflation induces gravitational waves, which could constrain our model parameters. Another interesting avenue is that signs of peaks in the curvature spectrum indicate primordial black hole formation [236, 248], and these features can also serve to constrain alternative early-universe models.

Bouncing cosmologies have attractive features as alternatives to inflation and successfully alleviate the initial singularity problem of standard inflationary models. In Part I,

we showed that natural inflation could indeed follow a bounce, and further investigation into the primordial power spectrum would help distinguish our model from competing inflationary scenarios. Although bouncing models do not resolve all the issues with early-universe cosmology, since fine-tuning of the initial conditions is still required, exploring the evolutionary and dynamical behavior of bouncing models within different theories of gravity could shed light on the nature of the inflaton, in ways standard inflation does not.

In developing a framework to test or constrain extended models of gravity, we considered the description of relativistic stars in the context of $f(R)$ theories of gravity.

In Part III, we presented a solution strategy to find exact static spherically symmetric solutions in $f(R)$ gravity and discussed the physical requirements and boundary conditions necessary to describe a relativistic star. To demonstrate the implementation of our mathematical scheme, we considered the simplest higher-order curvature correction to GR: a quadratic $f(R)$ model. Our field equations were modeled as a two-fluid system. To maintain generality, acknowledging that $f(R)$ models are inherently anisotropic, we considered a fluid source that included an anisotropic pressure contribution. We found that including anisotropy made it easier to find exact solutions using our reconstruction technique. The properties of our two new exact stellar solutions are summarized as follows:

1. Considering an interior Schwarzschild–Tolman IV metric solution as the description of our total fluid, we found a static spherically symmetric solution that describes a quasi-isotropic object with a shell and double layer. This solution is the first explicit example of an object with a double-layer structure. We found that the orthogonal pressure of the shell, including the double-layer contribution, is negative, while the other thermodynamic properties are positive. In the standard approach, the requirement for physicality would be that all thermodynamic quantities are positive. However, we found that the weak energy condition was satisfied; therefore, we interpreted the negative orthogonal pressure as a tension on the shell and the double layer.

2. We reconstructed an exact solution from a generic static spherically symmetric interior metric. The construction of the metric is analogous to the Tolman IV solution; therefore, we added a quartic radial term to the (0,0) component of the metric. This stellar solution describes a highly compact object at its center, since $c^2_{m,r}(r = 0) \simeq 0.8$, and its pressure and energy density profiles for baryonic matter exhibit the characteristics of standard solutions to the TOV equations, i.e., positive, monotonically decreasing profiles. Unlike the previous solution, this one does not feature a shell, and a smooth matching to the exterior Schwarzschild spacetime is possible. However, these solutions were obtained for a much smaller value of α than in the previous case.

Our research contributes to the taxonomy of static spherically symmetric spacetimes in the context of $f(R)$ models of gravity by developing a solution strategy for finding analytical solutions that describe the interior of compact stellar objects with appropriate physical properties, and by providing a means to test numerical studies using exact solutions. As far as we are aware, only numerical solutions to static spherically symmetric spacetimes exist in the context of $f(R)$ gravity. So, the solutions presented here are the first exact solutions to be found. With regard to the astrophysical interpretation of our solutions, such as describing neutron stars and further constraining our model parameters, determining the mass–radius relation and the maximum-mass limits is an important aspect to investigate. The challenge we face is that these calculations differ from the standard case. Instead of a one-dimensional figure associated with the variation of the parameter α, as often appears in the literature, in our case, we must consider all the parameters of the exact solutions we have derived. Therefore, the mass-to-radius analysis concerns a hypersurface in parameter space, and the standard analysis would be insufficient to fully understand the properties of the solutions.

Our results demonstrate the importance of defining the boundary when describing a realistic stellar object in gravity. There are works in the literature that attempt to describe neutron stars in extended models of gravity; however, a hard boundary is often

not defined and is placed an infinite radius away. This is an important issue to address, and more discussion should focus on it. It is essential to accurately describe what we consider realistic stellar models in gravity so that constraining model parameters or favoring/eliminating models can be done reliably. Therefore, it is worthwhile to investigate the matching of spacetimes to describe more realistic physical systems. For example, Clifton et al. [72] found that for $f(R) = R^n$ models, no known spherically symmetric vacuum solutions can be matched to an expanding Friedmann–Lemaître–Robertson–Walker background.

Another interesting avenue to pursue is adapting the work in Chapter 8 and the subsequent chapters to include magnetism to describe magnetars. Consequently, we could investigate the emission of gravitational waves produced by the magnetosphere. The examination of strong gravitational lensing effects could also be performed on the results in Chapter 11. The work of Nzioki et al. [216], using an $f(R) = R^n$ model, showed that the bending angle depends on the parameters of the theory of gravity and does not depend on the position of the observer. This allows one to directly constrain the function f and determine the nature of the gravitational interaction in the strong-field regime.

An important future direction is assessing how future cosmological and astrophysical observations could test the models developed in this thesis. For the early-universe scenarios of Parts I and II, forthcoming CMB missions such as *LiteBIRD* [12] and *CMB-S4* [3] will provide high-precision measurements of the tensor–scalar ratio and possible deviations from standard slow-roll behavior, thereby constraining bounce-induced features in the primordial spectrum. Likewise, large-scale surveys including the *Square Kilometer Array* (SKA) [50] will probe the small-scale structure and potential signatures associated with peaks in the curvature spectrum, offering a means to test scenarios that predict primordial black hole formation or other distinctive imprints from the bounce phase.

For the stellar models presented in Part III, future pulsar-timing observations with SKA [258], together with gravitational-wave measurements from neutron-star mergers, will tighten constraints on the mass–radius relation, tidal deformability, and strong-field

behavior of compact objects. Since these quantities depend sensitively on the parameters of $f(R)$ gravity, improved observations will assist in delimiting the viable region of parameter space for the exact solutions constructed here. In addition, strong-lensing measurements from upcoming surveys may further probe the dependence of lensing angles on the underlying gravitational theory [254].

These missions collectively provide a promising avenue for testing the predictions of the bouncing cosmologies and extended-gravity stellar models developed in this work, and for linking their theoretical features to measurable astrophysical phenomena.

In summary, this thesis has explored foundational and novel aspects of early-universe cosmology and stellar structure within extended theories of gravity, providing both theoretical insights and exact analytical solutions performed in a fully covariant manner where previously only numerical approaches were available. By addressing the limitations of inflationary cosmology through bouncing models, and by rigorously constructing physically viable relativistic stars in $f(R)$ gravity, this work contributes meaningfully to the ongoing effort to reconcile observational data with high-energy gravitational theories. The methods and results presented not only deepen our understanding of the early universe and compact objects but also offer new tools to constrain alternative models of gravity with greater precision. As the field moves toward an era of increasingly refined astrophysical observations, including gravitational wave astronomy and precision cosmology, the analytical frameworks and models developed here will serve as valuable benchmarks.

BIBLIOGRAPHY

[1] Arno A. Penzias and Robert W. Wilson: The cosmic microwave background. *Phys. Bull.*, 29(12):564, 1978. doi: 10.1088/0031-9112/29/12/026. 4

[2] On the concentration of relic magnetic monopoles in the universe. *Phys. Lett. B*, 79(3):239–241, 1978. ISSN 0370-2693. doi: https://doi.org/10.1016/0370-2693(78)90232-0. 4

[3] K. Abazajian et al. CMB-S4: Forecasting Constraints on Primordial Gravitational Waves. *ApJ*, 926(1):54, 2022. doi: 10.3847/1538-4357/ac1596. 22, 146

[4] T. M. C. Abbott et al. Dark Energy Survey Year 3 results: Cosmological constraints from galaxy clustering and weak lensing. *Phys. Rev. D*, 105(2):023520, 2022. doi: 10.1103/PhysRevD.105.023520. 1, 21

[5] M. Abdul Karim et al. DESI DR2 Results I: Baryon Acoustic Oscillations from the Lyman Alpha Forest. 3 2025. 79, 143

[6] A. Addazi, A. Marciano, and C. Qian. Testing the Anomalous Growth of the Black Hole Radius from AGN. *Galaxies*, 6(4):107, 2018. doi: 10.3390/galaxies6040107. 14

[7] N. Aghanim et al. Planck 2018 results. VI. Cosmological parameters. *Astron.*

Astrophys., 641:A6, 2020. doi: 10.1051/0004-6361/201833910. [Erratum: Astron.Astrophys. 652, C4 (2021)]. 1, 5

[8] Y. Akrami et al. Planck 2018 results. X. Constraints on inflation. *Astron. Astrophys.*, 641:A10, 2020. doi: 10.1051/0004-6361/201833887. 7, 21

[9] S. Alam et al. The clustering of galaxies in the completed SDSS-III Baryon Oscillation Spectroscopic Survey: cosmological analysis of the DR12 galaxy sample. *MNRAS*, 470(3):2617–2652, 2017. doi: 10.1093/mnras/stx721. 1

[10] A. Albrecht and P. J. Steinhardt. Cosmology for grand unified theories with radiatively induced symmetry breaking. *Phys. Rev. Lett.*, 48:1220–1223, 1982. doi: 10.1103/PhysRevLett.48.1220. 5

[11] M. Alishahiha, E. Silverstein, and D. Tong. DBI in the sky: Non-gaussianity from inflation with a speed limit. *Phys. Rev. D*, 70:123505, 2004. doi: 10.1103/PhysRevD.70.123505. 13, 56

[12] E. Allys et al. Probing Cosmic Inflation with the LiteBIRD Cosmic Microwave Background Polarization Survey. *PTEP*, 2023(4):042F01, 2023. doi: 10.1093/ptep/ptac150. 146

[13] R. A. Alpher, H. Bethe, and G. Gamow. The origin of chemical elements. *Phys. Rev.*, 73:803–804, 1948. doi: 10.1103/PhysRev.73.803. 4

[14] M. E. S. Alves, O. D. Miranda, and J. C. N. de Araujo. Probing the $f(R)$ formalism through gravitational wave polarizations. *Phys. Lett. B*, 679(4):401–406, 2009. doi: 10.1016/j.physletb.2009.08.005. 20

[15] M. F. S. Alves, L. F. M. A. M. Reis, and L. G. Medeiros. Gravitational waves from inspiraling black holes in quadratic gravity. *Phys. Rev. D*, 107:044017, 2023. doi: 10.1103/PhysRevD.107.044017. 21

[16] L. Amendola, M. Kunz, I. D. Saltas, and I. Sawicki. Fate of Large-Scale Structure in Modified Gravity After GW170817 and GRB170817A. *Phys. Rev. Lett.*, 120(13): 131101, 2018. doi: 10.1103/PhysRevLett.120.131101. 14

[17] L. Amendola et al. Cosmology and fundamental physics with the Euclid satellite. *Living Rev. Rel.*, 21(1):2, 2018. doi: 10.1007/s41114-017-0010-3. 22

[18] K. N. Ananda, S. Carloni, and P. K. S. Dunsby. The Evolution of cosmological gravitational waves in $f(R)$ gravity. *Phys. Rev. D*, 77:024033, 2008. doi: 10.1103/PhysRevD.77.024033. 100

[19] K. N. Ananda, S. Carloni, and P. K. S. Dunsby. A detailed analysis of structure growth in $f(R)$ theories of gravity. *Class. Quantum Grav.*, 26:235018, 2009. doi: 10.1088/0264-9381/26/23/235018.

[20] K. N. Ananda, S. Carloni, and P. K. S. Dunsby. A characteristic signature of fourth order gravity. *Springer Proc. Phys.*, 137:165–172, 2011. doi: 10.1007/978-3-642-19760-4_15. 100

[21] G. Antoniou, A. Papageorgiou, and P. Kanti. Probing Modified Gravity Theories with Scalar Fields Using Black-Hole Images. *Universe*, 9(3):147, 2023. doi: 10.3390/universe9030147. 14, 15

[22] M. Aparicio Resco, Á. de la Cruz-Dombriz, F. J. Llanes Estrada, and V. Zapatero Castrillo. On neutron stars in $f(R)$ theories: Small radii, large masses and large energy emitted in a merger. *Phys. Dark Univ.*, 13:147–161, 2016. doi: 10.1016/j.dark.2016.07.001. 16, 121

[23] A. S. Arapoglu, C. Deliduman, and K. Y. Eksi. Constraints on Perturbative $f(R)$ Gravity via Neutron Stars. *JCAP*, 07:020, 2011. doi: 10.1088/1475-7516/2011/07/020. 20, 124, 134

[24] C. Armendariz-Picon, T. Damour, and V. F. Mukhanov. k - inflation. *Phys. Lett. B*, 458:209–218, 1999. doi: 10.1016/S0370-2693(99)00603-6. 12

[25] C. Arnold, M. Leo, and B. Li. Realistic simulations of galaxy formation in $f(R)$ modified gravity. *Nature Astron.*, 3(10):945–954, 2019. doi: 10.1038/s41550-019-0823-y. 14

[26] A. V. Astashenok, S. Capozziello, and S. D. Odintsov. Magnetic Neutron Stars in $f(R)$ gravity. *Astrophys. Space Sci.*, 355(2):333–341, 2015. doi: 10.1007/s10509-014-2182-6. 15

[27] A. V. Astashenok, S. D. Odintsov, and Á. de la Cruz-Dombriz. The realistic models of relativistic stars in $f(R) = R + \alpha R^2$ gravity. *Class. Quantum Grav.*, 34(20):205008, 2017. doi: 10.1088/1361-6382/aa8971. 16, 121

[28] S. Bag, V. Sahni, Y. Shtanov, and S. Unnikrishnan. Emergent Cosmology Revisited. *JCAP*, 07:034, 2014. doi: 10.1088/1475-7516/2014/07/034. 11

[29] S. Bahamonde, M. Jamil, P. Pavlovic, and M. Sossich. Cosmological wormholes in $f(R)$ theories of gravity. *Phys. Rev. D*, 94:044041, Aug 2016. doi: 10.1103/PhysRevD.94.044041. 15

[30] V. Baibhav and D. Maity. Boson stars in higher-derivative gravity. *Phys. Rev. D*, 95:024027, 2017. doi: 10.1103/PhysRevD.95.024027. 15

[31] T. Baker, E. Bellini, P. G. Ferreira, M. Lagos, J. Noller, and I. Sawicki. Strong constraints on cosmological gravity from GW170817 and GRB 170817A. *Phys. Rev. Lett.*, 119(25):251301, 2017. doi: 10.1103/PhysRevLett.119.251301. 15, 19

[32] T. Baker, E. Barausse, A. Chen, C. de Rham, M. Pieroni, and G. Tasinato. Testing gravitational wave propagation with multiband detections. *JCAP*, 03:044, 2023. doi: 10.1088/1475-7516/2023/03/044. 15

[33] S. Banerjee, S. Bera, S. Banerjee, and T. P. Singh. Constraints on fourth order gravity from binary pulsars and gravitational waves. *Phys. Rev. D*, 96:084015, 2017. doi: 10.1103/PhysRevD.96.084015. 14, 15

[34] J. D. Barrow and M. P. Dabrowski. Oscillating Universes. *MNRAS*, 275:850–862, 1995. 8

[35] N. H. Barth and S. M. Christensen. Quantizing fourth-order gravity theories: The functional integral. *Phys. Rev. D*, 28:1876–1893, 1983. doi: 10.1103/PhysRevD.28.1876. 100

[36] D. Battefeld and P. Peter. A Critical Review of Classical Bouncing Cosmologies. *Phys. Rept.*, 571:1–66, 2015. doi: 10.1016/j.physrep.2014.12.004. 3, 7

[37] B. Bertotti, L. Iess, and P. Tortora. A test of general relativity using radio links with the Cassini spacecraft. *Nature*, 425:374–376, 2003. doi: 10.1038/nature01997. 1, 17

[38] D. Bessada, W. H. Kinney, and K. Tzirakis. Inflationary potentials in DBI models. *JCAP*, 09:031, 2009. doi: 10.1088/1475-7516/2009/09/031. 13

[39] G. Betschart and C. A. Clarkson. Scalar and electromagnetic perturbations on LRS class II space-times. *Class. Quantum Grav.*, 21:5587–5608, 2004. doi: 10.1088/0264-9381/21/23/018. 92

[40] A. Borde, A. H. Guth, and A. Vilenkin. Inflationary space-times are incomplete in past directions. *Phys. Rev. Lett.*, 90:151301, 2003. doi: 10.1103/PhysRevLett.90.151301. 7

[41] A. Bosma. *The distribution and kinematics of neutral hydrogen in spiral galaxies of various morphological types*. PhD thesis, University of Groningen, Netherlands, 1978. 2

[42] R. H. Brandenberger. Principles, progress and problems in inflationary cosmology. *AAPPS Bull.*, 11:20–29, 2001. 5

[43] R. H. Brandenberger. Lectures on the theory of cosmological perturbations. *Lect. Notes Phys.*, 646:127–167, 2004. doi: 10.1007/978-3-540-40918-2_5. 41

[44] R. H. Brandenberger. Initial conditions for inflation — A short review. *Int. J. Mod. Phys. D*, 26(01):1740002, 2016. doi: 10.1142/S0218271817400028. 6

[45] R. H. Brandenberger and P. Peter. Bouncing Cosmologies: Progress and Problems. *Found. Phys.*, 47(6):797–850, 2017. doi: 10.1007/s10701-016-0057-0. 7

[46] C. Brans and R. H. Dicke. Mach's principle and a relativistic theory of gravitation. *Phys. Rev.*, 124:925–935, 1961. doi: 10.1103/PhysRev.124.925. 22

[47] C. H. Brans. The Roots of scalar-tensor theory: An Approximate history. In *Santa Clara 2004: 1st International Workshop on Gravitation and Cosmology*, 6 2005. 22

[48] R. P. Breton, V. M. Kaspi, M. Kramer, M. A. McLaughlin, M. Lyutikov, S. M. Ransom, I. H. Stairs, R. D. Ferdman, F. Camilo, and A. Possenti. Relativistic Spin Precession in the Double Pulsar. *Science*, 321:104–107, 2008. doi: 10.1126/science.1159295. 20

[49] H. A. Buchdahl. On the gravitational field equations arising from the square of the Gaussian curvature. *Nuovo Cim.*, 23:141–157, 1962. doi: https://doi.org/10.1007/BF02733549. 17

[50] S. Camera et al. Cosmology on the Largest Scales with the SKA. *PoS*, AASKA14:025, 2015. doi: 10.22323/1.215.0025. 146

[51] M. Campbell. Reconstructing exact relativistic star solutions GitHub repository, 2025. URL `https://github.com/mariamcampbell/exact-relativistic-stars`. 180

[52] M. Campbell, R. Daniel, P. K. S. Dunsby, and C. van de Bruck. Bouncing cosmologies in the presence of a Dirac-Born-Infeld field. *Phys. Rev. D*, 110:043505, 2024. doi: 10.1103/PhysRevD.110.043505. 14, 52, 54, 143

[53] M. Campbell, S. Carloni, P. K. S. Dunsby, and N. F. Naidu. Some exact relativistic star solutions in $f(R)$ gravity. *Class. Quantum Grav.*, 42:085014, 2025. doi: 10.1088/1361-6382/adc8f2. 26, 84, 99, 120, 139, 180

[54] W. W. Campbell and R. Trumpler. Observations on the deflection of light in passing through the Sun's gravitational field, made during the total solar eclipse of September 21, 1923. *PASP*, 35(205):158, 1923. doi: 10.1088/123292a. 17

[55] S. Capozziello and F. Bajardi. Gravitational waves in modified gravity. *Int. J. Mod. Phys. D.*, 28(05):1942002, 2019. doi: 10.1142/S0218271819420021. 20

[56] S. Capozziello and G. Lambiase. The emission of Gamma Ray Bursts as a test-bed for modified gravity. *Phys. Lett. B*, 750:344–347, 2015. doi: 10.1016/j.physletb.2015.09.048. 14

[57] S. Carloni and D. Vernieri. Covariant Tolman-Oppenheimer-Volkoff equations. II. the anisotropic case. *Phys. Rev. D*, 97:124057, 2018. doi: 10.1103/PhysRevD.97.124057. 126, 139

[58] S. Carloni and D. Vernieri. Covariant Tolman-Oppenheimer-Volkoff equations. I. the isotropic case. *Phys. Rev. D*, 97:124056, 2018. doi: 10.1103/PhysRevD.97.124056. 139

[59] S. Carloni, P. K. S. Dunsby, and A. Troisi. The Evolution of density perturbations in $f(R)$ gravity. *Phys. Rev. D*, 77:024024, 2008. doi: 10.1103/PhysRevD.77.024024. 100

[60] S. M. Carroll. The Cosmological constant. *Living Rev. Rel.*, 4:1, 2001. doi: 10.12942/lrr-2001-1. 2

[61] S. M. Carroll, V. Duvvuri, M. Trodden, and M. S. Turner. Is Cosmic Speed-Up Due to New Gravitational Physics? *Phys. Rev. D*, 70:043528, 2004. doi: 10.1103/PhysRevD.70.043528. 24

[62] X. Chen. Running non-Gaussianities in DBI inflation. *Phys. Rev. D*, 72:123518, 2005. doi: 10.1103/PhysRevD.72.123518. 13

[63] A. D. Chernin. How Gamow calculated the temperature of the background radiation or a few words about the fine art of theoretical physics. *Physics-Uspekhi*, 37(8):813, 1994. doi: 10.1070/PU1994v037n08ABEH000041. 4

[64] T. Chiba, T. Okabe, and M. Yamaguchi. Kinetically driven quintessence. *Phys. Rev. D*, 62:023511, 2000. doi: 10.1103/PhysRevD.62.023511. 12

[65] L. P. Chimento and R. Lazkoz. Bridging geometries and potentials in DBI cosmologies. *Gen. Rel. Grav.*, 40:2543–2555, 2008. doi: 10.1007/s10714-008-0637-1. 13

[66] L. P. Chimento, R. Lazkoz, and M. G. Richarte. Enhanced Inflation in the Dirac-Born-Infeld framework. *Phys. Rev. D*, 83:063505, 2011. doi: 10.1103/PhysRevD.83.063505. 13

[67] S. R. Chowdhury and M. Khlopov. Gravitational waves in the extended theory of gravity. *Int. J. Mod. Phys. D*, 30(16):2140011, 2021. doi: 10.1142/S0218271821400113. 20

[68] T. Clifton. Alternative theories of gravity. Ph.D. Thesis, DAMTP University of Cambridge, 2006. 20, 140

[69] T. Clifton. Embedding Non-Linear Structures in $f(R)$ Cosmologies. In *14th Marcel Grossmann Meeting on Recent Developments in Theoretical and Experimental General Relativity, Astrophysics, and Relativistic Field Theories*, volume 2, pages 1253–1258, 2017. doi: 10.1142/9789813226609_0094. 18, 141

[70] T. Clifton and J. D. Barrow. The power of general relativity. *Phys. Rev. D*, 72: 103005, 2005. doi: 10.1103/PhysRevD.72.103005. 20

[71] T. Clifton, P. G. Ferreira, A. Padilla, and C. Skordis. Modified gravity and cosmology. *Phys. Rept.*, 513(1):1–189, 2012. doi: 10.1016/j.physrep.2012.01.001. 22

[72] T. Clifton, P. K. S. Dunsby, R. Goswami, and A. M. Nzioki. On the absence of the usual weak-field limit, and the impossibility of embedding some known solutions for isolated masses in cosmologies with $f(R)$ dark energy. *Phys. Rev. D*, 87(6):063517, 2013. doi: 10.1103/PhysRevD.87.063517. 18, 141, 146

[73] T. Clifton, C. S. Gallagher, S. Goldberg, and K. A. Malik. Viable gauge choices in cosmologies with nonlinear structures. *Phys. Rev. D*, 101(6):063530, 2020. doi: 10.1103/PhysRevD.101.063530. 42

[74] D. Clowe, M. Bradac, A. H. Gonzalez, M. Markevitch, S. W. Randall, C. Jones, and D. Zaritsky. A direct empirical proof of the existence of dark matter. *Astrophys. J. Lett.*, 648:L109–L113, 2006. doi: 10.1086/508162. 1

[75] A. A. Coley. *Dynamical systems and Cosmology*. Kluwer, Dordrecht, Netherlands, 2003. doi: 10.1007/978-94-017-0327-7. 56

[76] E. J. Copeland, A. R. Liddle, and D. Wands. Exponential potentials and cosmological scaling solutions. *Phys. Rev. D*, 57:4686–4690, 1998. doi: 10.1103/PhysRevD.57.4686. 67

[77] E. J. Copeland, M. Sami, and S. Tsujikawa. Dynamics of dark energy. *Int. J. Mod. Phys. D*, 15(11):1753–1935, 2006. doi: 10.1142/S021827180600942X. 67

[78] E. J. Copeland, S. Mizuno, and M. Shaeri. Cosmological dynamics of a dirac-born-infeld field. *Phys. Rev. D*, 81:123501, 2010. doi: 10.1103/PhysRevD.81.123501. 54, 78

[79] V. Corbin and N. J. Cornish. Detecting the cosmic gravitational wave background with the big bang observer. *Class. Quantum Grav.*, 23:2435–2446, 2006. doi: 10.1088/0264-9381/23/7/014. 10

[80] P. Creminelli and F. Vernizzi. Dark energy after GW170817 and GRB170817A. *Phys. Rev. Lett.*, 119:251302, Dec 2017. doi: 10.1103/PhysRevLett.119.251302. 15, 19

[81] J. Crowder and N. J. Cornish. Beyond LISA: Exploring future gravitational wave missions. *Phys. Rev. D*, 72:083005, 2005. doi: 10.1103/PhysRevD.72.083005. 10

[82] T. Damour. *Binary Systems as Test-Beds of Gravity Theories*, pages 1–41. Springer Netherlands, Dordrecht, 2009. ISBN 978-1-4020-9264-0. doi: 10.1007/978-1-4020-9264-0_1. 14, 15

[83] T. Damour. 1974: The discovery of the first binary pulsar. *Class. Quantum Grav.*, 32(12):124009, 2015. doi: 10.1088/0264-9381/32/12/124009. 17

[84] R. Daniel, M. Campbell, C. van de Bruck, and P. Dunsby. Transitioning from a bounce to R^2 inflation. *JCAP*, 2023(06):030, 2023. doi: 10.1088/1475-7516/2023/06/030. 28

[85] A. De Felice and S. Tsujikawa. f(R) theories. *Living Rev. Rel.*, 13:3, 2010. doi: 10.12942/lrr-2010-3. 99

[86] C. de Rham and A. J. Tolley. DBI and the Galileon reunited. *JCAP*, 05:015, 2010. doi: 10.1088/1475-7516/2010/05/015. 22

[87] C. de Rham, G. Gabadadze, and A. J. Tolley. Resummation of Massive Gravity. *Phys. Rev. Lett.*, 106:231101, 2011. doi: 10.1103/PhysRevLett.106.231101. 22

[88] P. C. M. Delgado, R. Durrer, and N. Pinto-Neto. The CMB bispectrum from bouncing cosmologies. *JCAP*, 11:024, 2021. doi: 10.1088/1475-7516/2021/11/024. 9

[89] M. S. R. Delgaty and K. Lake. Physical acceptability of isolated, static, spherically symmetric, perfect fluid solutions of Einstein's equations. *Comput. Phys. Commun.*, 115:395–415, 1998. doi: 10.1016/S0010-4655(98)00130-1. xxiv, 106, 108, 117

[90] N. Deruelle, M. Sasaki, and Y. Sendouda. Junction conditions in $f(R)$ theories of gravity. *Prog. Theor. Phys.*, 119(2):237–251, 2008. ISSN 0033-068X. doi: 10.1143/PTP.119.237. 18, 111

[91] R. H. Dicke and P. J. E. Peebles. The big bang cosmology - enigmas and nostrums. In S. W. Hawking and W. Israel, editors, *General Relativity: An Einstein centenary survey*, pages 504–517, 1979. 5

[92] A. D. Dolgov and M. Kawasaki. Can modified gravity explain accelerated cosmic expansion? *Phys. Lett. B*, 573:1–4, 2003. doi: 10.1016/j.physletb.2003.08.039. 24

[93] J. Droste. The field of a single centre in Einstein's theory of gravitation, and the motion of a particle in that field. *Koninklijke Nederlandse Akademie van Wetenschappen Proceedings Series B Physical Sciences*, 19:197–215, 1917. 16

[94] J. Droste. "Golden Oldie": The Field of a Single Centre in Einstein's Theory of Gravitation, and the Motion of a Particle in That Field. *Gen. Rel. Grav.*, 9:1545–1563, 2002. doi: 10.1023/A:1020747322668. 16

[95] M. J. Duff. M Theory (The Theory Formerly Known as Strings). *Int. J. Mod. Phys. A*, 11:5623–5642, 1996. doi: 10.1201/9781482268737-36. 2, 23

[96] P. K. S. Dunsby and G. F. R. Ellis. Perturbations of Cosmological Backgrounds. *Fundam. Theor. Phys.*, 100:493–508, 1999. doi: 10.1007/978-94-017-0934-7_29. 41, 44

[97] P. K. S. Dunsby, B. A. C. C. Bassett, and G. F. R. Ellis. Covariant analysis of gravitational waves in a cosmological context. *Class. Quantum Grav.*, 14:1215–1222, 1997. doi: 10.1088/0264-9381/14/5/023. 49

[98] F. W. Dyson, A. S. Eddington, and C. Davidson. A Determination of the Deflection of Light by the Sun's Gravitational Field, from Observations Made at the Total Eclipse of May 29, 1919. *Phil. Trans. Roy. Soc. Lond. A*, 220:291–333, 1920. doi: 10.1098/rsta.1920.0009. 17

[99] C. Ecker, T. Gorda, A. Kurkela, et al. Constraining the equation of state in neutron-star cores via the long-ringdown signal. *Nat. Commun.*, 16:1320, 2025. doi: 10.1038/s41467-025-56500-x. 19

[100] A. S. Eddington. *The Mathematical Theory of Relativity*. The University Press, Cambridge [Eng.], 1930. 16

[101] A. Einstein. Erklärung der perihelbewegung des merkur aus der allgemeinen relativitätstheorie. *Sitzungsberichte der preußischen Akademie der Wissenschaften*, 831: 839, 1915. 17

[102] A. Einstein. Approximative Integration of the Field Equations of Gravitation. *Sitzungsber. Preuss. Akad. Wiss. Berlin (Math. Phys.)*, 1916:688–696, 1916. 49

[103] A. Einstein. Kosmologische Betrachtungen zur allgemeinen Relativitätstheorie. *Sitzungsberichte der Königlich Preussischen Akademie der Wissenschaften*, pages 142–152, 1917. 2

[104] A. Einstein. Über Gravitationswellen. *Sitzungsber. Preuss. Akad. Wiss. Berlin (Math. Phys.)*, 1918:154–167, 1918. 49

[105] A. Einstein and A. Engel. *The Collected Papers of Albert Einstein: English Translation. The Berlin years.* Number v. 6. Princeton University Press, 1997. ISBN 9780691017341. 2

[106] A. Einstein and E. G. Straus. The influence of the expansion of space on the gravitation fields surrounding the individual stars. *Rev. Mod. Phys.*, 17:120–124, 1945. doi: 10.1103/RevModPhys.17.120. 18

[107] E. Elizalde. *The Hubble-Lemaître Law and the Expansion of the Universe*. Springer International Publishing, Cham, 2021. ISBN 978-3-030-80654-5. doi: 10.1007/978-3-030-80654-5_5. 4

[108] G. F. R Ellis. Editorial note to: E. Lifshitz, On the gravitational stability of the expanding universe. *Gen. Rel. Grav.*, 49, 02 2017. doi: 10.1007/s10714-016-2164-9. 49

[109] G. F. R. Ellis and R. Maartens. The emergent universe: Inflationary cosmology with no singularity. *Class. Quantum Grav.*, 21:223–232, 2004. doi: 10.1088/0264-9381/21/1/015. 3

[110] G. F. R. Ellis and H. van Elst. Cosmological Models (Cargèse lectures 1998). In *Theoretical and Observational Cosmology*, volume 541 of *NATO Advanced Study Institute (ASI) Series C*, pages 1–116, 1999. doi: 10.48550/arXiv.gr-qc/9812046. 92

[111] G. F. R. Ellis and J. Wainwright. *Dynamical Systems in Cosmology*. Cambridge University Press, 1997. 56

[112] G. F. R. Ellis, J. Murugan, and C. G. Tsagas. The Emergent universe: An Explicit construction. *Class. Quantum Grav.*, 21(1):233–250, 2004. doi: 10.1088/0264-9381/21/1/016. 3

[113] G. F. R. Ellis, E. Platts, D. Sloan, and A. Weltman. Current observations with a decaying cosmological constant allow for chaotic cyclic cosmology. *JCAP*, 04:026, 2016. doi: 10.1088/1475-7516/2016/04/026. 79, 143

[114] J. Emery, G. Tasinato, and D. Wands. Mixed non-Gaussianity in multiple-DBI inflation. *JCAP*, 05:021, 2013. doi: 10.1088/1475-7516/2013/05/021. 13

[115] C. W. F. Everitt et al. Gravity Probe B: Final Results of a Space Experiment to Test

General Relativity. *Phys. Rev. Lett.*, 106:221101, 2011. doi: 10.1103/PhysRevLett.106.221101. 20

[116] T. Evstafyeva, R. Ro şca Mead, U. Sperhake, and B. Brügmann. Boson stars in massless and massive scalar-tensor gravity. *Phys. Rev. D*, 108:104064, 2023. doi: 10.1103/PhysRevD.108.104064. 15

[117] J. M. Ezquiaga and M. Zumalacárregui. Dark Energy After GW170817: Dead Ends and the Road Ahead. *Phys. Rev. Lett.*, 119(25):251304, 2017. doi: 10.1103/PhysRevLett.119.251304. 15, 19

[118] S. M. Faber and J. S. Gallagher. Masses and mass-to-light ratios of galaxies. *Annu. Rev. Astron. Astrophys.*, 17:135–187, 1979. doi: 10.1146/annurev.aa.17.090179.001031. 2

[119] V. Faraoni. Matter instability in modified gravity. *Phys. Rev. D*, 74:104017, 2006. doi: 10.1103/PhysRevD.74.104017. 24

[120] P. Feola, X. J. Forteza, S. Capozziello, R. Cianci, and S. Vignolo. Mass-radius relation for neutron stars in $f(R) = R+\alpha R^2$ gravity: A comparison between purely metric and torsion formulations. *Phys. Rev. D*, 101:044037, 2020. doi: 10.1103/PhysRevD.101.044037. 16, 121

[121] R. C. Fernandez and A. de la Cruz-Dombriz. Toward a realistic Buchdahl limit in $f(R)$ theories of gravity. *Phys. Rev. D*, 111(6):064073, 2025. doi: 10.1103/PhysRevD.111.064073. 16

[122] A. Ferté and K. Hong. Results and forecasts on cosmic inflation from weak lensing. *Phys. Rev. D*, 109:103502, 2024. doi: 10.1103/PhysRevD.109.103502. 22

[123] A. Finke, S. Foffa, F. Iacovelli, M. Maggiore, and M. Mancarella. Modified gravitational wave propagation and the binary neutron star mass function. *Phys. Dark Univ.*, 36:100994, 2022. doi: 10.1016/j.dark.2022.100994. 14, 15

[124] E. B. Fomalont and S. M. Kopeikin. The measurement of the light deflection from Jupiter: Experimental Results. *Astrophys. J.*, 598:704–711, 2003. doi: 10.1086/378785. 17

[125] G. Gamow. The origin of elements and the separation of galaxies. *Phys. Rev.*, 74: 505–506, 1948. doi: 10.1103/PhysRev.74.505.2. 4

[126] G. Gamow. The Evolution of the Universe. *Nature*, 162(4122):680–682, 1948. doi: 10.1038/162680a0. 4

[127] A. Ganguly, R. Gannouji, R. Goswami, and S. Ray. Neutron stars in the Starobinsky model. *Phys. Rev. D*, 89:064019, 2014. doi: 10.1103/PhysRevD.89.064019. 16, 121

[128] A. Ganguly, R. Gannouji, R. Goswami, and S. Ray. Global structure of black holes via the dynamical system. *Class. Quantum Grav.*, 32(10):105006, 2015. doi: 10.1088/0264-9381/32/10/105006. 92

[129] T. Ghigna et al. The LiteBIRD mission to explore cosmic inflation. In *SPIE Astronomical Telescopes + Instrumentation 2024*, 6 2024. 22

[130] D. J. Gogoi and U. Dev Goswami. A new $f(R)$ gravity model and properties of gravitational waves in it. *Eur. Phys. J. C*, 80(12):1101, 2020. doi: 10.1140/epjc/s10052-020-08684-3. 20

[131] M. Goliath and G. F. R. Ellis. Homogeneous cosmologies with cosmological constant. *Phys. Rev. D*, 60:023502, 1999. doi: 10.1103/PhysRevD.60.023502. 57

[132] C. Gordon, D. Wands, B. A. Bassett, and R. Maartens. Adiabatic and entropy perturbations from inflation. *Phys. Rev. D*, 63:023506, 2000. doi: 10.1103/PhysRevD.63.023506. 42

[133] J. L. Greenstein, J. B. Oke, and H. L. Shipman. Effective Temperature, Radius, and Gravitational Redshift of Sirius B. *Astrophys. J.*, 169:563, 1971. doi: 10.1086/151174. 17

[134] Ö. Güngör and G. D. Starkman. A classical, non-singular, bouncing universe. *JCAP*, 04:003, 2021. doi: 10.1088/1475-7516/2021/04/003. 30, 32, 36, 51

[135] A. Guth and J. Silk. The Inflationary Universe: The Quest for a New Theory of Cosmic Origins. *Phys. Today*, 50(10):102, 1997. doi: 10.1063/1.881979. 5

[136] A. H. Guth. Inflationary universe: A possible solution to the horizon and flatness problems. *Phys. Rev. D*, 23:347–356, 1981. doi: 10.1103/PhysRevD.23.347. 5

[137] T. Harko, F. S. N. Lobo, M. K. Mak, and S. V. Sushkov. Modified-gravity wormholes without exotic matter. *Phys. Rev. D*, 87:067504, 2013. doi: 10.1103/PhysRevD.87.067504. 15

[138] E. R. Harrison. Normal Modes of Vibrations of the Universe. *Rev. Mod. Phys.*, 39: 862–882, 1967. doi: 10.1103/RevModPhys.39.862. 44

[139] E. R. Harrison. Fluctuations at the threshold of classical cosmology. *Phys. Rev. D*, 1:2726–2730, 1970. doi: 10.1103/PhysRevD.1.2726. 4

[140] S. W. Hawking. Perturbations of an Expanding Universe. *ApJ*, 145:544, 1966. doi: 10.1086/148793. 49

[141] S. W. Hawking and H. Bondi. The occurrence of singularities in cosmology. *Proceedings of the Royal Society of London. Series A. Mathematical and Physical Sciences*, 294(1439):511–521, 1966. doi: 10.1098/rspa.1966.0221. 2

[142] S. W. Hawking and H. Bondi. The occurrence of singularities in cosmology. II. *Proceedings of the Royal Society of London. Series A. Mathematical and Physical Sciences*, 295(1443):490–493, 1966. doi: 10.1098/rspa.1966.0255.

[143] S. W. Hawking and H. Bondi. The occurrence of singularities in cosmology. III. causality and singularities. *Proceedings of the Royal Society of London. Series A. Mathematical and Physical Sciences*, 300(1461):187–201, 1967. doi: 10.1098/rspa.1967.0164. 2

[144] S. W. Hawking, T. Hertog, and H. S. Reall. Trace anomaly driven inflation. *Phys. Rev. D*, 63:083504, 2001. doi: 10.1103/PhysRevD.63.083504. 7

[145] L. Heisenberg, M. Bartelmann, R. Brandenberger, and A. Refregier. Model independent analysis of supernova data, dark energy, trans-Planckian censorship and the swampland. *Phys. Lett. B*, 812:135990, 2021. doi: 10.1016/j.physletb.2020.135990. 14

[146] L. Herrera and N. O. Santos. Local anisotropy in self-gravitating systems. *Phys. Rep.*, 286:53–130, 1997. doi: 10.1016/S0370-1573(96)00042-7. 99

[147] K. Hinterbichler. Theoretical Aspects of Massive Gravity. *Rev. Mod. Phys.*, 84: 671–710, 2012. doi: 10.1103/RevModPhys.84.671. 22

[148] W. Hu and I. Sawicki. Models of $f(R)$ cosmic acceleration that evade solar system tests. *Phys. Rev. D*, 76:064004, 2007. doi: 10.1103/PhysRevD.76.064004. 140

[149] H. Huang, J. Kunz, and D. Mitra. Shadow images of compact objects in beyond Horndeski theory. *JCAP*, 05:007, 2024. doi: 10.1088/1475-7516/2024/05/007. 14, 15

[150] M.-X. Huang, G. Shiu, and B. Underwood. Multifield DBI Inflation and Non-Gaussianities. *Phys. Rev. D*, 77:023511, 2008. doi: 10.1103/PhysRevD.77.023511. 13

[151] J.-C. Hwang and H.-R. Noh. Gauge ready formulation of the cosmological kinetic theory in generalized gravity theories. *Phys. Rev. D*, 65:023512, 2002. doi: 10.1103/PhysRevD.65.023512. 42, 48, 50

[152] A. Ijjas. Cyclic completion of the anamorphic universe. *Class. Quantum Grav.*, 35 (7):075010, 2018. doi: 10.1088/1361-6382/aab086. 10

[153] A. Ijjas and P. J. Steinhardt. The anamorphic universe. *JCAP*, 10:001, 2015. doi: 10.1088/1475-7516/2015/10/001. 8

[154] A. Ijjas and P. J. Steinhardt. Bouncing cosmology made simple. *Class. and Quantum Grav.*, 35(13):135004, 2018. doi: 10.1088/1361-6382/aac482. 7

[155] A. Ijjas and P. J. Steinhardt. A new kind of cyclic universe. *Phys. Lett. B*, 795: 666–672, 2019. doi: 10.1016/j.physletb.2019.06.056. 3

[156] W. Israel. Singular hypersurfaces and thin shells in general relativity. *Nuovo Cim. B*, 44S10:1, 1966. doi: 10.1007/BF02710419. [Erratum: Nuovo Cim.B 48, 463 (1967)]. 110

[157] S. Kachru, R. Kallosh, A. D. Linde, J. M. Maldacena, L. P. McAllister, and S. P. Trivedi. Towards inflation in string theory. *JCAP*, 10:013, 2003. doi: 10.1088/1475-7516/2003/10/013. 12

[158] R. Kallosh, L. Kofman, and A. D. Linde. Pyrotechnic universe. *Phys. Rev. D*, 64: 123523, 2001. doi: 10.1103/PhysRevD.64.123523. 8

[159] R. Kallosh, L. Kofman, A. D. Linde, and A. A. Tseytlin. BPS branes in cosmology. *Phys. Rev. D*, 64:123524, 2001. doi: 10.1103/PhysRevD.64.123524.

[160] R. Kallosh, J. U. Kang, A. D. Linde, and V. Mukhanov. The New ekpyrotic ghost. *JCAP*, 04:018, 2008. doi: 10.1088/1475-7516/2008/04/018. 8

[161] D. J. Kapner, T. S. Cook, E. G. Adelberger, J. H. Gundlach, Blayne R. Heckel, C. D. Hoyle, and H. E. Swanson. Tests of the gravitational inverse-square law below the dark-energy length scale. *Phys. Rev. Lett.*, 98:021101, 2007. doi: 10.1103/PhysRevLett.98.021101. 20

[162] T. Katsuragawa, T. Nakamura, T. Ikeda, and S. Capozziello. Gravitational waves in $F(R)$ gravity: Scalar waves and the chameleon mechanism. *Phys. Rev. D*, 99: 124050, 2019. doi: 10.1103/PhysRevD.99.124050. 20

[163] S. Kecskemeti, J. Maiden, G. Shiu, and B. Underwood. DBI Inflation in the Tip Region of a Warped Throat. *JHEP*, 09:076, 2006. doi: 10.1088/1126-6708/2006/09/076. 13

[164] J. Khoury, B. A. Ovrut, P. J. Steinhardt, and N. Turok. The Ekpyrotic universe: Colliding branes and the origin of the hot big bang. *Phys. Rev. D*, 64:123522, 2001. doi: 10.1103/PhysRevD.64.123522. 7

[165] W. H. Kinney and K. Tzirakis. Quantum modes in DBI inflation: exact solutions and constraints from vacuum selection. *Phys. Rev. D*, 77:103517, 2008. doi: 10.1103/PhysRevD.77.103517. 13

[166] H. Kodama and M. Sasaki. Cosmological Perturbation Theory. *Prog. Theor. Phys. Suppl.*, 78:1–166, 1984. doi: 10.1143/PTPS.78.1. 41, 44

[167] H. Kragh. Hubble Law or Hubble-Lemaître Law? The IAU Resolution. *arXiv e-prints*, art. arXiv:1809.02557, 2018. doi: 10.48550/arXiv.1809.02557. 4

[168] M. Kramer, I. H. Stairs, R. N. Manchester, N. Wex, A. T. Deller, W. A. Coles, M. Ali, M. Burgay, F. Camilo, I. Cognard, T. Damour, G. Desvignes, R. D. Ferdman, P. C. C. Freire, S. Grondin, L. Guillemot, G. B. Hobbs, G. Janssen, R. Karuppusamy, D. R. Lorimer, A. G. Lyne, J. W. McKee, M. McLaughlin, L. E. Münch, B. B. P. Perera, N. Pol, A. Possenti, J. Sarkissian, B. W. Stappers, and G. Theureau. Strong-field gravity tests with the double pulsar. *Phys. Rev. X*, 11:041050, Dec 2021. doi: 10.1103/PhysRevX.11.041050. 17

[169] X.-M. Kuang, Z.-Y. Tang, B. Wang, and A. Wang. Constraining a modified gravity theory in strong gravitational lensing and black hole shadow observations. *Phys. Rev. D*, 106(6):064012, 2022. doi: 10.1103/PhysRevD.106.064012. 14, 15

[170] G. Lambiase, M. Sakellariadou, and A. Stabile. Constraints on extended gravity

models through gravitational wave emission. *JCAP*, 2021(03):014, 2021. doi: 10.1088/1475-7516/2021/03/014. 21

[171] D. Langlois, D. M. Sedrakian, and B. Carter. Differential rotation of relativistic superfluid in neutron stars. *MNRAS*, 297:1189, 1998. doi: 10.1046/j.1365-8711.1998.01575.x. 97

[172] D. Langlois, S. Renaux-Petel, D. A. Steer, and T. Tanaka. Primordial perturbations and non-Gaussianities in DBI and general multi-field inflation. *Phys. Rev. D*, 78:063523, 2008. doi: 10.1103/PhysRevD.78.063523. 13

[173] D. Langlois, S. Renaux-Petel, D. A. Steer, and T. Tanaka. Primordial fluctuations and non-Gaussianities in multi-field DBI inflation. *Phys. Rev. Lett.*, 101:061301, 2008. doi: 10.1103/PhysRevLett.101.061301. 13

[174] J.-L. Lehners. Ekpyrotic and Cyclic Cosmology. *Phys. Rept.*, 465:223–263, 2008. doi: 10.1016/j.physrep.2008.06.001. 8, 10

[175] G. Lemaître. A Homogeneous Universe of Constant Mass and Growing Radius Accounting for the Radial Velocity of Extragalactic Nebulae. *Annales Soc. Sci. Bruxelles A*, 47:49–59, 1927. doi: 10.1007/s10714-013-1548-3. 3

[176] P. S. Letelier. Anisotropic fluids with two-perfect-fluid components. *Phys. Rev. D*, 22:807–813, 1980. doi: 10.1103/PhysRevD.22.807. 99

[177] C. Li, R. H. Brandenberger, and Y.-K. E. Cheung. Big-Bounce Genesis. *Phys. Rev. D*, 90(12):123535, 2014. doi: 10.1103/PhysRevD.90.123535. 8

[178] A. R. Liddle and D. H. Lyth. *Cosmological inflation and large scale structure*. Cambridge University Press, 2000. ISBN 978-0-521-57598-0, 978-0-521-82849-9. doi: 10.1017/CBO9781139175180. 4

[179] S. L. Liebling and C. Palenzuela. Dynamical boson stars. *Living Rev. Rel.*, 26(1):1, 2023. doi: 10.1007/s41114-023-00043-4. 15

[180] E. M. Lifshitz. Republication of: On the gravitational stability of the expanding universe. *J. Phys. (USSR)*, 10(2):116, 1946. doi: 10.1007/s10714-016-2165-8. 49

[181] E. M. Lifshitz and I. M. Khalatnikov. Investigations in relativistic cosmology†. *Adv. Phys.*, 12(46):185–249, 1963. doi: 10.1080/00018736300101283. 49

[182] A. D. Linde. A New Inflationary Universe Scenario: A Possible Solution of the Horizon, Flatness, Homogeneity, Isotropy and Primordial Monopole Problems. *Phys. Lett. B*, 108:389–393, 1982. doi: 10.1016/0370-2693(82)91219-9. 5

[183] A. D. Linde. Chaotic inflation. *Phys. Lett. B*, 129(3):177–181, 1983. ISSN 0370-2693. doi: https://doi.org/10.1016/0370-2693(83)90837-7. 5

[184] J. Liu, Y.-F. Cai, and H. Li. Evidences for bouncing evolution before inflation in cosmological surveys. *J. Theor. Phys.*, 1:1–10, 2012. 8

[185] T. Liu, X. Zhang, and W. Zhao. Constraining $f(R)$ gravity in solar system, cosmology and binary pulsar systems. *Phys. Lett. B*, 777:286–293, 2018. ISSN 0370-2693. doi: https://doi.org/10.1016/j.physletb.2017.12.051. 14, 15

[186] F. S. N. Lobo. Wormhole geometries in modified gravity. *AIP Conference Proceedings*, 1458(1):447–450, 2012. ISSN 0094-243X. doi: 10.1063/1.4734456. 15

[187] L. Lombriser, A. Slosar, U. Seljak, and W. Hu. Constraints on $f(R)$ gravity from probing the large-scale structure. *Phys. Rev. D*, 85:124038, 2012. doi: 10.1103/PhysRevD.85.124038. 19

[188] F. Lucchin and S. Matarrese. Power-law inflation. *Phys. Rev. D*, 32:1316–1322, 1985. doi: 10.1103/PhysRevD.32.1316. 62

[189] J.-P. Luminet. Editorial note to 'The beginning of the world from the point of view of quantum theory'. *Gen. Rel. Grav.*, 43:2911–2928, 2011. doi: 10.1007/s10714-011-1213-7. 3

[190] J.-P. Luminet. Editorial note to "A Homogeneous Universe of Constant Mass and Increasing Radius accounting for the Radial Velocity of Extra–Galactic Nebulae" by Georges Lemaître (1927). *Gen. Rel. Grav.*, 45:1619–1633, 2013. doi: 10.1007/s10714-013-1547-4.

[191] J.-P. Luminet. Lemaître's Big Bang. *PoS*, FFP14:214, 2016. doi: 10.22323/1.224.0214. 3

[192] A. Lupsasca, D. R. Mayerson, B. Ripperda, and S. Staelens. *A Beginner's Guide to Black Hole Imaging and Associated Tests of General Relativity*, pages 183–237. 2024. doi: 10.1007/978-981-97-2871-8_6. 14, 15

[193] D. H. Lyth and A. Riotto. Particle physics models of inflation and the cosmological density perturbation. *Phys. Rept.*, 314:1–146, 1999. doi: 10.1016/S0370-1573(98)00128-8. 31

[194] C. F. B. Macedo, J. L. Rosa, and D. Rubiera-Garcia. Optical appearance of black holes surrounded by a dark matter halo. *JCAP*, 07:046, 2024. doi: 10.1088/1475-7516/2024/07/046. 14, 15

[195] K. A. Malik and D. Wands. Cosmological perturbations. *Phys. Rept.*, 475:1–51, 2009. doi: 10.1016/j.physrep.2009.03.001. 42

[196] S. Mastrogiovanni, D. Steer, and M. Barsuglia. Probing modified gravity theories and cosmology using gravitational-waves and associated electromagnetic counterparts. *Phys. Rev. D*, 102(4):044009, 2020. doi: 10.1103/PhysRevD.102.044009. 15

[197] C. H. McGruder and B. W. VanDerMeer. The 1916 PhD Thesis of Johannes Droste and the Discovery of Gravitational Repulsion. 1 2018. 16

[198] S. Mignemi and D. L. Wiltshire. Black holes in higher derivative gravity theories. *Phys. Rev. D*, 46:1475–1506, 1992. doi: 10.1103/PhysRevD.46.1475. 17, 121

[199] C. W. Misner. The Isotropy of the Universe. *ApJ*, 151:431, 1968. doi: 10.1086/149448. 4

[200] C. W. Misner, K. S. Thorne, and J. A. Wheeler. *Gravitation*. W. H. Freeman, San Francisco, 1973. ISBN 978-0-7167-0344-0, 978-0-691-17779-3. viii

[201] V. F. Mukhanov. *Physical Foundations of Cosmology*. Cambridge University Press, Oxford, 2005. ISBN 978-0-521-56398-7. doi: 10.1017/CBO9780511790553. 5

[202] V. F. Mukhanov, H. A. Feldman, and R. H. Brandenberger. Theory of cosmological perturbations. *Phys. Rep.*, 215(5-6):203–333, 1992. doi: 10.1016/0370-1573(92)90044-Z. 41

[203] D. J. Mulryne, R. Tavakol, J. E. Lidsey, and G. F. R. Ellis. An Emergent Universe from a loop. *Phys. Rev. D*, 71:123512, 2005. doi: 10.1103/PhysRevD.71.123512. 3

[204] J. Näf and P. Jetzer. On the $1/c$ expansion of $f(R)$ gravity. *Phys. Rev. D*, 81:104003, 2010. doi: 10.1103/PhysRevD.81.104003. 19, 20

[205] N. F. Naidu, S. Carloni, and P. K. S. Dunsby. Two-fluid stellar objects in general relativity: The covariant formulation. *Phys. Rev. D*, 104:044014, 2021. doi: 10.1103/PhysRevD.104.044014. 101, 104, 121, 139

[206] N. F. Naidu, S. Carloni, and P. K. S. Dunsby. Anisotropic two-fluid stellar objects in general relativity. *Phys. Rev. D*, 106:124023, 2022. doi: 10.1103/PhysRevD.106.124023. 101, 121, 139

[207] A. Narang, S. Mohanty, and S. Jana. Gravitational radiation from binary systems in $f(R)$ gravity: A semi-classical approach. *JCAP*, 03:008, 2023. doi: 10.1088/1475-7516/2023/03/008. 14, 15

[208] G. G. L. Nashed and S. Capozziello. Anisotropic compact stars in $f(R)$ gravity. *Eur. Phys. J. C*, 81(5):481, 2021. doi: 10.1140/epjc/s10052-021-09273-8. 99

[209] P. Navarro Moreno, A. Wojnar, and F. J. Llanes-Estrada. Testing gravity with the latent heat of neutron star matter. *JCAP*, 01:015, 2025. doi: 10.1088/1475-7516/2025/01/015. 14, 15

[210] C. Negrelli, L. Kraiselburd, S. Landau, and C. G. Scóccola. Testing Modified Gravity theory (MOG) with Type Ia Supernovae, Cosmic Chronometers and Baryon Acoustic Oscillations. *JCAP*, 07:015, 2020. doi: 10.1088/1475-7516/2020/07/015. 14

[211] H. K. Nguyen. Beyond Schwarzschild–de Sitter spacetimes: A new exhaustive class of metrics inspired by Buchdahl for pure R^2 gravity in a compact form. *Phys. Rev. D*, 106:104004, 2022. doi: 10.1103/PhysRevD.106.104004. 17

[212] A. Nicolis, R. Rattazzi, and E. Trincherini. The Galileon as a local modification of gravity. *Phys. Rev. D*, 79:064036, 2009. doi: 10.1103/PhysRevD.79.064036. 22

[213] S. Nojiri and S. D. Odintsov. Modified gravity with negative and positive powers of the curvature: Unification of the inflation and of the cosmic acceleration. *Phys. Rev. D*, 68:123512, 2003. doi: 10.1103/PhysRevD.68.123512. 24

[214] S. Nojiri and S. D. Odintsov. Modified gravity with $\ln(R)$ terms and cosmic acceleration. *Gen. Rel. Grav.*, 36:1765–1780, 2004. doi: 10.1023/B:GERG.0000035950.40718.48. 24

[215] M. Novello and S. E. Perez Bergliaffa. Bouncing Cosmologies. *Phys. Rept.*, 463:127–213, 2008. doi: 10.1016/j.physrep.2008.04.006. 7

[216] A. M. Nzioki, P. K. S. Dunsby, R. Goswami, and S. Carloni. A Geometrical Approach to Strong Gravitational Lensing in $f(R)$ Gravity. *Phys. Rev. D*, 83:024030, 2011. doi: 10.1103/PhysRevD.83.024030. 140, 146

[217] A. M. Nzioki, R. Goswami, and P. K. S. Dunsby. Jebsen-Birkhoff theorem and

its stability in $f(R)$ gravity. *Phys. Rev. D*, 89(6):064050, 2014. doi: 10.1103/PhysRevD.89.064050. 18

[218] V. K. Oikonomou. Effects of a pre-inflationary de Sitter bounce on the primordial gravitational waves in $f(R)$ gravity theories. *Nucl. Phys. B*, 984:115985, 2022. doi: 10.1016/j.nuclphysb.2022.115985. 9

[219] J. R. Oppenheimer and G. M. Volkoff. On massive neutron cores. *Phys. Rev.*, 55: 374–381, 1939. doi: 10.1103/PhysRev.55.374. 81, 85, 91, 103

[220] M. Ostrogradsky. Mémoires sur les équations différentielles, relatives au problème des isopérimètres. *Mem. Acad. St. Petersbourg*, 6(4):385–517, 1850. 24

[221] T. Padmanabhan. *Structure Formation in the Universe*. Cambridge University Press, 1993. ISBN 9780521424868. 4

[222] A. Paliathanasis, M. Tsamparlis, S. Basilakos, and J. D. Barrow. Dynamical analysis in scalar field cosmology. *Phys. Rev. D*, 91:123535, 2015. doi: 10.1103/PhysRevD.91.123535. 67

[223] T. Papanikolaou, S. Banerjee, Y-F Cai, S. Capozziello, and E. N. Saridakis. Primordial black holes and induced gravitational waves in non-singular matter bouncing cosmology. *JCAP*, 06:066, 2024. doi: 10.1088/1475-7516/2024/06/066. 52

[224] L. Parker and S. A. Fulling. Quantized matter fields and the avoidance of singularities in general relativity. *Phys. Rev. D*, 7:2357–2374, 1973. doi: 10.1103/PhysRevD.7.2357. 7

[225] W. Pauli. *Relativitätstheorie*. Springer, 2000. 16

[226] E. Pechlaner and R. Sexl. On quadratic lagrangians in general relativity. *Commun. Math. Phys.*, 2:165–175, 1966. 17

[227] P. J. E. Peebles. Large-scale background temperature and mass fluctuations due to scale-invariant primeval perturbations. *ApJL*, 263:L1–L5, 1982. doi: 10.1086/183911. 4

[228] P. J. E. Peebles. Discovery of the Hot Big Bang: What happened in 1948. *Eur. Phys. J. H*, 39:205–223, 2014. doi: 10.1140/epjh/e2014-50002-y. 4

[229] P. J. E. Peebles. Anomalies in physical cosmology. *Annals Phys.*, 447:169159, 2022. doi: 10.1016/j.aop.2022.169159. 1

[230] R. Penrose. Gravitational collapse and space-time singularities. *Phys. Rev. Lett.*, 14:57–59, 1965. doi: 10.1103/PhysRevLett.14.57. 2

[231] R. Penrose. Before the big bang: An outrageous new perspective and its implications for particle physics. *Conf. Proc. C*, 060626:2759–2767, 2006. 8

[232] R. Penrose. *Cycles of Time: An Extraordinary New View of the Universe*. Knopf Doubleday Publishing Group, 2011. ISBN 9780307596741. 8

[233] A. A. Penzias and R. G. Wilson. A measurement of excess antenna temperature at 4080-mc/s. *ApJ*, 142:419–421, 1965. 4

[234] S. Perlmutter et al. Measurements of Ω and Λ from 42 High Redshift Supernovae. *Astrophys. J.*, 517:565–586, 1999. doi: 10.1086/307221. 1, 2

[235] P. Peter and J.-P. Uzan. *Primordial Cosmology*. Oxford Graduate Texts. Oxford University Press, 2013. ISBN 978-0-19-966515-0, 978-0-19-920991-0. 56

[236] S. Pi and M. Sasaki. Primordial black hole formation in nonminimal curvaton scenarios. *Phys. Rev. D*, 108(10):L101301, 2023. doi: 10.1103/PhysRevD.108.L101301. 52, 143

[237] Planck Collaboration, Y. Akrami, et al. Planck 2018 results. IX. Constraints on

primordial non-Gaussianity. *Astron. Astrophys.*, 641:A9, 2020. doi: 10.1051/0004-6361/201935891. 21

[238] R. V. Pound and G. A. Rebka. Gravitational red-shift in nuclear resonance. *Phys. Rev. Lett.*, 3:439–441, 1959. doi: 10.1103/PhysRevLett.3.439. 17

[239] J. P. Preskill. Cosmological production of superheavy magnetic monopoles. *Phys. Rev. Lett.*, 43:1365–1368, 1979. doi: 10.1103/PhysRevLett.43.1365. 4

[240] B. Reina, J. M. M. Senovilla, and R. Vera. Junction conditions in quadratic gravity: thin shells and double layers. *Class. Quantum Grav.*, 33(10):105008, 2016. doi: 10.1088/0264-9381/33/10/105008. 139

[241] A. G. Riess, A. V. Filippenko, P. Challis, A. Clocchiatti, A. Diercks, P. M. Garnavich, R. L. Gilliland, C. J. Hogan, S. Jha, R. P. Kirshner, B. Leibundgut, M. M. Phillips, D. Reiss, B. P. Schmidt, R. A. Schommer, R. C. Smith, J. Spyromilio, C. Stubbs, N. B. Suntzeff, and J. Tonry. Observational evidence from supernovae for an accelerating universe and a cosmological constant. *Astron. J.*, 116(3):1009, 1998. doi: 10.1086/300499. 2

[242] W. Rindler. Visual horizons in world models. *MNRAS*, 116(6):662–677, 1956. ISSN 0035-8711. doi: 10.1093/mnras/116.6.662. 4

[243] J. L. Rosa. Junction conditions in gravity theories with extra scalar degrees of freedom. *Phys. Rev. D*, 109:064018, 2024. doi: 10.1103/PhysRevD.109.064018. 111

[244] C. Rovelli. Loop quantum gravity. *Living Rev. Rel.*, 1:1, 1998. doi: 10.12942/lrr-1998-1. 2

[245] C. Rovelli. *Quantum gravity*. Cambridge Monographs on Mathematical Physics. Univ. Pr., Cambridge, UK, 2004. doi: 10.1017/CBO9780511755804. 2

[246] V. C. Rubin and W. K. Ford, Jr. Rotation of the Andromeda Nebula from a Spectroscopic Survey of Emission Regions. *Astrophys. J.*, 159:379–403, 1970. doi: 10.1086/150317. 1

[247] R. K. Sachs and A. M. Wolfe. Perturbations of a cosmological model and angular variations of the microwave background. *Astrophys. J.*, 147:73–90, 1967. doi: 10.1007/s10714-007-0448-9. 49

[248] M. Sasaki, T. Suyama, T. Tanaka, and S. Yokoyama. Primordial black holes—perspectives in gravitational wave astronomy. *Class. Quantum Grav.*, 35 (6):063001, 2018. doi: 10.1088/1361-6382/aaa7b4. 52, 143

[249] I. Sawicki and W. Hu. Stability of cosmological solutions in $f(R)$ models of gravity. *Phys. Rev. D*, 75:127502, 2007. doi: 10.1103/PhysRevD.75.127502. 24

[250] K. Schwarzschild. On the gravitational field of a mass point according to Einstein's theory. *Sitzungsber. Preuss. Akad. Wiss. Berlin (Math. Phys.)*, 1916:189–196, 1916. 16

[251] J. M. M. Senovilla. Junction conditions for F(R)-gravity and their consequences. *Phys. Rev. D*, 88:064015, 2013. doi: 10.1103/PhysRevD.88.064015. 111, 113, 114

[252] J. M. M. Senovilla. Gravitational double layers. *Class. Quantum Grav.*, 31:072002, 2014. doi: 10.1088/0264-9381/31/7/072002. 111, 113, 114, 115

[253] J. M. M. Senovilla and D. Garfinkle. The 1965 penrose singularity theorem. *Class. Quantum Grav.*, 32(12):124008, 2015. doi: 10.1088/0264-9381/32/12/124008. 2

[254] A. J. Shajib, G. P. Smith, S. Birrer, A. Verma, N. Arendse, T. E. Collett, T. Daylan, and S. Serjeant. Strong gravitational lenses from the Vera C. Rubin Observatory. 6 2024. 22, 147

[255] I. I. Shapiro. Fourth Test of General Relativity. *Phys. Rev. Lett.*, 13(26):789–791, 1964. doi: 10.1103/PhysRevLett.13.789. 17

[256] I. I. Shapiro, M. E. Ash, R. P. Ingalls, W. B. Smith, D. B. Campbell, R. B. Dyce, R. F. Jurgens, and G. H. Pettengill. Fourth Test of General Relativity: New Radar Result. *Phys. Rev. Lett.*, 26(18):1132–1135, 1971. doi: 10.1103/PhysRevLett.26.1132. 17

[257] E. Silverstein and D. Tong. Scalar speed limits and cosmology: Acceleration from d-cceleration. *Phys. Rev. D*, 70:103505, 2004. doi: 10.1103/PhysRevD.70.103505. 13, 56

[258] R. Smits, M. Kramer, B. Stappers, D. R. Lorimer, J. Cordes, and A. Faulkner. Pulsar searches and timing with the square kilometre array. *Astron. Astrophys.*, 493:1161–1170, 2009. doi: 10.1051/0004-6361:200810383. 146

[259] T. P. Sotiriou. $f(R)$ gravity and scalar-tensor theory. *Class. Quantum Grav.*, 23: 5117–5128, 2006. doi: 10.1088/0264-9381/23/17/003. 23

[260] T. P. Sotiriou and V. Faraoni. $f(R)$ Theories Of Gravity. *Rev. Mod. Phys.*, 82: 451–497, 2010. doi: 10.1103/RevModPhys.82.451. 24

[261] M. Spalinski. On Power law inflation in DBI models. *JCAP*, 05:017, 2007. doi: 10.1088/1475-7516/2007/05/017. 13

[262] A. A. Starobinsky. A New Type of Isotropic Cosmological Models Without Singularity. *Phys. Lett. B*, 91:99–102, 1980. doi: 10.1016/0370-2693(80)90670-X. 6, 28, 121

[263] J. M. Stewart. Perturbations of Friedmann-Robertson-Walker cosmological models. *Class. Quantum Grav.*, 7:1169–1180, 1990. doi: 10.1088/0264-9381/7/7/013. 42

[264] J. M. Stewart and G. F. R. Ellis. Solutions of Einstein's equations for a fluid which exhibit local rotational symmetry. *J. Math. Phys.*, 9:1072–1082, 1968. doi: 10.1063/1.1664679. 92

[265] H. Sugai et al. Updated Design of the CMB Polarization Experiment Satellite LiteBIRD. *J. Low. Temp. Phys.*, 199(3-4):1107–1117, 2020. doi: 10.1007/s10909-019-02329-w. 22

[266] J. H. Taylor, Jr. Binary Pulsars and Relativistic Gravity. *J. Astrophys. Astron.*, 16:307, 1995. doi: 10.1007/BF02714841. 17

[267] R. C. Tolman. Static solutions of Einstein's field equations for spheres of fluid. *Phys. Rev.*, 55:364–373, 1939. doi: 10.1103/PhysRev.55.364. xxiv, 81, 85, 90, 103

[268] R. C. Tolman and M. Ward. On the behavior of non-static models of the universe when the cosmological term is omitted. *Phys. Rev.*, 39:835–843, 1932. doi: 10.1103/PhysRev.39.835. 8

[269] R. Trumpler. Final results on the light deflections in the Sun's gravitational field from observations made at the total solar eclipse of September 21, 1922. *PASP*, 40 (234):130, 1928. doi: 10.1086/123816. 17

[270] M. S. Turner. Cosmological parameters. *AIP Conf. Proc.*, 478(1):113–128, 1999. doi: 10.1063/1.59381. 2

[271] S. Vagnozzi and A. Loeb. The Challenge of Ruling Out Inflation via the Primordial Graviton Background. *Astrophys. J. Lett.*, 939(2):L22, 2022. doi: 10.3847/2041-8213/ac9b0e. 9

[272] H. van Elst and G. F. R. Ellis. The covariant approach to LRS perfect fluid spacetime geometries. *Class. Quantum Grav.*, 13(5):1099–1127, 1996. doi: 10.1088/0264-9381/13/5/023. 92

[273] S. Weinberg. The cosmological constant problem. *Rev. Mod. Phys.*, 61:1–23, 1989. doi: 10.1103/RevModPhys.61.1. 2

[274] S. Weinberg. The Cosmological constant problems. In *4th International Symposium on Sources and Detection of Dark Matter in the Universe (DM 2000)*, pages 18–26, 2 2000. doi: 10.1007/978-3-662-04587-9_2. 2

[275] S. Weinberg. *Cosmology*. Oxford University Press, New York, 2008. ISBN 978-0-19-852682-7. 5

[276] J. M. Weller, C. van de Bruck, and D. F. Mota. Inflationary predictions in scalar-tensor DBI inflation. *JCAP*, 06:002, 2012. doi: 10.1088/1475-7516/2012/06/002. 13

[277] H. Weyl. Gravitation and electricity. *Sitzungsber. Preuss. Akad. Wiss. Berlin (Math. Phys.)*, 1918:465, 1918. 17

[278] B. Whitt. Fourth Order Gravity as General Relativity Plus Matter. *Phys. Lett. B*, 145:176–178, 1984. doi: 10.1016/0370-2693(84)90332-0. 17, 100

[279] B. Whitt. Stability of Schwarzschild black holes in fourth-order gravity. *Phys. Rev. D*, 32:379–388, 1985. doi: 10.1103/PhysRevD.32.379. 24

[280] C. M. Will. The Confrontation between General Relativity and Experiment. *Living Rev. Rel.*, 17:4, 2014. doi: 10.12942/lrr-2014-4. 1

[281] E. Witten. String theory dynamics in various dimensions. *Nucl. Phys. B*, 443: 85–126, 1995. doi: 10.1201/9781482268737-32. 2, 23

[282] R. P. Woodard. Avoiding dark energy with 1/R modifications of gravity. *Lect. Notes Phys.*, 720:403–433, 2007. doi: 10.1007/978-3-540-71013-4_14. 24

[283] R. P. Woodard. Ostrogradsky's theorem on Hamiltonian instability. *Scholarpedia*, 10(8):32243, 2015. doi: 10.4249/scholarpedia.32243. 24

[284] M. Wyman. Galilean-invariant scalar fields can strengthen gravitational lensing. *Phys. Rev. Lett.*, 106:201102, 2011. doi: 10.1103/PhysRevLett.106.201102. 22

[285] S. S. Yazadjiev, D. D. Doneva, K. D. Kokkotas, and K. V. Staykov. Non-perturbative and self-consistent models of neutron stars in R-squared gravity. *JCAP*, 06:003, 2014. doi: 10.1088/1475-7516/2014/06/003. 16, 121

[286] Ya. B. Zel'dovich. Cosmological constant and elementary particles. *JETP Lett.*, 6: 883, 1967. 2

[287] Ya. B. Zel'dovich. The cosmological constant and the theory of elementary particles. *Soviet Physics Uspekhi*, 11(3):381, 1968. doi: 10.1070/PU1968v011n03ABEH003927. 2

[288] Ya. B. Zel'dovich. Gravitational instability: An Approximate theory for large density perturbations. *Astron. Astrophys.*, 5:84–89, 1970. 4

[289] X. Zhang, T. Liu, and W. Zhao. Gravitational radiation from compact binary systems in screened modified gravity. *Phys. Rev. D*, 95:104027, 2017. doi: 10.1103/PhysRevD.95.104027. 14, 15

[290] H.-B. Zheng, M.-Q. Wu, G.-P. Li, and Q.-Q. Jiang. Shadows and accretion disk images of charged rotating black hole in modified gravity theory. *Eur. Phys. J. C*, 85(1):46, 2025. doi: 10.1140/epjc/s10052-025-13791-0. 14, 15

APPENDIX A

COMPLETE ANALYTICAL SOLUTIONS TO RELATIVISTIC STARS

This appendix lists the new exact solutions obtained from the reconstruction technique used in Secs. 11.3 and 11.4 for Starobinsky gravity, as appeared in [53]. A link to the GitHub repository containing the Mathematica notebooks and the python file used to calculate and plot these solutions is in [51].

A.1 Interior Schwarzschild-Tolman IV spacetime

We provide the full expressions for the solution in Sec. 11.3, along with the surface quantities on $\mathcal{S}$ describing the shell and the double layer.

A.1.1 The complete jump quantities

$$[\phi]^{+}_{-} \equiv \phi^{\mathcal{S}} = \frac{\sqrt{A^2 + r_b^2}\sqrt{\mathcal{R}^2 - r_b^2}}{\mathcal{R}\sqrt{A^2 + 2r_b^2}}, \tag{A.1}$$

$$[\mathcal{A}]^{+}_{-} = \mathcal{A}^{\mathcal{S}} = \frac{\mu_1 r_b^2 \sqrt{A^2 + r_b^2}\sqrt{\mathcal{R}^2 - r_b^2}}{\mathcal{R}\sqrt{A^2 + 2r_b^2}\left(-2c_1\sqrt{3 - \mu_1 r_b^2} + 2\mu_1 r_b^2 - 6\right)}, \tag{A.2}$$

$$[X]^{+}_{-} = X^{\mathcal{S}} = -\frac{2r_b\sqrt{\mathcal{R}^2 - r_b^2}\sqrt{A^2 + r_b^2}\left(-2x_{11} + 2x_{12} - c_1^2\sqrt{3 - r_b^2\mu_1}x_{13} + c_1 x_{10}\right)}{\mathcal{R}^3\left(A^2 + 2r_b^2\right)^{7/2}\left(3 - r_b^2\mu_1\right)^{3/2}\left(\mu_1 r_b^2 - c_1\sqrt{3 - r_b^2\mu_1} - 3\right)^3}, \tag{A.3}$$

where

$$x_1 = 2\mathcal{R}^2A^6 + 12\mathcal{R}^2r_b^2A^4 + \left(4\mathcal{R}^2 - 6A^2\right)r_b^6 + \left(6A^2\mathcal{R}^2 - 9A^4\right)r_b^4, \tag{A.4}$$

$$x_2 = 8r_b^8 - 2\left(A^2 - 2\mathcal{R}^2\right)r_b^6 + \left(6A^2\mathcal{R}^2 - 15A^4\right)r_b^4 + 2\left(A^6 + 13\mathcal{R}^2A^4\right)r_b^2 + 4A^6\mathcal{R}^2, \tag{A.5}$$

$$x_3 = 16r_b^6 + 6\left(3A^2 - 2\mathcal{R}^2\right)r_b^4 - \left(A^4 + 26\mathcal{R}^2A^2\right)r_b^2 + 4A^4\left(A^2 + \mathcal{R}^2\right), \tag{A.6}$$

$$x_4 = 32r_b^8 + 2\left(A^2 - 26\mathcal{R}^2\right)r_b^6 - \left(71A^4 + 130\mathcal{R}^2A^2\right)r_b^4 + \left(8A^6 + 38\mathcal{R}^2A^4\right)r_b^2 + 5A^6\mathcal{R}^2, \tag{A.7}$$

$$x_5 = 16r_b^6 + 6\left(A^2 - 6\mathcal{R}^2\right)r_b^4 - \left(31A^4 + 86\mathcal{R}^2A^2\right)r_b^2 + 4A^4\left(A^2 + \mathcal{R}^2\right), \tag{A.8}$$

$$x_6 = 12r_b^8 - 6A^2r_b^6 - 2\left(16A^4 + 5\mathcal{R}^2A^2\right)r_b^4 + 3\left(A^6 + 13\mathcal{R}^2A^4\right)r_b^2 + 6A^6\mathcal{R}^2, \tag{A.9}$$

$$x_7 = 60r_b^8 + 4\left(A^2 - 5\mathcal{R}^2\right)r_b^6 - \left(103A^4 + 68\mathcal{R}^2A^2\right)r_b^4 + 3\left(5A^6 + 43\mathcal{R}^2A^4\right)r_b^2 + 19A^6\mathcal{R}^2, \tag{A.10}$$

$$x_8 = 112r_b^8 + \left(70A^2 - 92\mathcal{R}^2\right)r_b^6 - 3\left(35A^4 + 74\mathcal{R}^2A^2\right)r_b^4 + 2\left(14A^6 + 53\mathcal{R}^2A^4\right)r_b^2 + 13A^6\mathcal{R}^2, \tag{A.11}$$

$$x_9 = 4r_b^6 + 3\left(A^2 - 2\mathcal{R}^2\right)r_b^4 - 2\left(2A^4 + 7\mathcal{R}^2A^2\right)r_b^2 + A^4\left(A^2 + \mathcal{R}^2\right), \tag{A.12}$$

$$x_{10} = r_b^4x_6\mu_1^4 - 3r_b^2x_7\mu_1^3 + 9x_8\mu_1^2 - 432x_9\mu_1 - 486\left(A^2 + 2\mathcal{R}^2\right)\left(5A^2 + 2r_b^2\right), \tag{A.13}$$

$$x_{11} = \left(r_b^2x_1\mu_1^3 - 3x_2\mu_1^2 + 9x_3\mu_1 + 27\left(A^2 + 2\mathcal{R}^2\right)\left(5A^2 + 2r_b^2\right)\right)\left(3 - r_b^2\mu_1\right)^{3/2}, \tag{A.14}$$

$$x_{12} = \left(A^2 + 2\mathcal{R}^2\right)c_1^3\left(5A^2 + 2r_b^2\right)\left(r_b^2\mu_1 - 3\right)^3, \tag{A.15}$$

$$x_{13} = r_b^2 \left(12 r_b^8 + 2\left(A^2 - 8\mathcal{R}^2\right) r_b^6 - 6\left(4A^4 + 7\mathcal{R}^2 A^2\right) r_b^4 + 3\left(A^6 + 5\mathcal{R}^2 A^4\right) r_b^2 + 2A^6\mathcal{R}^2\right) \mu_1^3$$
$$- 3x_4\mu_1^2 + 18x_5\mu_1 + 162\left(A^2 + 2\mathcal{R}^2\right)\left(5A^2 + 2r_b^2\right). \tag{A.16}$$

The Ricci scalar on the surface $\mathcal{S}$ is given by Eq. (A.17), evaluated at r_b using the parameter values from Figs. 11.1–11.5.

A.1.2 The Ricci scalar:

$$R(r) = \frac{1}{B}\left(2\left(A^4\left(3c_1^2 z^3 + c_1 a_1 + z a_2\right) + A^2\left(c_1^2 z^3\left(7r^2 + 3\mathcal{R}^2\right) + c_1 a_3 + z a_4\right)\right.\right.$$
$$\left.\left. + 2r^2\left(c_1^2 z^3\left(3r^2 + \mathcal{R}^2\right) + 3c_1 a_5 + z a_6\right)\right)\right), \tag{A.17}$$

where $z = \sqrt{3 - \mu_1 r^2}$, and

$$a_1 = 9\mu_1^2 r^4 - 2\mu_1 r^2\left(\mu_1\mathcal{R}^2 + 24\right) + 9\left(\mu_1\mathcal{R}^2 + 6\right), \tag{A.18}$$

$$a_2 = 6\mu_1^2 r^4 - 2\mu_1 r^2\left(\mu_1\mathcal{R}^2 + 15\right) + 9\left(\mu_1\mathcal{R}^2 + 3\right), \tag{A.19}$$

$$a_3 = 22\mu_1^2 r^6 + \mu_1 r^4\left(\mu_1\mathcal{R}^2 - 117\right) - 6r^2\left(2\mu_1\mathcal{R}^2 - 21\right) + 54\mathcal{R}^2, \tag{A.20}$$

$$a_4 = 15\mu_1^2 r^6 - \mu_1 r^4\left(2\mu_1\mathcal{R}^2 + 75\right) + r^2\left(6\mu_1\mathcal{R}^2 + 63\right) + 27\mathcal{R}^2, \tag{A.21}$$

$$a_5 = 3\mu_1^2 r^6 - 16\mu_1 r^4 + r^2\left(18 - \mu_1\mathcal{R}^2\right) + 6\mathcal{R}^2, \tag{A.22}$$

$$a_6 = 6\mu_1^2 r^6 - \mu_1 r^4\left(\mu_1\mathcal{R}^2 + 30\right) + 3r^2\left(\mu_1\mathcal{R}^2 + 9\right) + 9\mathcal{R}^2, \tag{A.23}$$

$$B = \mathcal{R}^2\left(A^2 + 2r^2\right)^2 z\left(c_1 z - \mu_1 r^2 + 3\right)^2. \tag{A.24}$$

A.1.3 Total energy density:

$$\mu^{\text{tot}} = \frac{3A^4 + A^2\left(7r^2 + 3\mathcal{R}^2\right) + 2r^2\left(3r^2 + \mathcal{R}^2\right)}{\mathcal{R}^2\left(A^2 + 2r^2\right)^2}. \tag{A.25}$$

A.1.4 Total radial pressure:

$$p_r^{\text{tot}} = \frac{4\left(A^2+r^2\right)\left(\mathcal{R}^2-r^2\right)}{r^2\mathcal{R}^2\left(A^2+2r^2\right)}\left(-\frac{\mathcal{R}^2\left(A^2+2r^2\right)}{4\left(A^2+r^2\right)\left(\mathcal{R}^2-r^2\right)}+\frac{\mu_1 r^2}{-2c_1 z+2\mu_1 r^2-6}+\frac{1}{4}\right). \tag{A.26}$$

A.1.5 Total isotropic pressure:

$$\begin{aligned} p^{\text{tot}} = \frac{1}{3B}\Big(&-\left(A^4\left(3c_1^2z^3+2c_1b_1+zb_2\right)\right)-A^2\left(c_1^2z^3\left(7r^2+3\mathcal{R}^2\right)+2c_1b_3+zb_4\right)\\ &-2r^2\left(c_1^2z^3\left(3r^2+\mathcal{R}^2\right)+2c_1b_5+3zb_6\right)\Big), \end{aligned} \tag{A.27}$$

where

$$b_1 = \mu_1\left(6\mu_1 r^4-2r^2\left(\mu_1\mathcal{R}^2+15\right)+9\mathcal{R}^2\right)+27, \tag{A.28}$$

$$b_2 = \mu_1 r^2\left(9\mu_1 r^2-4\mu_1\mathcal{R}^2-42\right)+18\mu_1\mathcal{R}^2+27, \tag{A.29}$$

$$b_3 = r^2\left(\mu_1 r^2\left(15\mu_1 r^2-2\mu_1\mathcal{R}^2-75\right)+6\mu_1\mathcal{R}^2+63\right)+27\mathcal{R}^2, \tag{A.30}$$

$$b_4 = r^2\left(\mu_1 r^2\left(23\mu_1 r^2-7\mu_1\mathcal{R}^2-108\right)+30\mu_1\mathcal{R}^2+63\right)+27\mathcal{R}^2, \tag{A.31}$$

$$b_5 = r^2\left(\mu_1 r^2\left(6\mu_1 r^2-\mu_1\mathcal{R}^2-30\right)+3\mu_1\mathcal{R}^2+27\right)+9\mathcal{R}^2, \tag{A.32}$$

$$b_6 = r^2\left(\mu_1 r^2\left(3\mu_1 r^2-\mu_1\mathcal{R}^2-14\right)+4\mu_1\mathcal{R}^2+9\right)+3\mathcal{R}^2. \tag{A.33}$$

A.1.6 Total orthogonal pressure:

$$\begin{aligned} p_\perp^{\text{tot}} =&\frac{1}{B}\left(A^4\left(-c_1^2z^3+c_1d_1+zd_2\right)-A^2\left(c_1^2z^3\left(2r^2+\mathcal{R}^2\right)+3c_1d_3+zd_4\right)\right.\\ &\left.-2r^4\left(c_1^2z^3-c_1d_1+zd_5\right)\right), \end{aligned} \tag{A.34}$$

where

$$d_1 = \mu_1 r^2 \left(-4\mu_1 r^2 + \mu_1 \mathcal{R}^2 + 21\right) - 6\mu_1 \mathcal{R}^2 - 18, \tag{A.35}$$

$$d_2 = \mu_1 r^2 \left(-3\mu_1 r^2 + \mu_1 \mathcal{R}^2 + 15\right) - 6\mu_1 \mathcal{R}^2 - 9, \tag{A.36}$$

$$d_3 = r^2 \left(\mu_1 \left(3\mu_1 r^4 - 16 r^2 + \mathcal{R}^2\right) + 12\right) + 6\mathcal{R}^2, \tag{A.37}$$

$$d_4 = r^2 \left(\mu_1 r^2 \left(7\mu_1 r^2 - \mu_1 \mathcal{R}^2 - 36\right) + 9\mu_1 \mathcal{R}^2 + 18\right) + 9\mathcal{R}^2, \tag{A.38}$$

$$d_5 = \mu_1 r^2 \left(3\mu_1 r^2 - \mu_1 \mathcal{R}^2 - 15\right) + 6\mu_1 \mathcal{R}^2 + 9. \tag{A.39}$$

A.2 A Generic Interior Metric

We present the full expressions for the solution discussed in Sec. 11.4.

A.2.1 Model parameter relations through the junction conditions:

$$\mathfrak{D}_3 = \frac{3\left(12\mathfrak{D}_1^3 r_b^4 + \mathfrak{D}_1^2 r_b^2 \left(49\mathfrak{D}_2 r_b^4 + 13\right) + 10\mathfrak{D}_2 r_b^2 \left(3\mathfrak{D}_2^2 r_b^8 + 1\right) + \mathfrak{D}_1 \left(\mathfrak{D}_2 r_b^4 \left(61\mathfrak{D}_2 r_b^4 + 30\right) + 5\right)\right)}{2\mathfrak{D}_2 r_b^4 \left(\mathfrak{D}_2 r_b^4 \left(11\mathfrak{D}_2 r_b^4 + 36\right) - 11\right) + \mathfrak{D}_1 r_b^2 \left(\mathfrak{D}_2 r_b^4 \left(37\mathfrak{D}_2 r_b^4 + 14\right) - 3\right) + 3\mathfrak{D}_1^2 \left(\mathfrak{D}_2 r_b^8 + r_b^4\right)}, \tag{A.40}$$

$$\begin{aligned}\mathfrak{D}_4 = \frac{1}{\mathfrak{d}_1} \Big(&36\mathfrak{D}_1^4 r_b^6 + 3\mathfrak{D}_1^3 r_b^4 \left(69\mathfrak{D}_2 r_b^4 + 25\right) + 4\mathfrak{D}_1^2 r_b^2 \left(\mathfrak{D}_2 r_b^4 \left(71\mathfrak{D}_2 r_b^4 + 80\right) + 18\right) \\ &+10\mathfrak{D}_2 r_b^2 \left(\mathfrak{D}_2 r_b^4 \left(23 - \mathfrak{D}_2 r_b^4 \left(3\mathfrak{D}_2 r_b^4 + 31\right)\right) + 3\right) \\ &+\mathfrak{D}_1 \left(\mathfrak{D}_2 r_b^4 \left(\mathfrak{D}_2 r_b^4 \left(41\mathfrak{D}_2 r_b^4 + 129\right) + 287\right) + 15\right)\Big),\end{aligned} \tag{A.41}$$

$$\begin{aligned}\mathfrak{D}_5 = \frac{1}{\mathfrak{d}_1} \Big(&16\mathfrak{D}_2^2 r_b^4 \left(\mathfrak{D}_2 r_b^4 \left(2\mathfrak{D}_2 r_b^4 + 7\right) - 7\right) + 8\mathfrak{D}_1 \mathfrak{D}_2 r_b^2 \left(\mathfrak{D}_2 r_b^4 + 1\right) \left(5\mathfrak{D}_2 r_b^4 - 12\right) \\ &-6\mathfrak{D}_1^3 \left(5\mathfrak{D}_2 r_b^6 + r_b^2\right) - 4\mathfrak{D}_1^2 \left(\mathfrak{D}_2 r_b^4 \left(10\mathfrak{D}_2 r_b^4 + 21\right) + 3\right)\Big),\end{aligned} \tag{A.42}$$

where

$$\begin{aligned}\mathfrak{d}_1 =& r_b^2 \left(5\mathfrak{D}_2 r_b^4 + 3\mathfrak{D}_1 r_b^2 + 1\right) \left(3\mathfrak{D}_1^2 \left(\mathfrak{D}_2 r_b^6 + r_b^2\right) + \mathfrak{D}_1 \left(\mathfrak{D}_2 r_b^4 \left(37\mathfrak{D}_2 r_b^4 + 14\right) - 3\right)\right) \\ &+2\mathfrak{D}_2 r_b^2 \left(\mathfrak{D}_2 r_b^4 \left(11\mathfrak{D}_2 r_b^4 + 36\right) - 11\right)\Big).\end{aligned} \tag{A.43}$$

A.2.2 Ricci scalar:

$$R(r)=\frac{2\left(-11\mathfrak{D}_2^2\mathfrak{D}_3\mathfrak{D}_5r^{12}+\mathfrak{D}_2\mathfrak{b}_1r^{10}-\mathfrak{b}_2r^8-\mathfrak{b}_3r^6+\mathfrak{b}_4r^4-\mathfrak{b}_5r^2-3\left(\mathfrak{D}_1-\mathfrak{D}_3+\mathfrak{D}_4\right)\right)}{\left(\mathfrak{D}_2r^4+\mathfrak{D}_1r^2+1\right)^2\left(\mathfrak{D}_3r^2+1\right)^2}, \tag{A.44}$$

where

$$\mathfrak{b}_1=\mathfrak{D}_2\mathfrak{D}_3\left(\mathfrak{D}_3-7\mathfrak{D}_4\right)-3\left(5\mathfrak{D}_2+6\mathfrak{D}_1\mathfrak{D}_3\right)\mathfrak{D}_5, \tag{A.45}$$

$$\begin{aligned}\mathfrak{b}_2=&\mathfrak{D}_2\mathfrak{D}_3\left(\mathfrak{D}_2-2\mathfrak{D}_1\mathfrak{D}_3\right)+11\mathfrak{D}_2\left(\mathfrak{D}_2+\mathfrak{D}_1\mathfrak{D}_3\right)\mathfrak{D}_4+25\mathfrak{D}_1\mathfrak{D}_2\mathfrak{D}_5\\&+6\left(\mathfrak{D}_1^2+3\mathfrak{D}_2\right)\mathfrak{D}_3\mathfrak{D}_5,\end{aligned} \tag{A.46}$$

$$\begin{aligned}\mathfrak{b}_3=&6\mathfrak{D}_2^2+2\left(-\mathfrak{D}_3^2+6\mathfrak{D}_4\mathfrak{D}_3+9\mathfrak{D}_1\mathfrak{D}_4+12\mathfrak{D}_5\right)\mathfrak{D}_2\\&+\mathfrak{D}_1\left(10\mathfrak{D}_3\mathfrak{D}_5+\mathfrak{D}_1\left(-\mathfrak{D}_3^2+3\mathfrak{D}_4\mathfrak{D}_3+9\mathfrak{D}_5\right)\right),\end{aligned} \tag{A.47}$$

$$\begin{aligned}\mathfrak{b}_4=&2\left(\mathfrak{D}_3-3\mathfrak{D}_4\right)\mathfrak{D}_1^2-\left(-2\mathfrak{D}_3^2+5\mathfrak{D}_4\mathfrak{D}_3+9\mathfrak{D}_2+15\mathfrak{D}_5\right)\mathfrak{D}_1-2\mathfrak{D}_2\left(\mathfrak{D}_3+9\mathfrak{D}_4\right)\\&-3\mathfrak{D}_3\mathfrak{D}_5,\end{aligned} \tag{A.48}$$

$$\mathfrak{b}_5=\left(2\mathfrak{D}_1^2+\left(10\mathfrak{D}_4-4\mathfrak{D}_3\right)\mathfrak{D}_2+\mathfrak{D}_3\left(\mathfrak{D}_4-\mathfrak{D}_3\right)+5\mathfrak{D}_5\right). \tag{A.49}$$

A.2.3 Total energy density:

$$\mu^{\text{tot}}=\frac{-3r^4\mathfrak{D}_3\mathfrak{D}_5+r^2\left(\mathfrak{D}_3{}^2-\mathfrak{D}_3\mathfrak{D}_4-5\mathfrak{D}_5\right)+3\mathfrak{D}_3-3\mathfrak{D}_4}{\left(r^2\mathfrak{D}_3+1\right)^2} \tag{A.50}$$

A.2.4 Total radial pressure:

$$\begin{aligned}p_r^{\text{tot}}=&\frac{1}{\left(r^2\mathfrak{D}_3+1\right)\left(r^4\mathfrak{D}_2+r^2\mathfrak{D}_1+1\right)}\left(5r^6\mathfrak{D}_2\mathfrak{D}_5+r^4(3\mathfrak{D}_1\mathfrak{D}_5-\mathfrak{D}_2\mathfrak{D}_3+5\mathfrak{D}_2\mathfrak{D}_4)\right.\\&\left.+r^2(-\mathfrak{D}_1\mathfrak{D}_3+3\mathfrak{D}_1\mathfrak{D}_4+4\mathfrak{D}_2+\mathfrak{D}_5)+2\mathfrak{D}_1-\mathfrak{D}_3+\mathfrak{D}_4\right)\end{aligned} \tag{A.51}$$

A.2.5 Total orthogonal pressure

$$p_{\perp}^{\rm tot} = \frac{1}{(r^2\mathfrak{D}_3+1)^2\,(r^4\mathfrak{D}_2+r^2\mathfrak{D}_1+1)^2}\left(7r^{12}{\mathfrak{D}_2}^2\mathfrak{D}_3\mathfrak{D}_5 + r^{10}\mathfrak{g}_1 + r^8\mathfrak{g}_2 + r^6\mathfrak{g}_3 + r^4\mathfrak{g}_4 + r^2\mathfrak{g}_5 + 2\mathfrak{D}_1 - \mathfrak{D}_3 + \mathfrak{D}_4\right), \tag{A.52}$$

where

$$\mathfrak{g}_1 = \mathfrak{D}_2(11\mathfrak{D}_1\mathfrak{D}_3\mathfrak{D}_5 + 4\mathfrak{D}_2\mathfrak{D}_3\mathfrak{D}_4 + 10\mathfrak{D}_2\mathfrak{D}_5), \tag{A.53}$$

$$\mathfrak{g}_2 = 3\mathfrak{D}_3\mathfrak{D}_5\left({\mathfrak{D}_1}^2 + 4\mathfrak{D}_2\right) + 6\mathfrak{D}_1\mathfrak{D}_2\mathfrak{D}_3\mathfrak{D}_4 + 16\mathfrak{D}_1\mathfrak{D}_2\mathfrak{D}_5 + {\mathfrak{D}_2}^2(\mathfrak{D}_3 + 7\mathfrak{D}_4), \tag{A.54}$$

$$\mathfrak{g}_3 = \mathfrak{D}_2(\mathfrak{D}_1\mathfrak{D}_3 + 11\mathfrak{D}_1\mathfrak{D}_4 + 8\mathfrak{D}_3\mathfrak{D}_4 + 16\mathfrak{D}_5) + \mathfrak{D}_1(\mathfrak{D}_1\mathfrak{D}_3\mathfrak{D}_4 + 5\mathfrak{D}_5(\mathfrak{D}_1 + \mathfrak{D}_3)) + 4{\mathfrak{D}_2}^2, \tag{A.55}$$

$$\mathfrak{g}_4 = -{\mathfrak{D}_1}^2(\mathfrak{D}_3 - 3\mathfrak{D}_4) + 2\mathfrak{D}_1(3\mathfrak{D}_2 + \mathfrak{D}_3\mathfrak{D}_4 + 4\mathfrak{D}_5) + 4\mathfrak{D}_2(\mathfrak{D}_3 + 3\mathfrak{D}_4) + \mathfrak{D}_3\mathfrak{D}_5, \tag{A.56}$$

$$\mathfrak{g}_5 = {\mathfrak{D}_1}^2 - \mathfrak{D}_1\mathfrak{D}_3 + 5\mathfrak{D}_1\mathfrak{D}_4 + 8\mathfrak{D}_2 + 2\mathfrak{D}_5. \tag{A.57}$$

A.2.6 Total isotropic pressure

$$p^{\rm tot} = \frac{19r^{12}{\mathfrak{D}_2}^2\mathfrak{D}_3\mathfrak{D}_5 + r^{10}\mathfrak{h}_1 + r^8\mathfrak{h}_2 + r^6\mathfrak{h}_3 + r^4\mathfrak{h}_4 + r^2\mathfrak{h}_5 + 6\mathfrak{D}_1 - 3\mathfrak{D}_3 + 3\mathfrak{D}_4}{3\,(r^2\mathfrak{D}_3+1)^2\,(r^4\mathfrak{D}_2+r^2\mathfrak{D}_1+1)^2} \tag{A.58}$$

where

$$\mathfrak{h}_1 = \mathfrak{D}_2(5\mathfrak{D}_5(6\mathfrak{D}_1\mathfrak{D}_3 + 5\mathfrak{D}_2) - \mathfrak{D}_2\mathfrak{D}_3(\mathfrak{D}_3 - 13\mathfrak{D}_4)), \tag{A.59}$$

$$\mathfrak{h}_2 = \mathfrak{D}_5\left(9{\mathfrak{D}_1}^2\mathfrak{D}_3 + 40\mathfrak{D}_1\mathfrak{D}_2 + 30\mathfrak{D}_2\mathfrak{D}_3\right) + \mathfrak{D}_2(\mathfrak{D}_2(5\mathfrak{D}_3 + 19\mathfrak{D}_4) - 2\mathfrak{D}_1\mathfrak{D}_3(\mathfrak{D}_3 - 10\mathfrak{D}_4)), \tag{A.60}$$

$$\begin{aligned}\mathfrak{h}_3 = {} & \mathfrak{D}_2\left(6\mathfrak{D}_1(\mathfrak{D}_3 + 5\mathfrak{D}_4) - 2{\mathfrak{D}_3}^2 + 22\mathfrak{D}_3\mathfrak{D}_4 + 38\mathfrak{D}_5\right) \\ & + \mathfrak{D}_1\left(\mathfrak{D}_1\left(-{\mathfrak{D}_3}^2 + 5\mathfrak{D}_3\mathfrak{D}_4 + 13\mathfrak{D}_5\right) + 14\mathfrak{D}_3\mathfrak{D}_5\right) + 12{\mathfrak{D}_2}^2,\end{aligned} \tag{A.61}$$

$$\mathfrak{h}_4 = -{\mathfrak{D}_1}^2(\mathfrak{D}_3 - 9\mathfrak{D}_4) + 2\mathfrak{D}_1\left(9\mathfrak{D}_2 - {\mathfrak{D}_3}^2 + 4\mathfrak{D}_3\mathfrak{D}_4 + 10\mathfrak{D}_5\right) + 10\mathfrak{D}_2(\mathfrak{D}_3 + 3\mathfrak{D}_4) + 3\mathfrak{D}_3\mathfrak{D}_5, \tag{A.62}$$

$$\mathfrak{h}_5 = 4{\mathfrak{D}_1}^2 - 2\mathfrak{D}_1(\mathfrak{D}_3 - 7\mathfrak{D}_4) + 20\mathfrak{D}_2 + \mathfrak{D}_3(\mathfrak{D}_4 - \mathfrak{D}_3) + 5\mathfrak{D}_5. \tag{A.63}$$

APPENDIX B

PARAMETER SAMPLING FOR STELLAR INTERIORS IN QUADRATIC GRAVITY

This appendix describes the sampling method of the model parameters for the analytical solutions found in Sec. 11.3.

Random values were generated for each parameter, μ, A, $\mathcal{R}$, and c_1 using the built-in functions in Mathematica. Choosing a sample size of 500 values, the parameter values were sampled in the following way:

The central point in the parameter space is $(\mu_1, c_1, A, \mathcal{R}) = (-1.25, 0.3, 1.5, 7.3)$ and the radius of the sphere is chosen to be `meanradius` $= 1$ with a perturbed radius of `sigmaradius` $= 0.05$ from the central point. A list of values for the radial distance, polar, and azimuthal angles are generated using the built-in Mathematica functions as follows:

$\theta =$ `RandomVariate[NormalDistribution[0, N[Pi]], Numpoints];`

$\phi =$ `RandomVariate[NormalDistribution[0, 2N[Pi]], Numpoints];`

radius $=$ `RandomVariate[NormalDistribution[meanradius, sigmaradius], Numpoints];`.

To generate random numbers for the model parameters, constrained to a sphere of radius 1, but shifted from the central point, the following were calculated:

$$\mu_1 = \mu_1 \text{ central value} + (\text{radius } \cdot \sin(\theta) \cdot \cos(\phi)),$$

$$c_1 = c_1 \text{ central value} + (\text{radius } \cdot \sin(\theta) \cdot \sin(\phi)),$$

$$A = A \text{ central value} + (\text{radius } \cdot \cos(\theta)),$$

$$\mathcal{R} = \texttt{RandomVariate[PoissonDistribution[}\mathcal{R} \text{ central value}\texttt{], Numpoints]}.$$